Title
The Toxic Effects of Nanoparticles in Bacterial Cells

Author
Kaweeteerawat, Chitrada

Publication Date
2015

Peer reviewed|Thesis/dissertation

UNIVERSITY OF CALIFORNIA

Los Angeles

The Toxic Effects of Nanoparticles in Bacterial Cells

A dissertation submitted in partial satisfaction of the requirements for the degree Doctor of Philosophy in Molecular Toxicology

By

Chitrada Kaweeteerawat

2015

ABSTRACT OF THE DISSERTATION

The Toxic Effects of Nanoparticles in Bacterial Cells

by

Chitrada Kaweeteerawat

Doctor of Philosophy in Molecular Toxicology

University of California, Los Angeles, 2015

Professor Hilary Godwin, Chair

ABSTRACT

The overarching goal of the work described herein is to elucidate which physicochemical properties contribute to the toxicity of nanoparticles and whether nanoparticles have any special toxicological properties compared to their bulk or micron-sized analogs. We focused specifically on a series of 24 metal oxide nanoparticles (NPs) and on metal (Cu and Ag) NPs and investigated their impacts on enteric bacteria (*Escherichia coli* and *Lactobacillus brevis*). For the MOx NPs, we determined that the conduction band energy and hydration energy of the metal correlated most strongly with the toxicity of the nanoparticles in *E. coli*. Using a series of sub-

lethal assays, we demonstrated that the most toxic MOx NPs resulted in ROS generation and membrane damage. For both the Cu and Ag NPs, we compared the magnitude and mechanisms of toxicity to the corresponding metal ions (Cu^{2+} and Ag^{+}), and in the case of Cu NPs, we also compared the magnitude and mechanisms of toxicity of the NPs to their micron-sized analogs in both *E. coli* and *L. brevis*. In the case of the Cu NPs, we found that, although the magnitude of toxicity of the different Cu species correlates with the amount of bioavailable copper, the mechanisms of toxicity for the Cu NPs were significantly different from those of ionic and micron-sized Cu species. In the case of the Ag NP (Ag-BPEI), we performed a genome-wide gene expression analysis in *E. coli* and compared the results to that of Ag^{+}. This study revealed that the genes up and down regulated by Ag-BPEI are distinct from those affected by Ag^{+}. Taken together, these studies provide important insights both into how to develop new MOx NPs that are safer by design and provide important insights into the unique toxicological properties of some Cu and Ag NPs.

The dissertation of Chitrada Kaweeteerawat is approved.

Michael D. Collins

Donatello Telesca

Robert Schiestl

Hilary A. Godwin, Committee Chair

University of California, Los Angeles 2015

To my friends and family for their infinite support throughout life

Abbreviation Used Herein

E. coli	*Escherichia coli*
L. brevis	*Lactobacillus brevis*
NPs	nanoparticles
MOx	metal oxide
GDS	gene deletion strains
DCFH	Dichloro-dihydro-fluorescein diacetate
H_2DCFDA	2',7'-dichloro-dihydro-fluorescein diacetate
PI	Propidium Iodide
SVM	support vector machine
SAR	structure activity relationship
ROS	reactive oxygen species

TABLE OF CONTENTS

LIST OF FIGURES AND TABLES

For Chapter 2 (previously published in *Environmental Science and Technology*):

For Chapter 3 (manuscript submitted for publication to *ACS Nano*):

For Chapter 4:

For APPENDIX 1 (Supporting Information for Chapter 2):

For APPENDIX 2 (Supporting Information for Chapter 3):

For APPENDIX 3 (Supporting Information for Chapter 4):

ACKNOWLEDGEMENTS

First and foremost, I would like to thank my advisor, Dr. Hilary Godwin, who has been so much more to me than an academic advisor. She is also my role model for how to be successful in science while at the same time be sensitive and kind towards others. I always received constant support, encouragement and wonderful advice from her. Somehow, she is capable of guiding me in the right direction scientifically and at the same time building my confidence and inspiring me. Hilary also taught an academic writing class I took which has been a critical key to my career as a scientist. It is such a positive and efficient process to work with Hilary, for whom I am forever grateful. I also want to thank my committee members Dr. Michael Collins, Dr. Robert Schiestl and Dr. Donatello Telesca for their wisdom, advice and continuing support throughout the years. Particularly, Dr. Collins who taught the Fundamentals of Toxicology class, which I considered my most favorite, fun and enjoyable class I have taken at UCLA. I am confident that this class will be very beneficial to me as a future toxicologist. He also allowed me to TA in his class, which have been a great honor and pleasure to me.

I also owe many thanks to Dr. Angela Ivask who mentored me during my rotation and the first three years of my time in the Godwin lab. She showed me so many valuable techniques, gave me crucial advice and inspired me. I also considered her to be a great friend who made my life at UCLA so delightful. I also want to thanks the member of UC-CEIN: Xiang Wang, Sijie Lin, Ivy Ji, Ruibin Li, Bingbing Sun, Olivia Osbourne, Paul Chang, Tian Xia, Huan Meng, Wendy Kong, Vi Hyunh and David Avery for their support as well as great talks and laughs during lunch time. Particularly, I want to thank Xiang Wang who sat next to me and always helped me with Excel, Endnote and other experimental designs. My deepest gratitude also goes

to Kevin Roy, who is my best friend and is always there to support me. He also made me the best person I can be as a scientist and in other areas of life.

As a graduate student, I received financial support (including tuition, fees, stipend and health insurance) from the Royal Thai Government as well as from the University of California, Center for Environmental Implications of Nanotechnology (UC-CEIN). The research presented in this work was supported by funding from the National Science Foundation and the Environmental Protection Agency under Cooperative Agreement Number DBI-0830117 and DBI-12266377 to UC-CEIN.

Chapter 2 is a version of a previous publication, which appeared in *Environmental Science and Technology* (*ES&T*) 49(2):1105-12 on January 2015. I would like to acknowledge the contributions of the co-authors in the paper: Specifically I would like to thank Rong Liu, Cecile Low-Kam, Heidi Fischer, Yoram Cohen and Donatello Telesca for statistical analysis and SAR (Rong); Patricia Holden, Andre Nel for reading through and help revise the manuscript; Zhaoxia Ji, Suman Pokhrel, Chong Hyun Chang, Jeffrey Zink, Lutz Mädler for synthesizing and characterizing the metal oxide nanoparticles; Angela Ivask, Haiyuan Zhang for the help with designing the experiments. Hilary Godwin is the principle investigator who provided ideas, helped to design the experiments, assisted with trouble-shooting problem and with writing and editing the manuscript.

Chapter 3 was submitted as a manuscript to *ACS Nano* on April 3, 2015 and was under review as of June 2, 2015. I would like to express my immense gratitude towards the following co-authors: Chong Hyun Chang, Kevin Roy, Rong Liu, Ruibin Li, Daniel Toso, Heidi Fischer, Angela Ivask, Zhaoxia Ji, Jeffrey Zink, Z. Hong Zhou, Guillaume Chanfreau, Donatello Telesca,

Yoram Cohen, Patricia Holden, Andre Nel and Hilary Godwin. Specifically, I would like to thank Daniel Toso and Z. Hong Zhou for performing tomography imaging and 3D reconstruction; Kevin Roy and Guillaume Chanfreau for performing gel electrophoresis, DNA imaging and quantification; Chong Hyun Chang for performing TEM imaging and ICP-OES; Ruibin Li for con-focal microscopy; Rong Liu, Heidi Fischer, Donatello Telesca and Yoram Cohen for statistical analysis; Zhaoxia Ji and Jeffrey Zink for characterizing of the nanoparticles; Angela Ivask, Patricia Holden, Z. Hong Zhou and Andre Nel for providing helpful feedback on the manuscript preparation and Hilary Godwin for supervising the project, providing guidance, helping to design the experiments and assisting with writing and editing the manuscript.

For the work presented in Chapter 4, I would like to acknowledge the contributions of the following co-authors: Angela Ivask, Rong Liu, Amro ElBadawy, Chong Hyun Chang, Zhaoxia Ji, Yoram Cohen, Jeffrey Zink, Thabet Tolaymat, Patricia Holden, Andre Nel and Hilary Godwin. Specifically, I would like to thank Angela Ivask for her assistance with designing and performing the growth-inhibition experiments; Rong Liu and Yoram Cohen for statistical analysis; Zhaoxia Ji, Jeffrey Zink and Chong Hyun Chang for particle characterization; Amro ElBadawy and Thabet Tolaymat for synthesizing and characterizing the nanoparticles; Angela Ivask, Patricia Holden and Andre Nel for providing helpful feedback on the manuscript and Hilary Godwin for supervising the project. I also would like to extend my gratitude to the UCLA Clinical Microarray Core (CMC) and Jose Solis for microarray analysis and his assistance preparing the methods section of the manuscript.

Chitrada Kaweeteerawat

EDUCATION

2010……..…… M.S., Bioscience (Molecular Genetics), Graduate School of Science, Osaka University, Osaka, Japan

2007……..… B.S. (Biology) Highest Honors, Chiang Mai University, Chiang Mai, Thailand.

HONORS

2009 – 2015…..... Full scholarship from the Royal Thai Government for Ph.D. study

2007 – 2009..... Full scholarship for graduate Master of Science program from the Japanese government (Monbukagakusho: MEXT)

2001 – 2007……..……..... Full scholarship for high school and undergraduate studies from the Thai government, under the Development and Promotion of Science and Technology Talents Project (DPST)

PUBLICATIONS

Kaweeteerawat C, Ivask A, Liu R, Zhang H, Chang CH, Lowkam C, Fischer HJ, Ji Z, Pokhrel S, Cohen Y, Telesca D, Zink J, Mädler L, Holden PA, Nel A and Godwin HA. *Toxicity of Metal Oxide Nanoparticles in Escherichia coli Correlates with Conduction Band Energy and Hydration Energy*. **Environ. Sci. Technol**., *2015*, 49 (2): 1105-12.

AWARDS

- Student merit award (first place) from Society of Risk Analysis (SRA) Dose-response specialty group (Denver, CO, December 8-10, 2014)

- Student and young professionals travel award to present a poster at the Nano Risk Analysis II workshop (Washington DC, September 15-16, 2014)

- Student research project award from California Unified Program Agency, CUPA (San Francisco, CA, February 5, 2014)

- Student travel award from Society of Environmental Toxicology and Chemistry (SETAC) to attend the 34th annual meeting (Nashville, TN, November 17-21, 2013)

- Student travel award from Sustainable Nanotechnology Organization (SNO) to attend the 2nd annual conference (Santa Barbara, CA, November 3-5, 2013)

- Student travel award from American College of Toxicology (ACT) to attend the 34th annual meeting (San Antonio, TX, November 3-6, 2013)

- Sustainable Research Showcase Award from UCLA Sustainable Resource Center (UCLA, CA, May 8, 2013)

- Student research project award from California Unified Program Agency, CUPA (Garden Grove, CA, February 6, 2013)

- Student travel award from American College of Toxicology (ACT) to attend the 33rd annual meeting (Orlando, FL, November 4-7, 2012)

CHAPTER 1

Introduction and Overview of the Organization of the Thesis

The rapidly growing field of nanotechnology has enabled a vast array of applications in both industrial and consumer products. Nanoparticles and nanotechnology-enabled products have contributed to the development of various fields such as medicine, energy resources, agriculture, electronics and materials science.[1-3] In the field of medicine, nanotechnology has facilitated the development of novel methods of target-based therapeutic DNA/drug delivery, imaging for diagnostics or the construction of tissue-engineered 3D organs.[4,5] In the field of energy and environmental sustainability, nanotechnologies have contributed to the development of high-performance solar cells, batteries for energy storage for hybrid/electric cars, hydrogen fuel cells for vehicles or high-tensile materials for rotor blades used in windmills.[6-8]

Among all nanoparticles in use commercially, metal oxide nanoparticles (MOx NPs), copper nanoparticles (Cu NPs) and silver nanoparticles (Ag NPs) are among the most extensively used materials.[9] MOx NPs, including ZnO and TiO_2 NPs have been substantially used in sunscreens due to their excellent ability to reflect sunlight.[10] Other materials such as SiO_2 NPs have been utilized in products as diverse as batteries, paints, adhesives and high-definition television,[11] whereas, functionalized ZnO NPs have been developed as selective killers of proliferating cells and as antimicrobial drugs.[12] Ag NPs are frequently used in odor resistant textiles, food storage containers, antiseptic spray, wound dressings and bandages, largely due to their excellent antibacterial properties.[13] Cu NPs are used as lubricants, conducting polymers, surfactants and catalysts in chemical reactions as well as deodorants, food additives and as antifouling agents in paint.[14] Key questions that have emerged about these materials are: (1)

how do the physical chemical properties of MOx NPs impact their toxicity, and is it possible to develop new MOx NPs that have desirable materials properties but are "safer by design"[15] and (2) are there toxicological properties specific to Cu and Ag NPs that are distinct from their ionic analogs and hence make them fundamentally "new" materials?

Within the UC Center for Environmental Implications of Nanotechnology (UC-CEIN), researchers have looked at each of these issues across a wide range of different organisms and ecosystems.[16] For examples, they have found that toxic MOx NPs lead to lethality in zebra fish embryos as well as pulmonary inflammation and cytokine response in mammalian cells.[17,18] In this work, I have implemented high-throughput screening approaches to study the toxicity of MOx in bacteria. **Chapter 2** describes the use of growth-inhibition assays and a suite of sub-lethal assays to discover the magnitude as well as the mechanisms of toxicity of 24 different MOx NPs in bacteria (*Escherichia coli*). Moreover, by studying the same 24 MOx NPs in two evolutionarily distant species, *namely* mammalian cell line and bacterial cells, it is possible to generalize the toxic effect of NPs across the evolutionary tree.

Similarly, the UC-CEIN is focused on understanding mechanisms of toxicity of Cu NPs, which are extensively used as antimicrobials or as anti-fouling agents in coating materials.[14] The center systematically explores the toxic effects of Cu NPs in various aspects of toxicity such as terrestrial impacts, marine and freshwater hazardous assessment, fate and transport, life cycle analysis, as well as exposure modeling and structure activity relationship of the Cu NPs.[19-22] In **Chapter 3** of this study, the magnitude as well as mechanisms of toxicity of Cu NPs was evaluated and systematically compared with micron-sized and ionic Cu species, in two species of environmentally relevant bacteria, *Escherichia coli* (gram negative) and *Lactobacillus brevis*

(gram positive). These two phyla of bacteria also play critical roles in wastewater streams and septic tanks.[19,23]

Previous members of UC-CEIN and the Godwin lab also demonstrated that Ag NPs and ionic silver affect bacteria differently using a genome-wide single gene deletion strains (GDS).[24] However, GDS analysis cannot be performed in essential genes since it is impossible to construct a deletion mutant of an essential gene and the results from GDS can only be complemented with results from microarray analysis.[25] In **Chapter 4**, I report microarray studies using the same Ag NPs (Ag-BPEI) and ionic Ag to explore the mechanisms of toxicity, as well as the stress response of bacterial cells to Ag insults at the gene expression level.

In **Chapter 5**, I describe the overarching conclusions of this study and recommendations for future studies to improve the field of nanotoxicology. Supplemental information for **Chapter 2** is described in **Appendix 1**. Supplemental information for **Chapter 3** is described in **Appendix 2**. Finally, supplemental information for **Chapter 4** is described in **Appendix 3**.

As toxicologists and regulators struggle to keep pace with the rate of which introduction of new nanoparticles are introduced into the marketplace, a detailed understanding of the molecular mechanisms of toxicity of the novel particles is critical to comprehend the potentially adverse effects of the nanoparticles. The suite of assays implemented here will allow for discovering the magnitude as well as key features of the mechanisms of toxicity of poorly characterized nanoparticles. Moreover, a thorough understanding of the relationship between the physicochemical properties of particles and their toxicities will allow for the design of safer nanoparticles that still exhibit superior characteristics over conventional materials. In the systematic comparison between toxicity of particles at nano-scale and micron-sized particles as

well as ionic species, unique toxicity of particles at nano-scale was observed. Finally, microarray analysis revealed that nanoparticles lead to up-/down-regulation of the gene expression differently from ionic counterparts.

References

1. de Morais, M. G.; Martins, V. G.; Steffens, D.; Pranke, P.; da Costa, J. A., Biological Applications of Nanobiotechnology. *J. Nanosci. Nanotechnol.* **2014,** *14*, 1007-17.

2. Iavicoli, I.; Leso, V.; Ricciardi, W.; Hodson, L. L.; Hoover, M. D., Opportunities and Challenges of Nanotechnology in the Green Economy. *Environ. Health* **2014,** *13*, 78.

3. Chaudhary, S.; Mehta, S. K., Selenium Nanomaterials: Applications in Electronics, Catalysis and Sensors. *J. Nanosci. Nanotechnol.* **2014,** *14*, 1658-74.

4. Pelipenko, J.; Kocbek, P.; Kristl, J., Critical Attributes of Nanofibers: Preparation, Drug Loading, and Tissue Regeneration. *Int. J. Pharm.* **2015,** *484*, 57-74.

5. Hopley, E. L.; Salmasi, S.; Kalaskar, D. M.; Seifalian, A. M., Carbon Nanotubes Leading the Way Forward in New Generation 3D Tissue Engineering. *Biotechnol. Adv.* **2014,** *32*, 1000-14.

6. Lin, C. C.; Han, H. V.; Chen, H. C.; Chen, K. J.; Tsai, Y. L.; Lin, W. Y.; Kuo, H. C.; Yu, P., Highly Efficient Multiple-Layer CdS Quantum Dot Sensitized III-V Solar Cells. *J. Nanosci. Nanotechnol.* **2014,** *14*, 1051-63.

7. Mohana Reddy, A. L.; Gowda, S. R.; Shaijumon, M. M.; Ajayan, P. M., Hybrid Nanostructures for Energy Storage Applications. *Adv. Mater.* **2012,** *24*, 5045-64.

8. Cosnier, S.; Holzinger, M.; Le Goff, A., Recent Advances in Carbon Nanotube-Based Enzymatic Fuel Cells. *Front. Bioeng. Biotechnol.* **2014,** *2*, 45.

9. The Project on Emerging Nanotechnologies: http://www.nanotechproject.org (accessed April 18, 2015).

10. Smijs, T. G.; Pavel, S., Titanium Dioxide and Zinc Oxide Nanoparticles in Sunscreens: Focus on Their Safety and Effectiveness. *Nanotechnol. Sci. Appl.* **2011,** *4*, 95-112.

11. Morse, D. E., Silicon Biotechnology: Harnessing Biological Silica Production to Construct New Materials. *Trends Biotechnol.* **1999,** *17*, 230-232.

12. Rasmussen, J. W.; Martinez, E.; Louka, P.; Wingettt, D. G., Zinc Oxide Nanoparticles for Selective Destruction of Tumor Cells and Potential for Drug Delivery Applications. *Expert Opin. Drug Del.* **2010,** *7*, 1063-1077.

13. Wei, L.; Lu, J.; Xu, H.; Patel, A.; Chen, Z. S.; Chen, G., Silver Nanoparticles: Synthesis, Properties, and Therapeutic Applications. *Drug Discov. Today* **2014,** *19*.

14. Anyaogu, K. C.; Fedorov, A. V.; Neckers, D. C., Synthesis, Characterization, and Antifouling Potential of Functionalized Copper Nanoparticles. *Langmuir* **2008,** *24*, 4340-6.

15. Sotiriou, G. A.; Watson, C.; Murdaugh, K. M.; Darrah, T. H.; Pyrgiotakis, G.; Elder, A.; Brain, J. D.; Demokritou, P., Engineering Safer-By-Design, Transparent, Silica-Coated ZnO Nanorods with Reduced DNA Damage Potential. *Environ. Sci. Nano* **2014,** *1*, 144-153.

16. Godwin, H. A.; Chopra, K.; Bradley, K. A.; Cohen, Y.; Harthorn, B. H.; Hoek, E. M. V.; Holden, P.; Keller, A. A.; Lenihan, H. S.; Nisbet, R. M., et al., The University of California Center for the Environmental Implications of Nanotechnology. *Environ. Sci. Techol.* **2009,** *43*, 6453-6457.

17. Lin, S.; Zhao, Y.; Ji, Z.; Ear, J.; Chang, C. H.; Zhang, H.; Low-Kam, C.; Yamada, K.; Meng, H.; Wang, X., et al., Zebrafish High-Throughput Screening to Study the Impact of Dissolvable Metal Oxide Nanoparticles on the Hatching Enzyme, ZHE1. *Small* **2013,** *9*, 1776-85.

18. Zhang, H. Y.; Ji, Z. X.; Xia, T.; Meng, H.; Low-Kam, C.; Liu, R.; Pokhrel, S.; Lin, S. J.; Wang, X.; Liao, Y. P., et al., Use of Metal Oxide Nanoparticle Band Gap to Develop a Predictive

Paradigm for Oxidative Stress and Acute Pulmonary Inflammation. *ACS Nano* **2012,** *6*, 4349-4368.

19. Lin, S. J.; Taylor, A. A.; Ji, Z. X.; Chang, C. H.; Kinsinger, N. M.; Ueng, W.; Walker, S. L.; Nel, A. E., Understanding the Transformation, Speciation, and Hazard Potential of Copper Particles in a Model Septic Tank System Using Zebrafish to Monitor the Effluent. *ACS Nano* **2015,** *9*, 2038-2048.

20. Hong, J.; Rico, C. M.; Zhao, L.; Adeleye, A. S.; Keller, A. A.; Peralta-Videa, J. R.; Gardea-Torresdey, J. L., Toxic Effects of Copper-Based Nanoparticles or Compounds to Lettuce (Lactuca sativa) and Alfalfa (Medicago sativa). *Environ. Sci. Process Impacts* **2015,** *17*, 177-85.

21. Conway, J. R.; Adeleye, A. S.; Gardea-Torresdey, J.; Keller, A. A., Aggregation, Dissolution, and Transformation of Copper Nanoparticles in Natural Waters. *Environ. Sci. Technol.* **2015,** *49*, 2749-56.

22. Adeleye, A. S.; Conway, J. R.; Perez, T.; Rutten, P.; Keller, A. A., Influence of Extracellular Polymeric Substances on the Long-Term Fate, Dissolution, and Speciation of Copper-Based Nanoparticles. *Environ. Sci. Technol.* **2014,** *48*, 12561-8.

23. Marcus, I. M.; Wilder, H. A.; Quazi, S. J.; Walker, S. L., Linking Microbial Community Structure to Function in Representative Simulated Systems. *Appl. Environ. Microb.* **2013,** *79*, 2552-9.

24. Ivask, A.; Elbadawy, A.; Kaweeteerawat, C.; Boren, D.; Fischer, H.; Ji, Z.; Chang, C. H.; Liu, R.; Tolaymat, T.; Telesca, D., et al., Toxicity Mechanisms in *Escherichia coli* Vary for Silver Nanoparticles and Differ from Ionic Silver. *ACS Nano* **2014,** *8*, 374-86.

25. Fry, R. C.; Begley, T. J.; Samson, L. D., Genome-Wide Responses to DNA-Damaging Agents. *Annu. Rev. Microbiol.* **2005,** *59*, 357-77.

CHAPTER 2

Toxicity of Metal Oxide Nanoparticles in *Escherichia coli* Correlates with Conduction Band Energy and Hydration Energy (This chapter has been published previously in *Environmental Science and Techonology*, ***2015***, 49 (2): 1105-12)

ABSTRACT

Metal oxide (MOx) nanoparticles (NPs) are used for a host of applications such as electronics, cosmetics, construction and medicine and, as a result, the safety of these materials to humans and the environment is of considerable interest. A prior study of 24 MOx NPs in mammalian cells revealed that some of these materials show hazard potential. Here, we report the growth inhibitory effects of the same series of MOx NPs in the bacterium *Escherichia coli*, and show that toxicity trends observed in *E. coli* parallel those seen previously in mammalian cells. Of the 24 materials studied, only ZnO, CuO, CoO, Mn_2O_3, Co_3O_4, Ni_2O_3 and Cr_2O_3 were found to exert significant growth inhibitory effects; these effects were found to relate to membrane damage and oxidative stress responses in minimal trophic media. A correlation of the toxicological data with physico-chemical parameters of MOx NPs revealed that the probability of a MOx NP being toxic increases with increasing hydration energy and as the conduction band energy approaches those of biological molecules. These observations are consistent with prior results observed in mammalian cells, revealing that mechanisms of toxicity of MOx NPs are consistent across two very different taxa. These results suggest that studying nanotoxicity in *E. coli* may help to predict toxicity patterns in higher organisms.

INTRODUCTION

Metal oxide nanoparticles (MOx NPs) are among the most commonly used categories of nanomaterials and have been widely used in diverse commercial and industrial products ranging from medicine, to electronics, to alternative energy. For example, ZnO and TiO_2 NPs have been used extensively in sunscreens due to their excellent ability to reflect sunlight.[1] SiO_2 NPs have been utilized in products such as batteries, paints, and adhesives.[2] Functionalized ZnO NPs have been developed as selective killers of proliferating cells[3] and as antimicrobial drugs.[4] Because MOx NPs are used in such a broad range of applications, many types of organisms could potentially be exposed to them. As a result, we are particularly interested in studies that help to elucidate which properties of MOx NPs result in toxicity in organisms from different taxa. Armed with this information, a manufacturer could ideally design a NP with desired materials properties that, at the same time, does not show inadvertent toxicity to organisms that are likely to be exposed to products containing these NPs.

Several prior studies have shown that MOx NPs adversely affect biological systems in various model organisms. For example, ZnO NPs have been shown to interfere with embryo-hatching in zebra-fish[5] and cause an inflammatory response in mice.[6] Studies of the microbial impact of MOx NPs also indicate that the materials (such as ZnO and TiO_2) reduce biomass, metabolic activities and biodiversity of soil bacteria.[7,8] The ability of MOx to generate reactive oxygen species (ROS) that leads to cellular oxidative stress is often thought to be a primary mechanistic pathways of MOx NP toxicity.[9,10] Consistent with this, elevated intracellular ROS and oxidative damage has previously been observed in human and bacterial cells treated with MOx NPs.[11,12] Moreover, disruption of bacterial cell membrane integrity and loss of energy generation potential were found to be important mechanisms of toxicity for TiO_2, CeO_2 and

ZnO.[13] In mammalian cells, the toxicity of 24 different MOx NPs was shown to be associated with the accumulation of ROS, membrane leakage, perturbed intracellular calcium flux and mitochondrial membrane depolarization.[14]

Studies of physicochemical properties of NPs that affect cellular toxicity are particularly important as this information can be generalized to better predict the toxicity of novel NPs and help to guide manufacturers to design safer NPs. In addition, an understanding of how physicochemical properties impact toxicity of NPs can help regulators assign new materials into likely hazard categories. Recently, some of us demonstrated that conduction band energy and metal dissolution are the best predictors of toxicity for 24 MOx NPs in mammalian cells.[14] This includes a demonstration that the overlap of conduction band energy with biological redox potential of the cell (-4.2 to -4.8 eV) was predictive of toxicity. We hypothesized that this overlap allows for the transfer of electrons between biomolecules and the NPs, which creates free radicals and contributes to oxidative stress. Of 24 MOx NPs studied, all those that had a conduction band energy that overlaps with the biological redox potential (Ni_2O_3, CoO, Cr_2O_3, Co_3O_4 and Mn_2O_3), with the exception of TiO_2, were found to be toxic in mammalian cells. One possible explanation for the lack of toxicity in TiO_2 is that conduction band energy of TiO_2 is extremely close to the upper edge of cellular redox potential, which may not provide enough of a driving force for electron transfer.[14] The other parameter that was shown to correlate strongly with MOx toxicity was metal ion dissolution: particles with a high rate of dissolution (ZnO and CuO) were also found to be highly toxic.[14-16] However, the question still remained whether these physicochemical properties were also the best predictors of toxicity in other organisms, particularly ones from very different taxa.

To test whether the same trends were observed in a completely different organism, we used growth inhibition test to study toxicity of 24 MOx NPs (Al_2O_3, CeO_2, Co_3O_4, CoO, Cr_2O_3, CuO, Fe_2O_3, Fe_3O_4, Gd_2O_3, HfO_2, In_2O_3, La_2O_3, Mn_2O_3, Ni_2O_3, NiO, Sb_2O_3, SiO_2, SnO_2, TiO_2, WO_3, Y_2O_3, Yb_2O_3, ZnO and ZrO_2) in the bacterium *E. coli*. In addition to growth inhibition assays that indicate general toxicity of NPs, a suite of fluorometric assays (including assays for membrane damage, biotic/abiotic ROS generation) was used to study the detailed mechanisms of toxicity of these MOx NPs. We found that particles that were previously identified to be toxic in mammalian cells (ZnO, CuO, CoO, Mn_2O_3, Co_3O_4, Ni_2O_3 and Cr_2O_3)[14,17] also exhibit adverse effects on growth, excite membrane damage, and induce ROS production in bacterial cells. We also found that conduction band and hydration energy can predict the potential for adverse biological effects in *E. coli* (a prokaryotic) system in the same way as for mammalian (eukaryotic) systems. This study sheds light into the use bacterial cells for rapid screening of general toxicity and hazardous ranking of NPs. The suite of sub-lethal assays could also be applied in the future to other bacteria that perform critical roles in the ecosystems to thoroughly understand the environmental impact of NPs.

MATERIALS AND METHODS

1.1 **Materials and instrumentation**

The bacterium used for this study was *Escherichia coli* strain ATCC 25922, a standard strain widely used for antimicrobial disk susceptibility tests.[13] Reagent grade water used in all experimental procedures was prepared using a Milli-Q water purification system (Millipore, Bedford, MA). Bacterial growth media (LB Lennox) was obtained from EMD Chemicals (Merck, Darmstadt, Germany). The pH of the final media was adjusted to 7. All toxicological

assays were conducted on cultures grown in an environmentally-relevant media: Modified Minimal Davis, MMD media (1 L H_2O containing 0.7 g K_2HPO_4; 0.2 g KH_2PO_4; 0.66 g $(NH_4)_2SO_4$; 0.5 g sodium citrate; 0.1 g $MgSO_4 \bullet 7H_2O$; 3.31g D-glucose, pH 6.9). Humic acid (HA) was obtained from Sigma-Aldrich (CA, USA). A 0.5 mg/mL HA stock solution was prepared immediately prior to use. The final concentration of HA used in the test solutions was 0.01 mg/mL. Phosphate buffered saline (PBS, KH_2PO_4 1.5 mM, NaCl 155.2 mM and $Na_2HPO_4 \bullet 7H_2O$, pH 7.4) was obtained as a solution from GIBCO (Invitrogen, CA, USA). Centrifugation was conducted in an Eppendorf 5424 centrifuge.

1.2. Preparation and characterization of nanomaterials

Metal oxide nanoparticles were synthesized or purchased from commercially-available sources, as described in **Table 2.1**. A flame spray pyrolysis (FSP) reactor was used to perform the in-house synthesis of CuO, Co_3O_4, Fe_3O_4, Sb_2O_3, TiO_2, WO_3 and ZnO as described previously.[14] Stock solutions of 20 mg/mL of each of the 24 MOx NPs were prepared in Milli-Q water followed by 15 minute sonication in a water-bath sonicator (40 kHz, Brandson 2510, Emerson Industrial Automation, MO) and were then stored at 4ºC. MMD media supplemented with 0.01% HA was used to dilute the particles to working concentrations. Humic acid (HA) was added to MMD media as a dispersing agent and was chosen because of its relevance for environmental systems. The concentration of 0.01 % added HA was selected because lower concentrations of HA did not prevent aggregation of representative MOx NPs. (**See Table A1.1** in the **Appendix 1**) The hydrodynamic size of the MOx NPs (for NP concentrations of 100 mg/L) in MMD media supplemented with 0.01% HA was measured by dynamic light scattering (DLS, ZetaPALS, Brookhaven Instruments Corporation inc., NY). To quantify metal ion

dissolution, 1 mg/mL of NPs was dispersed in MMD supplemented with 0.01% humic acid and kept at 37 ºC for 24 hours. This solution was then centrifuged at 21,130 RCF for 30 min to separate the particles from dissolved metal ions. The resulting dissolved ion concentrations (in the liquid fraction) for Al_2O_3, CeO_2, Gd_2O_3, HfO_2, In_2O_3, La_2O_3, Sb_2O_3, SiO_2, SnO_2, TiO_2, WO_3, Y_2O_3, Yb_2O_3 and ZrO_2 were then measured by Inductively Coupled Plasma Mass Spectrometry (ICP-MS, Perkin-Elmer SCIEX Elan DRCII). Atomic Absorption Spectrophotometry (AAS, AAnalyst 700, Perkin-Elmer) was used to measure the concentration of dissolved ions in the liquid fraction for the remainder of the particles (Co_3O_4, CoO, Cr_2O_3, CuO, Fe_2O_3, Fe_3O_4, Mn_2O_3, Ni_2O_3, NiO and ZnO). To determine the total amount of metal ion present in each sample (prior to centrifugation), a solution containing 100 mg/L of NPs was treated with 5 mL of pure HNO_3 and evaporated to completion at 95 ºC. The sample was then dissolved in 3 mL of 5% HNO_3 and analyzed by mass spectrometry (ICP-MS).

1.3 Growth inhibition studies and calculation of IC_{50} values

To assess the half-maximal inhibitory concentration (IC_{50}) for each NP, growth inhibition curves were constructed. 50 µL of a step-wise concentration gradient (0, 7.8, 15.6, 31.2, 62.5, 125, 250 and 500 mg/L) of MOx NPs was prepared in MMD supplemented with 0.01% humic acid, and placed in a 384-well transparent microplate (Greiner bio one, catalog #781186). A log-phase culture of *E. coli* (OD_{600} between 0.5-0.7) was then inoculated into each well using a disposable plastic pinhead (Genetix). The microplates were incubated at 37 ^{0}C in the dark and optical density at 600 nm (OD_{600}) was measured every 30 min for 24 hours using a Synergy plate reader (BioTek, VT). A growth inhibition curve was constructed by plotting the OD_{600} at 24 hours post exposure as a function of concentration for each of the NPs. At least 9 replicates were

performed for each concentration to obtain accurate IC_{50} values for each NP. The resulting curves for all 24 MOx NPs were fitted using a log-logistic model, $c+(d-c)/(1+\exp(b(\log(x)-\log(e))))$, with the **drc** package in the statistical software program R.[18] This model fixes constraints on the shape of the curve while allowing for flexibility to account for different shaped curves. The equations and parameters used to calculate the IC_{50} are shown in **Figure A1.1** (in **Appendix 1**). The area under the growth inhibition curve was used as an additional measure of global toxicity. The area was computed with the "grofit" package of the R software, which approximates the area under a smoothed curve.

1.4 Sub-lethal assays

To study cellular ROS generation, H_2DCFDA (2',7'-dichlorodihydrofluorescein diacetate, Molecular Probes, D399) was dissolved in ethanol to a concentration of 1.5 mg/mL. A fresh stock was prepared immediately prior to use each time this assay was performed. In the assay, H_2DCFDA crosses the cell membrane and is hydrolyzed by intracellular esterases to nonfluorescent dichlorofluorescin (DCFH). DCFH is then converted to the highly fluorescent 2′,7′--dichlorofluorescein (DCF) in the presence of intracellular reactive oxygen species.[19] H_2DCFDA was added to cells that had been treated with NPs in the dark for 24 hours at final concentration of 15 ng/mL. After 30 minutes of incubation, 100 μL of the mixture was aliquoted into 96 well-plates (Costar, catalog #3915) and the fluorescence was measured using a microplate reader (excitation/emission at 485/530 nm) (SpectraMax MS, Molecular Devices, CA). In this assay, a 1% solution of H_2O_2 was used as positive control. To measure the ability of the MOx NPs to generate *abiotic* ROS, the acetate group of H_2DCFDA was cleaved by 0.1 M NaOH at room temperature for 30 minutes.[20] The dye was diluted with MMD media to a

concentration of 300 ng/mL and then added to each sample in the 96 well-plate (Costar, catalog #3915), to yield a final dye concentration of 30 ng/mL.

To study whether MOx NPs can damage bacterial cell membranes, a live/dead BacLight Bacteria Viability kit (L7012, Molecular Probes) was utilized. PI and SYTO 9 were mixed according to the manufacturer's instructions;[21] 0.15 μL of 3.34 mM SYTO 9 dye and 0.15 μL of 20 mM Propidium iodide were added to 100 μL of a cell culture that had been treated with NPs in the dark for 24 hours in a 96 well plate (Costar, catalog #3915). The fluorescence signal was measured by a microplate reader (SpectraMax MS, Molecular Devices, CA) with excitation at 485; emission was monitored at 530 and 630 nm.

RESULTS AND DISCUSSION

A prior study in mammalian cells by UC CEIN researchers demonstrated that conduction band energy and metal ion dissolution correlate with toxicity of MOx NPs.[14] We wished to determine whether these trends hold true for other organisms as well, and as a result investigated the impacts of the same series of 24 MOx NPs in *E. coli*.

Acquisition and physiochemical characteristics of 24 metal oxide nanoparticles

17 out of 24 MOx NPs were purchased from commercial sources as shown in **Table 2.1**. The other seven particles (Co_3O_4, CuO, Fe_3O_4, Sb_2O_3, TiO_2,WO_3, ZnO) were synthesized in-house by flame spray pyrolysis, which allows accurate control over particle size. Primary size of the particles which determined by TEM analysis was reported previously[14] (**Table 2.1**). The hydrodynamic diameter of all of the particles tested in Milli-Q water was between ~110 - 310 nm, while the hydrodynamic diameter of the particles in bacterial (MMD) media with 0.01%

humic acid (HA) was in the range of 105 – 470 nm. These results agree with the previous finding that the hydrodynamic diameters of these MOx NPs in cell culture media tend to be larger than their size in pure water, most likely because of the increased ionic strength in test media compare to water.[22] Humic acid was added to the MMD media to prevent aggregation. Indeed, even though 0.01% HA was added as dispersing agent, the hydrodynamic size of 20 of the 24 MOx particles was only slightly higher in MMD media than in water (**Table 2.1**). Only Yb_2O_3 and WO_3 retained their hydrodynamic diameter when transferred from water to HA-supplemented MMD media and the hydrodynamic diameter of TiO_2 and HfO_2 decreased in HA-supplemented MMD media compared to that seen in deionized water (**Table 2.1**).

Growth inhibition effect of 24 metal oxide nanoparticles

The dose-dependent bacteriostatic properties of each of the 24 metal oxide nanoparticles were determined by constructing growth inhibition curves (**Figure 2.1**; **Figure A1.2** in **Appendix 1** provides individual growth curves for each of the NPs with error bars). In this experiment, a log-phase culture of *E. coli* was inoculated into a step-wise concentration gradient of 24 MOx NPs, ranging from 7.8 to 500 mg/L. Cell density was monitored for 24 hours. A dose-dependent decline in growth (as measured by OD_{600} at 24 hours) in *E. coli* was observed for seven (Co_3O_4, CoO, Cr_2O_3, CuO, Mn_2O_3, Ni_2O_3 and ZnO) of the 24 NPs with the rest of the materials showing no significant perturbation of growth. The IC_{50} values were determined to be 33, 39, 43, 70, 138, 181 and 232 mg/L for ZnO, CuO, CoO, Mn_2O_3, Co_3O_4, Ni_2O_3 and Cr_2O_3, respectively, while the rest of the particles exhibited IC_{50} values that were ≥ 500 mg/L (**Table 2.1**). IC_{50} values > 500 mg/L could not be determined because at high NP concentrations, the suspensions became too opaque and the NPs no longer remained stably suspended. Because

aggregation of the NPs interfered with our assay results, 0.01% humic acid was added to the MMD media in which the 24 MOx NPs were dispersed. We also determined the area under the dose-response curve to provide a continuous measure of toxicity, which was needed for the modeling portion of the study (see below). The seven materials that resulted in bacterial growth inhibition exhibited smaller values for area under the curve compared to the rest of the particles (**Figure A1.3** in **Appendix 1**).

Results from sub-lethal assays

To determine mechanism(s) of toxicity of the MOx NPs, we screened all of the 24 particles using a suite of sub-lethal assays for membrane damage, *biotic* ROS generation and *abiotic* ROS generation.

Membrane damage

To study the effects of the MOx NPs on the cell membrane of *E. coli*, we used a PI/SYTO dye combination assay. While green fluorescent SYTO reagent stains the DNA of all cells, PI only permeates the membrane of damaged or dying cells, leading to red staining. Thus, a low green to red ratio indicates a high fraction of dead cells or cells with compromised membranes. The seven materials that led to reduced bacterial growth (Co_3O_4, CoO, Cr_2O_3, CuO, Mn_2O_3, Ni_2O_3 and ZnO, **Figure 2.1**) also exhibited a significantly lower green/red fluorescence ratio than any of the non-toxic materials, as shown in **Figure 2.2**, suggesting that these particles may induce membrane leakage that eventually leads to cell death in *E. coli.* The same approach was used previously to assess membrane integrity in *E. coli* exposed to TiO_2, CeO_2 and ZnO by Horst *et al.*[13] The results reported herein are also consistent with previous findings in mammalian

cells, which indicated that the same seven particles reduced growth and caused membrane damage in human bronchial epithelial (BEAS-2B) and murine myeloid cells (RAW 264.7).[14]

Elevated ROS was observed only in cells treated with toxic particles

Intracellular generation of ROS has previously been implicated as a primary mediator of NP toxicity in various organisms.[10-14,23,24] To see whether ROS damage plays an important role in the toxicity of MOx NPs in *E. coli*, we measured the amount of intracellular ROS using H_2DCFDA, which fluoresces in response to ROS inside cells.[13] An elevated amount of intracellular ROS was observed in all of the toxic particles (Co_3O_4, CoO, Cr_2O_3, CuO, Mn_2O_3, Ni_2O_3 and ZnO) with Mn_2O_3 generating the strongest effect (**Figure 2.2)**. The correlation coefficient between biotic ROS generation and IC_{50} was determined to be -0.84 (**Table A1.2** in **Appendix 1**) suggesting that ROS plays an important role in NP toxicity. This finding is consistent with results previously reported by Premanathan *et al*., who showed that ROS-induced apoptosis is the principal mechanism of toxicity for ZnO nanoparticles in bacterial and human cells.[25] Likewise, Wang *et al*. previously reported that cellular injury and DNA damage in human cells after treated with CuO NPs was primarily mediated by ROS generation.[26]

Abiotic ROS generation property of metal oxide nanoparticles

Elevated ROS levels inside cells can result from two distinct pathways. In the first possible pathway, MOx NPs directly donate or receive electrons to or from bio-molecules and hence generate "abiotic ROS". In the second possible pathway, NPs cause toxicity due to one or more other mechanisms, which subsequently results in cellular stress and generation of biotic ROS. Examples of pathways that indirectly result in generation of biotic ROS include, but are not

limited to, disruption of cellular homeostasis,[27] elevation of DNA lesions,[28] membrane damage or loss of membrane potential.[29] Accumulation of ROS is often a hallmark of cells undergoing apoptosis or necrosis.[30,31] To further differentiate between direct and indirect mechanisms of ROS production by MOx NPs in bacteria, the ability of MOx NPs to produce ROS was measured under abiotic conditions.

H_2DCFDA cannot be used directly to measure abiotic ROS because the ester group on this molecule must be cleaved (to yield DCFH) before DCFH can react with ROS and produce fluorescence. In cells, the ester group is cleaved by non-specific esterases produced by the bacterium. To cleave H_2DCFDA in situ in the absence of cells, H_2DCFDA was treated with NaOH (Materials and methods and **Figure A1.4** in **Appendix 1**). The resulting solution was then added to gradient concentrations of MOx NPs ranging from 7.8 to 500 mg/L. A dose-dependent increase in fluorescent signal due to oxidation of the dye was observed for Co_3O_4, Mn_2O_3, CuO, Ni_2O_3 and CoO (**Figure 2.2**). Interestingly, neither ZnO nor Cr_2O_3 – both of which exhibit very low IC_{50} values (33 and 232 mg/L respectively, reflecting their high toxicity) produce ROS under abiotic conditions. These data demonstrate that the cellular toxicity and oxidative stress observed in *E. coli* treated with MOx NPs must result from either the direct transfer of electrons to/from NPs and the cells and/*or* from the downstream effects of other mechanisms of toxicity.

Several mechanisms that might be responsible for the toxicity of ZnO and Cr_2O_3 NPs have been proposed. Recently, ZnO nanoparticles were shown to be internalized into cells and to cause DNA damage in human nasal mucosa and epidermal cells by Hackenberg *et al.*[30] and Sharma *et al.*[32] Moreover, studies in *E. coli* have been reported in which ZnO NPs were shown to cause membrane disorganization, which leads to downstream intracellular (biotic) ROS generation and lethality.[33] For Cr_2O_3, prior studies have revealed that toxicity might be the result

of the particles increasing caspase-3 activity, which leads to apoptosis in human cell lines.[34] Based on a prior report of flow cytometry studies on *E. coli*, toxicity in this organism likely resulted from internalization of Cr_2O_3.[35] Taken together, these data suggest that other toxic pathways in addition to direct generation of ROS lead to cellular oxidative stress and cell death when *E. coli* is exposed to ZnO and Cr_2O_3. Conversely, the other MOx NPs that showed significant toxicity (Co_3O_4, CoO, CuO, Mn_2O_3 and Ni_2O_3) all resulted in significant abiotic ROS generation and hence their toxicity is likely due at least in part to the MOx NP serving directly as electron donors or acceptors.

Correlation between growth inhibition, membrane damage and reactive oxygen species generation

To determine whether the results from the growth assay (IC_{50}) and sub-lethal assays (membrane damage, biotic ROS generation and abiotic ROS generation) are correlated with each other, the correlation coefficient was calculated for data between all of the assays (**Table A1.2** in **Appendix 1**). Strong correlations between IC_{50} values and the results from each of the three of the sub-lethal assays were observed (correlation coefficient = -0.84, -0.79 and 0.82 for biotic ROS generation, abiotic ROS generation and membrane damage respectively). In addition, a moderate correlation was observed for the results of each assay in the suite of sub-lethal assays with each other (the absolute values of the correlation coefficients were all between 0.66 – 0.76; see **Table A1.2**). The results suggest that oxidative stress and perturbation of membrane integrity are important pathways of toxicity for MOx NPs in *E. coli* and that oxidative stress and membrane damage are correlated.

Demonstration of conduction band energy and hydration energy as main parameters to predict structure activity relationship in 24 MOx NPs

Previously, Nel and coworkers demonstrated that MOx NPs that have conduction band energy levels (Ec) between -4.2 to -4.8 eV (which overlaps with the redox potentials of biological molecules) could participate in electron transfer to/from biomolecules, resulting in oxidative stress that leads to lethality.[14] In addition, they demonstrated that the extent of metal ion dissolution was an important predictor of toxicity in mammalian cells. We wished to test whether the same trend held true for toxicity in *E. coli*. The method we used to explore correlation between fundamental physico-chemical properties of MOx NP and their toxicity in *E. coli* is nano-SARs. However, because dissolution is not a fundamental physico-chemical property (but rather is an observable experimental parameter), we chose to investigate whether the toxicity outcome in *E. coli* correlated with energy at the conduction band and hydration energy (ΔH_{hyd}). The hydration energy is the energy released upon attachment of water molecules to ions or the measurement of the affinity of water molecule to ions and is an intrinsic characteristic of NPs that directly reflect the rate of dissolution. Lower H_{hyd} was proposed to correlate with greater transportation across membrane and thus, higher toxicity.[36] A subset of us previously demonstrated that Structure Activity Relationship (SAR) using hydration energy and energy at conduction band predicted toxicity of MOx NPs in mammalian cells.[37] The results from this prior study suggested that the probability of MOx being toxic increases when the energy at conduction band of the particle falls into the range of redox potentials of biological molecules together with having lower level hydration energy. We arrived at the same toxicity class definition (toxic versus nontoxic) for this set of MOx NPs in bacteria as was observed and published in mammalian cells. Based on this class definition, a range of nano-SARs were

developed for the this set of MOx NPs.[37] From an initial pool of thirty physicochemical descriptors (including fundamental MOx properties, energies/enthalpy, NP size distribution, surface charge and energy structures), conduction band and hydration energies (estimated via Latimer's equation, $\Delta H_{hyd} = -631.184Z^2/(r+50)$ eV where Z is the charge on the cation, r is the cationic radius) were identified as being strongly correlated with the toxicity of MOx NPs. The Support Vector Machine (SVM), based nano-SAR development using the two energies, arrived at a classification accuracy as high as 91.5%. The classification boundary of toxic particles in the nano-SAR (**Figure 2.3**) encompasses the range of $E_C \sim$ [-5.47, -3.71] eV and $\Delta H_{hyd} > -70$ eV, which is consistent with previously suggested toxicity mechanisms for MOx NPs and metal ions[36,38]. In previous work, it had been postulated that a conduction band energy (E_C) within [-4.84, -4.12] eV (the estimated range of standard redox potential couples in biological media) is suggestive of the potential for electron transfer to occur between cellular redox couples and NP surfaces. Because humic acid (HA) could potentially facilitate the extracellular electron transfer (EET)[39] between electrons at conduction band and the bacterial cells and hence impact our results, we used the lowest concentration of HA that still resulted in well-dispersed suspensions of the NPs. (See **Table A1.1** in **Appendix 1**) Also, the observation that the probability of MOx NPs being classified as toxic increases with lower hydration energy is consistent with prior studies on metal ion toxicity, which demonstrated increased transportation of metal ion across cell membranes for metal ions of lower hydration energy (those considered to be "permeators").[36] It is notable that we also constructed nano-SAR using redox potential and hydration energy as descriptors. However, the accuracy of this model was reduced to 74%, suggesting that the parameters that are most likely to correlate with toxicity of MOx NPs are conduction band and hydration energies. This predictive paradigm underscored the assertion that

toxicity of nanoparticles to biological systems (mammalian cells or bacterial cells) most likely depends on intrinsic properties of the particles. In addition, these results suggest that for MOx NPs, toxicological mechanisms are likely to disrupt fundamental functions that are conserved throughout evolutionary lineages (*e.g.*, causing oxidative stress or destroying cell membrane). Moreover, since this study arrived at the same toxic classification as mammalian cells, we can confidently use conduction band energy and hydration energy as parameters to predict toxic outcomes of living organisms exposed to MOx NPs. This will enable engineer to design safer products and help regulator in prioritizing the particles that are "likely to be toxic" for further study.

Many studies have indicated that metal ion dissolution from nanoparticles plays an important role in inducing toxicity.[6,40,41] To determine whether this also holds true for MOx NPs in *E. coli*, the extent of dissolution of the 24 MOx NPs was measured by Atomic Absorption Spectroscopy (AAS) analysis and/or inductive coupled plasma mass spectrometry (ICP-MS) (**Materials and Methods**). Most of the particles dissolved less than 1.63% during the first 24 hours (which corresponds to the time course of the longest assay, which was for growth inhibition). The only exceptions were CuO and ZnO, which dissolved by 7.89% and 5.27% respectively in 24 hours (**Figure A1.5** in **Appendix 1** and **Table 2.1**). This result is consistent with previous findings in mammalian media that CuO and ZnO exhibit the highest amount of metal ion dissolution of all of the 24 metal particles tested.

In conclusion, this study demonstrates that out of 24 MOx NPs studied, only seven (ZnO, CuO, CoO, Mn_2O_3, Co_3O_4, Ni_2O_3 and Cr_2O_3) exert toxicity in *E. coli* bacterium. Based on the results reported herein, we conclude that the most likely mechanisms of toxicity include ROS generation and membrane damage. Our results parallel those previously reported for the toxicity

of the same 24 MOx NPs in mammalian cells. These results showing that mechanisms of toxicity of MOx NPs are the same for two cells types from very different taxa suggest that studying nanotoxicity in *E. coli* may help to predict toxicological outcomes in higher organisms. The micro-titer plate based assays described herein represent a reliable, rapid method for analyzing the toxicity of large numbers of different NPs under a variety of different conditions, and have the potential to bridge the gap between the rate of synthesis of novel NPs and the rate of toxicological analysis. The toxicity paradigms developed in this study could be applied to other bacteria that play crucial roles in the ecosystems in order to fully understand the environmental impacts of nanoparticles.

Supporting information of **Chapter 2** is found in **Appendix 1** which contains the calculation of IC_{50} from growth-inhibition curves (**Figure A1.1**); Individual growth inhibition curve including error bars for each of the 24 MOx NPs (**Figure A1.2**); Area under growth-inhibition curve for 24 metal oxide nanoparticles in *E. coli* (**Figure A1.3**); DCFH can be used to measured abitic ROS generation (**Figure A1.4**); Metal ion dissolution(**Figure A1.5**); Quantitative effects of humic acid on aggregation of nanoparticles (**Table A1.1**) and correlations between results obtained from diffferent assays performed on MOx NPs (**Table A1.2**).

(A) (B)

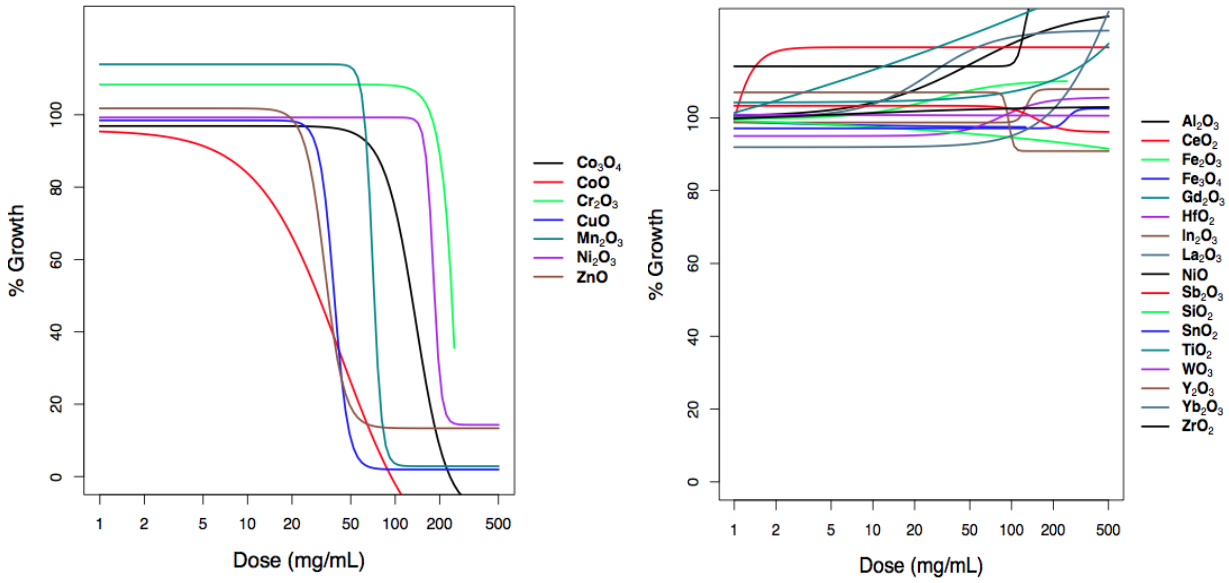

Figure 2.1. Inhibition of *E.coli* growth by 24 MOx NPs. Log-phase *E. coli* cultures were treated with different concentrations of MOx NPs ranging from 0 – 500 mg/L in 384 well plates in the presence of MMD media supplemented with 0.01% humic acid. The OD_{600} at 24 hours was used to calculate the percent growth inhibition compared to the untreated (control) culture. Dose-dependent growth inhibition was observed in seven out of the 24 particles tested (Co_3O_4, CoO, Cr_2O_3, CuO, Mn_2O_3, Ni_2O_3 and ZnO), suggesting that these particles are toxic to *E. coli*. Curves shown are the fit to the average of at least nine independent measurements. (A) Growth inhibition curves for toxic NPs (B) Growth inhibition curves for non-toxic NPs. Individual growth curves for each metal oxide species that include errors bars are provided in **Figure A1.2** in **Appendix 1**.

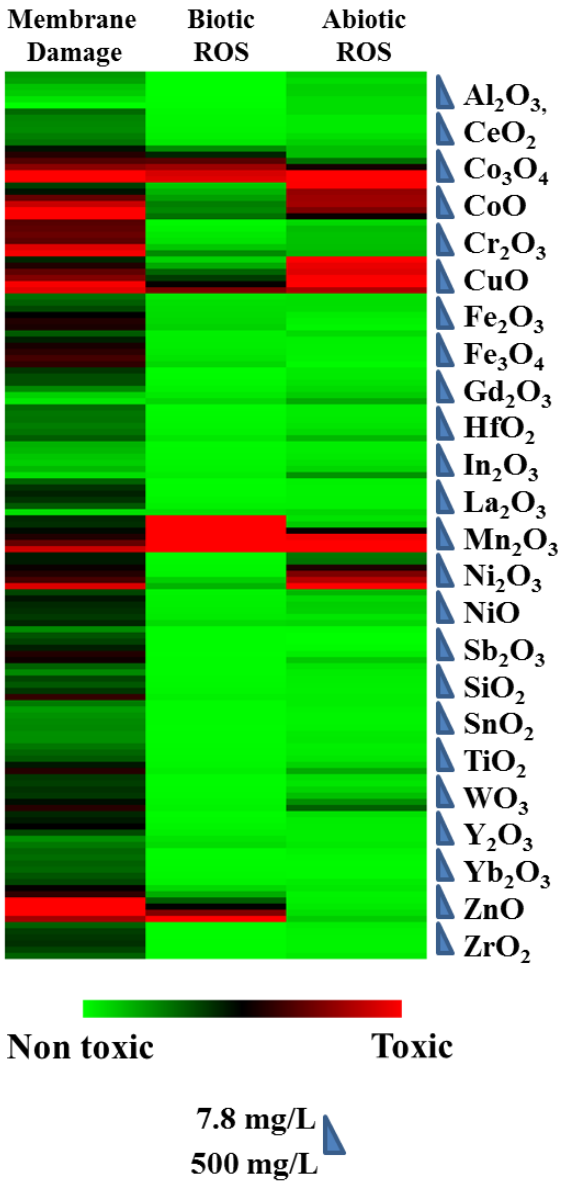

Figure 2.2. Heat map to summarize toxic effects of 24 MOx NPs. Fluorescence-based assays including membrane damage (PI/SYTO), biotic ROS generation (H_2DCFDA) and abiotic ROS generation (DCFH) were developed to study possible mechanistic pathways of toxicity of MOx NPs. Cells treated with a step-wise gradient concentration of NPs (7.8 – 500 mg/L) were mixed with a fluorescence dye (PI/SYTO, H_2DCFDA, DCFH for membrane damage, biotic ROS and abiotic ROS respectively). At least three replicates were performed for each concentration in

each of the assays. The toxicological outcomes were calculated from the fluorescence ratio observed for each NP compared to that observed for the negative control with buffer only. Positive controls used in this study were ethanol for membrane damage and H_2O_2 for biotic/abiotic ROS generation. A red color indicates that the result is more similar to the positive control, while a green color indicates that the result is more similar to the negative control. All seven of the toxic particles resulted in a high degree of membrane damage and accumulation of cellular ROS. However, only five out of seven particles were shown to be strong oxidizing agents under abiotic conditions.

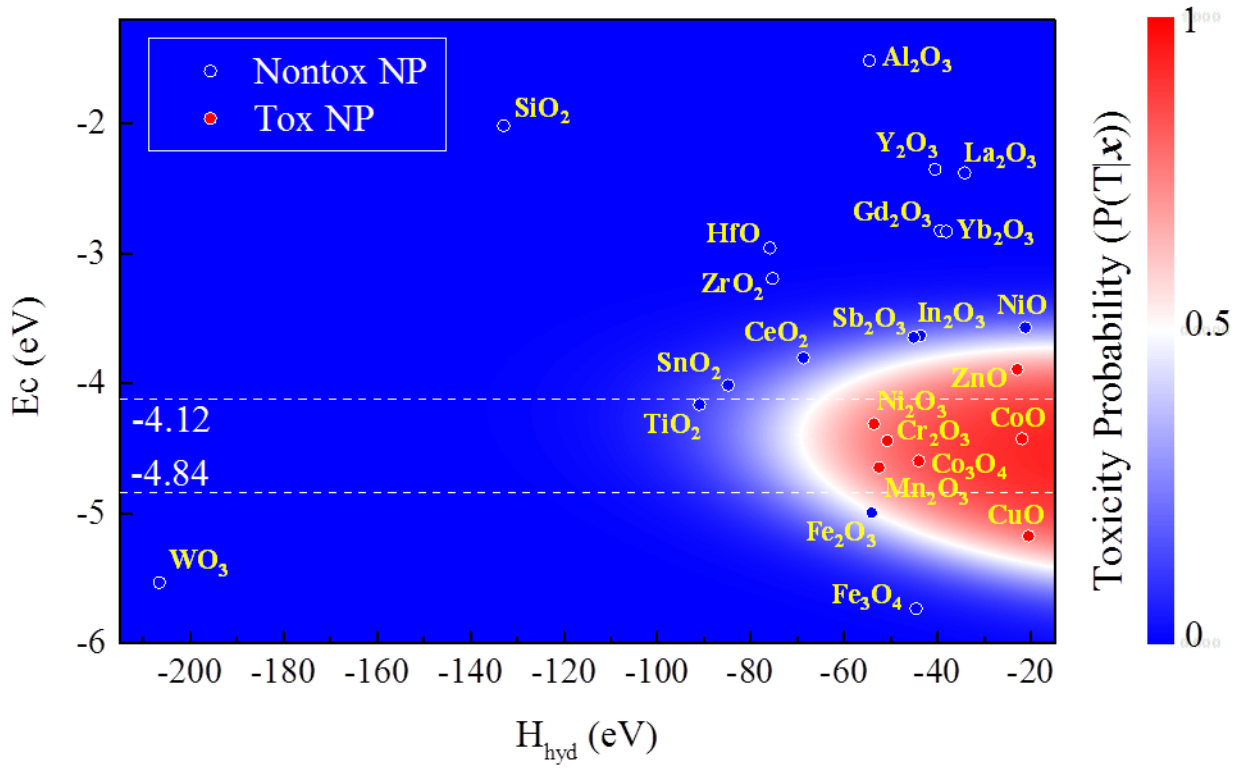

Figure 2.3. Use of band gap energy and hydration energy as parameters to predict toxicological outcomes of 24 MOx NPs. The probability of toxicity of each NP (*x*) was calculated using a support vector machine (SVM)-based nano-structure activity relationship (SAR) with the conduction band energy (E_C) and hydration enthalpy (ΔH_{hyd}). The nano-SAR arrived at a classification accuracy of 91.5%, with the posterior toxicity probability P(T|***x***) (i.e., the probability that NP ***x*** belongs to toxic class) is depicted via the color map in the descriptor space (where blue = 0 and red = 1). The contour for P(T|***x***) = 0.5 is outlined, which defines the nano-SAR classification boundary. NP bounded by this boundary is classified as toxic and those outside are classified as non-toxic. The nano-SAR classification boundary encompasses the range of Ec ~ [-5.47, -3.71] eV and ΔH_{hyd} < -70 eV.

Table 2.1. Source information, primary and hydrodynamic size, metal ion dissolution and IC_{50} of MOx NPs

Metal oxide nanoparticle	source	catalog number	diameter (nm)			metal ion dissolution (%)	IC_{50} (mg/L)
			primary[#]	water	MMD+ 0.01% HA		
Al_2O_3	Meliorium Technologies	Al_2O_3 NPs, 10 nm	14.7 ± 5.2	282.9 ± 3.7	317.5 ± 4.9	0.8 ± 0.10**	>500
CeO_2	Meliorium Technologies	CeO_2 NPs, 8 nm	18.3 ± 6.8	197.6 ± 7.0	317 ± 6 3.6	0.0 ± 0.0**	>500
Co_3O_4	In house synthesis	-	10.0 ± 2.4	174.5 ± 4.1	374.5 ± 17.7	0.05 ± 0.02*	138 (130-146)
CoO	SkySpring Nanomaterials	2310SC	71.8 ± 16.2	184.8 ± 11.4	228.5 ± 3.5	0.48 ± 0.04*	43 (25 - 72)
Cr_2O_3	US Research Nanomaterials, Inc.	US3060	193.0 ± 90.0	256.4 ± 5 .4	460 ± 62.2	0.09 ± 0.01*	232 (218 - 247)
CuO	In house synthesis	-	12.8 ± 3.4	263.3 ± 4.5	392.5 ± 60.1	7.9 ± 0.6*	39 (36 - 41)
Fe_2O_3	US Research Nanomaterials, Inc.	US3200	12.3 ± 2.9	144.7 ± 2.7	233.5 ± 3.5	0.1 ± 0.0*	>500
Fe_3O_4	In house synthesis	-	12.0 ± 3.2	198.4 ± 4.1	232.5 ±3 7.47	0.04 ± 0.0*	>500
Gd_2O_3	Nanostructured & Amorphous Materials, Inc.	2681RE	43.8 ± 15.8	195.7 ± 4.3	244.5 ± 7.8	0.01 ± 0.0**	>500
HfO_2	US Research Nanomaterials, Inc.	US3245	28.4 ± 7.3	291.8 ± 11.2	247.5 ± 2.1	0.02 ± 0.0**	>500
In_2O_3	US Research Nanomaterials, Inc.	US3250	59.6 ± 19.0	192.2 ± 2.1	232.5 ± 0.7	0.06 ± 0.00**	>500
La_2O_3	Nanostructured & Amorphous Materials, Inc.	2920RE	24.6 ± 5.3	211.0 ± 10.5	240.5 ± 0.7	0.00 ± 0.00**	>500
Mn_2O_3	Nanostructured & Amorphous Materials, Inc.	3610FY	51.5 ± 7.3	286.8 ± 2.8	412 ± 14.2	0.03 ± 0.01*	70 (62 - 79)
Ni_2O_3	SkySpring Nanomaterials	5420SC	140.6 ± 52.5	311.4 ± 7.1	351.5 ± 7.8	0.60 ± 0.2*	181 (176 - 186)

Metal oxide nanoparticles	source	catalog number	diameter (nm)			metal ion dissolution (%)	IC_{50} (mg/L)
			primary[#]	water	MMD + 0.01% HA		
NiO	Sigma-Aldrich	637130	13.1 ± 5.9	228.0 ± 5.7	472 ± 47.1	0.3 ± 0.01*	>500
Sb_2O_3	In house synthesis	-	11.8 ± 3.3	147.6 ± 1.8	205.5 ± 0.7	1.2 ± 0.1**	>500
SiO_2	Nanostructured & Amorphous Materials, Inc.US	4850MR	13.5 ± 4.2	113.4 ± 4.2	193.5 ± 2.1	0.0 5 ± 0.01**	>500
SnO_2	Research Nanomaterials, Inc.	US3460	62.4 ± 13.2	203.7 ± 4.7	293 ± 91.9	0.00 ± 0.00**	>500
TiO_2	In house synthesis	-	12.6 ± 4.3	166.0 ± 6.3	104.5 ± 0.7	0.03 ± 0.01**	>500
WO_3	In house synthesis	-	16.6 ± 4.3	176.6 ± 1.8	164.5 ± 9.1	1.6 ± 0.8**	>500
Y_2O_3	Meliorium Technologies	Y_2O_3 NPs, 8-10 nm	32.7 ± 8.1	312.2 ± 15.4	378 ± 21.2	0.02 ± 0.00**	>500
Yb_2O_3	MKNano	MKN-Yb_2O_3-090	61.7 ± 11.3	230.7 ± 1.8	249 ± .2	0.04 ± 0.02**	>500
ZnO	In house synthesis	-	22.6 ± 5.1	204.5 ± 15.1	357 ± 31.1	5.3 ± 1.9*	33 (32 - 35)
ZrO_2	US Research Nanomaterials, Inc.	US3600	40.1 ± 12.6	306.5 ± 10.3	377.6 ± 15.6	0.02 ± 0.00**	>500

[#] primary size of the particles obtained by TEM and reported in a previous study (reference 15)

* by AAS analysis

** by ICP-MS

REFERENCES

1. Nohynek, G. J.; Dufour, E. K., Nano-sized cosmetic formulations or solid nanoparticles in sunscreens: a risk to human health? *Arch. Toxicol.* **2012,** *86*, (7), 1063-1075.

2. Jaganathan, H.; Godin, B., Biocompatibility assessment of Si-based nano- and micro-particles. *Adv. Drug. Deliver. Rev.* **2012,** *64*, (15), 1800-1819.

3. Taccola, L.; Raffa, V.; Riggio, C.; Vittorio, O.; Iorio, M. C.; Vanacore, R.; Pietrabissa, A.; Cuschieri, A., Zinc oxide nanoparticles as selective killers of proliferating cells. *Int. J. Nanomed.* **2011,** *6*, (6), 1129-1140.

4. Padmavathy, N.; Vijayaraghavan, R., Enhanced bioactivity of ZnO nanoparticles-an antimicrobial study. *Sci. Technol. Adv. Mat.* **2008,** *9*, (3), 1-7.

5. Lin, S.; Zhao, Y.; Xia, T.; Meng, H.; Ji, Z.; Liu, R.; George, S.; Xiong, S.; Wang, X.; Zhang, H., et al., High content screening in zebrafish speeds up hazard ranking of transition metal oxide nanoparticles. *ACS Nano* **2011,** *5*, (9), 7284-7295.

6. Xia, T.; Zhao, Y.; Sager, T.; George, S.; Pokhrel, S.; Li, N.; Schoenfeld, D.; Meng, H.; Lin, S.; Wang, X., et al., Decreased dissolution of ZnO by iron doping yields nanoparticles with reduced toxicity in the rodent lung and zebrafish embryos. *ACS Nano* **2011,** *5*, (2), 1223-1235.

7. Ge, Y.; Schimel, J. P.; Holden, P. A., Evidence for negative effects of TiO(2) and ZnO nanoparticles on soil bacterial communities. *Environ. Sci. Technol.* **2011,** *45*, (4), 1659-1664.

8. Ge, Y.; Schimel, J. P.; Holden, P. A., The identification of soil bacteria susceptible to TiO2 and ZnO nanoparticles. *Appl. Environ. Microbiol.* **2012,** *78*, (18), 6749-6758.

9. Stohs, S. J.; Bagchi, D., Oxidative mechanisms in the toxicity of metal ions. *Free Radical Biol. Med.* **1995,** *18*, (2), 321-336.

10. Song, M. F.; Li, Y. S.; Kasai, H.; Kawai, K., Metal nanoparticle-induced micronuclei and oxidative DNA damage in mice. *J. Clin. Biochem. Nutr.* **2012,** *50*, (3), 211-216.

11. Naqvi, S.; Samim, M.; Abdin, M.; Ahmed, F. J.; Maitra, A.; Prashant, C.; Dinda, A. K., Concentration-dependent toxicity of iron oxide nanoparticles mediated by increased oxidative stress. *Int. J. Nanomed.* **2010,** *5*, (5), 983-989.

12. Pujalte, I.; Passagne, I.; Brouillaud, B.; Treguer, M.; Durand, E.; Ohayon-Courtes, C.; L'Azou, B., Cytotoxicity and oxidative stress induced by different metallic nanoparticles on human kidney cells. *Part. Fibre. Toxicol.* **2011,** *8*, (10), 1-16.

13. Horst, A. M.; Vukanti, R.; Priester, J. H.; Holden, P. A., An assessment of fluorescence- and absorbance-based assays to study metal-oxide nanoparticle ROS production and effects on bacterial membranes. *Small* **2013,** *9*, (9-10), 1753-64.

14. Zhang, H. Y.; Ji, Z. X.; Xia, T.; Meng, H.; Low-Kam, C.; Liu, R.; Pokhrel, S.; Lin, S. J.; Wang, X.; Liao, Y. P., et al., Use of Metal Oxide Nanoparticle Band Gap to Develop a Predictive Paradigm for Oxidative Stress and Acute Pulmonary Inflammation. *ACS Nano* **2012,** *6*, 4349-4368.

15. Pokhrel, S.; Nel, A. E.; Madler, L., Custom-designed nanomaterial libraries for testing metal oxide toxicity. *Accounts Chem. Res.* **2013,** *46*, (3), 632-41.

16. George, S.; Pokhrel, S.; Xia, T.; Gilbert, B.; Ji, Z. X.; Schowalter, M.; Rosenauer, A.; Damoiseaux, R.; Bradley, K. A.; Madler, L., et al., Use of a Rapid Cytotoxicity Screening Approach To Engineer a Safer Zinc Oxide Nanoparticle through Iron Doping. *ACS Nano* **2010,** *4*, (1), 15-29.

17. Zhang, H. Y.; Pokhrel, S.; Ji, Z. X.; Meng, H.; Wang, X.; Lin, S. J.; Chang, C. H.; Li, L. J.; Li, R. B.; Sun, B. B., et al., PdO Doping Tunes Band-Gap Energy Levels as Well as Oxidative

Stress Responses to a Co3O4 p-Type Semiconductor in Cells and the Lung. *J. Am. Chem. Soc.* **2014,** *136*, (17), 6406-6420.

18. Ritz, C.; Streibig, J. C., Bioassay analysis using R. *J. Stat. Softw.* **2005,** *12*, (5), 1-22.

19. Ding, X.; Yu, Q.; Xu, N.; Wang, Y.; Cheng, X.; Qian, K.; Zhao, Q.; Zhang, B.; Xing, L.; Li, M., Ecm7, a regulator of HACS, functions in calcium homeostasis maintenance, oxidative stress response and hyphal development in Candida albicans. *Fungal. Genet. Biol.* **2013,** *57*, 23-32.

20. Chin, R. M.; Fu, X.; Pai, M. Y.; Vergnes, L.; Hwang, H.; Deng, G.; Diep, S.; Lomenick, B.; Meli, V. S.; Monsalve, G. C., et al., The metabolite alpha-ketoglutarate extends lifespan by inhibiting ATP synthase and TOR. *Nature* **2014,** *510*, (7505), 397-401.

21. Zvab, U.; Marusic, M. B.; Stangar, U. L., Microplate-based assays for the evaluation of antibacterial effects of photocatalytic coatings. *Appl. Microbiol. Biot.* **2012,** *96*, (5), 1341-1351.

22. Kato, H.; Fujita, K.; Horie, M.; Suzuki, M.; Nakamura, A.; Endoh, S.; Yoshida, Y.; Iwahashi, H.; Takahashi, K.; Kinugasa, S., Dispersion characteristics of various metal oxide secondary nanoparticles in culture medium for in vitro toxicology assessment. *Toxicol. In Vitro* **2010,** *24*, 1009-1018.

23. Ivask, A.; Suarez, E.; Patel, T.; Boren, D.; Ji, Z.; Holden, P.; Telesca, D.; Damoiseaux, R.; Bradley, K. A.; Godwin, H., Genome-wide bacterial toxicity screening uncovers the mechanisms of toxicity of a cationic polystyrene nanomaterial. *Environ. Sci.Technol.* **2012,** *46*, (4), 2398-2405.

24. Li, Y.; Zhang, W.; Niu, J.; Chen, Y., Mechanism of photogenerated reactive oxygen species and correlation with the antibacterial properties of engineered metal-oxide nanoparticles. *ACS Nano* **2012,** *6*, (6), 5164-5173.

25. Premanathan, M.; Karthikeyan, K.; Jeyasubramanian, K.; Manivannan, G., Selective toxicity of ZnO nanoparticles toward Gram-positive bacteria and cancer cells by apoptosis through lipid peroxidation. *Nanomedicine-UK* **2011,** *7*, (2), 184-192.

26. Wang, Z.; Li, N.; Zhao, J.; White, J. C.; Qu, P.; Xing, B., CuO nanoparticle interaction with human epithelial cells: cellular uptake, location, export, and genotoxicity. *Chem. Res. Toxicol.* **2012,** *25*, (7), 1512-1521.

27. Srivastava, S.; Dubey, R. S., Manganese-excess induces oxidative stress, lowers the pool of antioxidants and elevates activities of key antioxidative enzymes in rice seedlings. *Plant Growth Regul.* **2011,** *64*, (1), 1-16.

28. Chiang, H. M.; Xia, Q.; Zou, X.; Wang, C.; Wang, S.; Miller, B. J.; Howard, P. C.; Yin, J. J.; Beland, F. A.; Yu, H., et al., Nanoscale ZnO induces cytotoxicity and DNA damage in human cell lines and rat primary neuronal cells. *J. Nanosci. Nanotechno.* **2012,** *12*, (3), 2126-2135.

29. Hussain, S.; Al-Nsour, F.; Rice, A. B.; Marshburn, J.; Yingling, B.; Ji, Z.; Zink, J. I.; Walker, N. J.; Garantziotis, S., Cerium dioxide nanoparticles induce apoptosis and autophagy in human peripheral blood monocytes. *ACS Nano* **2012,** *6*, (7), 5820-5829.

30. Hackenberg, S.; Scherzed, A.; Technau, A.; Kessler, M.; Froelich, K.; Ginzkey, C.; Koehler, C.; Burghartz, M.; Hagen, R.; Kleinsasser, N., Cytotoxic, genotoxic and pro-inflammatory effects of zinc oxide nanoparticles in human nasal mucosa cells in vitro. *Toxicol. In Vitro* **2011,** *25*, (3), 657-663.

31. Morgan, M. J.; Liu, Z. G., Reactive oxygen species in TNFalpha-induced signaling and cell death. *Mol. Cells* **2010,** *30*, (1), 1-12.

32. Sharma, V.; Anderson, D.; Dhawan, A., Zinc oxide nanoparticles induce oxidative stress and genotoxicity in human liver cells (HepG2). *J. Biomed. Nanotechnol.* **2011,** *7*, (1), 3782-3788.

33. Brayner, R.; Ferrari-Iliou, R.; Brivois, N.; Djediat, S.; Benedetti, M. F.; Fievet, F., Toxicological impact studies based on Escherichia coli bacteria in ultrafine ZnO nanoparticles colloidal medium. *Nano Lett.* **2006,** *6*, (4), 866-870.

34. Horie, M.; Nishio, K.; Endoh, S.; Kato, H.; Fujita, K.; Miyauchi, A.; Nakamura, A.; Kinugasa, S.; Yamamoto, K.; Niki, E., et al., Chromium(III) oxide nanoparticles induced remarkable oxidative stress and apoptosis on culture cells. *Environ. Toxicol.* **2011,** *28*, (2), 61-75.

35. Khatoon, I.; Vajpayee, P.; Singh, G.; Pandey, A. K.; Dhawan, A.; Gupta, K. C.; Shanker, R., Determination of Internalization of Chromium Oxide Nano-Particles in Escherichia coli by Flow Cytometry. *J. Biomed. Nanotechnol.* **2011,** *7*, (1), 168-169.

36. Thevenod, F., Catch me if you can! Novel aspects of cadmium transport in mammalian cells. *Biometals* **2010,** *23*, (5), 857-875.

37. Liu, R.; Zhang, H. Y.; Ji, Z. X.; Rallo, R.; Xia, T.; Chang, C. H.; Nel, A.; Cohen, Y., Development of structure-activity relationship for metal oxide nanoparticles. *Nanoscale* **2013,** *5*, (12), 5644-53.

38. Burello, E.; Worth, A. P., A theoretical framework for predicting the oxidative stress potential of oxide nanoparticles. *Nanotoxicology* **2011,** *5*, (2), 228-235.

39. Tang, J.; Liu, Y.; Yuan, Y.; Zhou, S., Humic acid-enhanced electron transfer of in vivo cytochrome c as revealed by electrochemical and spectroscopic approaches. *J. Environ. Sci. (China)* **2014,** *26*, (5), 1118-24.

40. Xia, T.; Kovochich, M.; Liong, M.; Madler, L.; Gilbert, B.; Shi, H.; Yeh, J. I.; Zink, J. I.; Nel, A. E., Comparison of the mechanism of toxicity of zinc oxide and cerium oxide nanoparticles based on dissolution and oxidative stress properties. *ACS Nano* **2008,** *2*, (10), 2121-2134.

41. Bondarenko, O.; Ivask, A.; Kakinen, A.; Kahru, A., Sub-toxic effects of CuO nanoparticles on bacteria: kinetics, role of Cu ions and possible mechanisms of action. *Environ. Pollut.* **2012,** *169*, (2012), 81-89.

CHAPTER 3

Cu Nanoparticles Have Different Impacts in *E. coli* and *L. brevis* Than Their Micron-Sized and Ionic Analogs (This chapter was submitted as a manuscript to *ACS Nano* on April 3, 2015 and was under review as of June 2, 2015)

ABSTRACT

Copper formulations have been used for decades for antimicrobial and antifouling applications. With the development of nano-formulations of copper that are more effective than their ionic and micron-sized analogs, a key regulatory question is whether these materials should be treated as new or existing materials. To address this issue, here we compare the magnitude and mechanisms of toxicity of a series of Cu species, including nano Cu, nano CuO, nano $Cu(OH)_2$ (CuPro and Kocide), micro Cu, micro CuO, ionic Cu^{2+} ($CuCl_2$ and $CuSO_4$) in two species of bacteria (*Escherichia coli and Lactobacillus brevis*). Our results reveal that Cu and CuO nanoparticles (NPs) are more toxic than their micron-sized counterparts, with toxicities approaching that of the ionic Cu species. Strikingly, these NPs showed distinct differences in their mode of toxicity when compared to the ionic and micron-sized Cu, highlighting the unique toxicity properties of materials at the nanoscale. Critically, *in vitro* DNA damage assays reveal that both nano Cu and micron-sized Cu are capable of causing complete degradation of plasmid DNA but electron tomography result shows that only nanoformulations of Cu are internalized as whole particles inside of cells. These studies suggest that nano Cu may have unique genotoxicity in bacteria compared to ionic and micron-sized Cu. As a result of these studies, we recommend that nanoformulations of Cu be regulated as new materials.

Keywords: copper, nanoparticle, nanotoxicology, ecotoxity, antimicrobial, antifouling, genotoxicity

INTRODUCTION

Nanomaterials have contributed to rapid advances in diverse fields including engineering, materials development, medicine, energy conservation as well as space technology. For nano-enabled products to be brought to market and have a sustainable future, we need to understand their toxicity and ecotoxicity. Of particular concern are nanoformulations of Cu, which are used as lubricants, conducting polymers, surfactants and catalysts in chemical reactions[1, 2] as well as drugs, deodorants, food additives and as antifouling agents in paint.[3, 4] Nanoformulations of Cu that are used commercially in environmental settings include nano $Cu(OH)_2$ (*e.g.*, CuPro and Kocide), nano CuO (n-CuO) and nano Cu (n-Cu). Many of the current and proposed applications for these materials take advantage of the potent antibacterial properties of Cu species. However, because of their antibacterial properties, Cu-based nanoparticles (Cu NPs) may also have unwanted effects in ecosystems. A central question is whether the magnitude and/or mechanisms of toxicity of Cu-based nanoparticles are the same as, or different from, those of other Cu formulations that are already on the market.

Cu-based nanoparticles have been shown to exhibit toxicity against a wide-range of environmentally-relevant organisms. For example, CuO nanoparticles have been shown to induce growth inhibition and lead to cellular oxidative stress in green alga[5], compromise the health of daphnia[6] and lead to neurotoxic effects in mussels.[7] Moreover, Cu nanoparticles have also been shown to cause gill injury and acute lethality in zebrafish.[8] In the bacterium *Escherichia coli*, CuO nanoparticles induce cytotoxicity and oxidative stress in.[9] There is also evidence to suggest that Cu-based nanoparticles may pose a threat to human health: CuO NPs

were found to cause acute pulmonary inflammation and lethality in human mesenchymal stem cells.[10, 11]

To address the question of whether the toxicology of nanoparticles is unique, it is critical to conduct side-by-side comparisons between nanoparticles and their ionic and micron-sized counterparts under comparable conditions. For metallic nanoparticles, some researchers have suggested that the toxicity of the nanoparticles is due to dissolved metal ions, and hence metal nanoparticles simply constitute a novel delivery mechanism for an existing agent.[12] For instance, Alvarez and co-workers reported that the toxicity of silver nanoparticles corresponds to the rate of the release of silver ions into solution, and that no particle-specific effects were observed when conducting the experiments in a completely anaerobic condition in bacteria.[12] By contrast, other studies have shown that some (but not all) Ag nanoparticles exhibit mechanisms of toxicity that are different from their ionic analogs. For instance, studies comparing the toxicity of various Ag NPs with ionic Ag^+ using microarray analysis[13] and genome-wide single gene deletion mutants in *E. coli*[14] revealed that the pathways involved in the response of this bacterium are different for different Ag NPs and differ from those seen for Ag^+. In the gene deletion strain studies, the toxicity of Ag-BPEI, which is a cationic Ag NP, was shown to involve pathways similar to that of PS-NH_2, a cationic NP that contains no Ag^+.[14] Moreover, in erythroid (mammalian) cells, silver nanoparticles have been found to disrupt transcription by inhibiting RNA polymerase, a process that was distinctly different from cytotoxic pathways induced by silver ions.[15]

Similarly, reports as to whether Cu nanoparticles are toxic simply because they release Cu ions or whether they can exhibit nano-specific toxicity has been a subject of debate in the literature. Bondarenko and coworkers have reported studies comparing nano CuO to $CuSO_4$

and micron-sized CuO in *E. coli*.[16] Based on their results, they suggested that nano CuO was toxic from copper ion release into solution because all three copper species resulted in biotic production of reactive oxygen species (ROS) and single-stranded DNA damage; additionally, these effects could be inhibited by addition of a Cu-chelating agent (EDTA).[16] By contrast, in a separate study of *Pseudomanas chlororaphis*, only CuO nanoparticles, but not their bulk or ionic counterparts, were found to modify bacterial metabolism and cellular reprogramming.[17] In addition, a study in the microcrustacean *Daphnia magna* and in the bacterium *Vibrio fischeri* revealed that CuO particles at the nano-size are more toxic than their bulk analogs.[18]

These somewhat conflicting results point to the need for a systematic and thorough analysis of the difference in toxicity mechanisms for multiple species of bacteria from related Cu species at the nano-size and the micron-size in comparison to ionic Cu. Here, we demonstrate the use of a suite of sub-lethal assays consisting of membrane damage, cellular ROS generation, electron transport activity and membrane potential to unveil the molecular mechanisms of toxicity of a panel of nanoparticles (n-Cu, n-CuO, n-$Cu(OH)_2$) compared to their micron-sized analogs (m-Cu and m-CuO) as well as ionic Cu ($CuCl_2$ and $CuSO_4$). In addition, we explored whether each of the Cu species was able to produce ROS abiotically, so that we could determine whether ROS generation observed *in vivo* was due to direct generation of ROS by the copper species themselves or whether it is due to downstream effects in cells. In addition, we used microscopy to study whether intact Cu nanoparticles were able to enter bacteria. We also used an *in vitro* DNA damage assay that allowed for exploring which types of damage (*i.e.*, single strand break versus double strand break versus complete degradation) were caused by each of the Cu species. We studied the toxicity of the Cu species in two very different taxa of bacteria: *E. coli*, a gram negative bacterium, and *Lactobacillus brevis*, a gram positive bacterium.

Gram negative bacteria have consisting of a double layer with a high lipid content whereas gram positive bacteria have a thick, but single-layered cell wall with low lipid content and a high content of peptidoglycan. As a result, the susceptibility of gram negative and gram positive bacteria to toxins is often quite different; typically gram negative bacteria are more resistant to (and gram positive bacteria more sensitive to) external insults.[19, 20] We intentionally selected two different species of enteric bacteria so that we could explore possible implications of Cu-based nanoparticles entering into liquid waste treatment systems that rely on microorganisms. These studies reveal significant differences between the toxicity of the various Cu species both *in vitro* and *in vivo,* and that *L. brevis* (the gram positive bacterium) is more sensitive to all of the Cu species than *E. coli* (the gram negative bacterium). Critically, we found that Cu NPs are internalized into *E. coli*, and cause DNA damage *in vitro* and cellular oxidative stress *in vivo* in both species. These results have important implications for both the regulation of Cu-based nanoparticles and for the design of safer products containing Cu species.

RESULTS AND DISCUSSION

Cu species varied in size from nanoscale to microscale

In this study, we selected Cu particles that varied in size (nanoscale to microscale) as well as in their chemical composition (elemental Cu and CuO and $Cu(OH)_2$) and compared their properties to ionic Cu. The Cu species used herein and their sources are described in **Table A2.1** in **Appendix 2**). All told, eight different Cu species were studied: nano Cu (n-Cu), nano CuO (n-CuO), nano $Cu(OH)_2$ (n-$Cu(OH)_2$), micro Cu (m-Cu), micro CuO (m-CuO), and ionic Cu (two forms, $CuCl_2$ and $CuSO_4$). Because n-$Cu(OH)_2$ constitutes the most widely-used class of nano-

sized Cu fungicide/bactericides, we tested two different commercial sources of n-$Cu(OH)_2$ (CuPro (n-$Cu(OH)_2$-a) and Kocide (n-$Cu(OH)_2$-b)) to determine whether there are any manufacturer-dependent differences in environmental effects for this class of Cu NPs. In addition, two different forms of ionic Cu^{2+} ($CuCl_2$ and $CuSO_4$) were tested as controls. The toxic effects of these particles were determined in *Escherichia coli* and *Lactobacillus brevis*: *E. coli* is a gram negative bacterium and *L. brevis* is a gram positive bacterium. Critically, both of these species of bacteria are important enteric bacteria. Both species play important roles in human health and in wastewater treatment (*E. coli* and *L. brevis* are also representatives of the phyla *Proteobacteria* and *Firmicutes*, two of the four bacterial phyla found previously in septic tanks[21]) and hence the impacts of Cu nanoparticles on these species can provide important insights into potentially downstream impacts of using Cu nanoparticles as fungicides and biocides in the environment.

The primary sizes (diameter) of the particles (as shown in **Table 3.1**) were less than 1,000 nm for all of the nano-scale particles (n-Cu, n-CuO, n-$Cu(OH)_2$-a and n-$Cu(OH)_2$-b) and ranged from 200 nm to >10 μm for micro-scaled particles (m-Cu and m-CuO). The hydrodynamic diameter of these particles in purified water was less than 1,400 nm for all of the nano-scaled particles and ranged in size between ~1,300 nm and > 3 μM for the micro-scaled particles. When dispersed in *E. coli* minimal (MMD) media, the average hydrodynamic diameter of the particles was approximately the same as that observed in purified water (see **Table 3.1**). However, when the particles were dispersed in Lactobacilli MRS broth, the average hydrodynamic diameter was slightly larger (280-1,600 nm for nano-scaled particles and > 3 μM for micro-sized particles) than that observed in purified water. This slight increase of hydrodynamic diameter found in nutrient-rich Lactobacilli MRS broth might be the result of

adsorption of proteins from the media onto the surface of the particles.[22] All of the particles remained stable in both *E. coli* and *L. brevis* media after 24 hours as shown in **Table 3.1**, when dispersed using humic acid as described in the **Materials and Methods**. The zeta potential of the particles ranged from -16.5 to -53.8 mV in purified water (**Table 3.1**). The percentage of Cu ion dissolution from each particle in purified water, *E. coli* MMD media and *Lactobacilli* media are provided in the **Table 3.2**. n-Cu and the two n-$Cu(OH)_2$ nanoparticles (CuPro and Kocide) dissolved more than the rest of the particles in both bacterial media studied, but still not completely (10%, 10% and 11% in MMD media and 21%, 22% and 18% in *Lactobacillus* media after 24 hours for n-Cu, n-$Cu(OH)_2$-a and n-$Cu(OH)_2$-b, respectively). Interestingly, for all of the particles studied, the particles dissolved most in the *Lactobacilli* media, an intermediate amount in the MMD media, and least in purified water. This dissolution trend presumably reflects the greater ionic strength and organic materials present in *Lactobacilli* media > MMD media > water; increasing ionic strength and the presence of some organic species have both been shown previously to facilitate the dissolution of Cu ions from the particles.[23]

Bacteria exhibit differential sensitivities to different Cu species, with gram positive bacteria more sensitive than gram negative bacteria

To study the antibacterial effects of Cu particles, growth inhibition assays were performed on both *E. coli* and *L. brevis*. Dose-dependent declines in bacterial growth were observed for all of the Cu species tested in both species of bacteria (**Figure A2.1 A**, *E. coli*; **B**, *L. brevis* and **Figure A2.2** in **Appendix 2** showing individual growth-inhibition curves with error bars for each of the Cu species in *E. coli*, **A** and *L. brevis*, **B**) but the magnitude of the toxicity (as measured by IC_{50}) differed significantly between the Cu species studied and between the two

species of bacteria (**Table 3.2**). Markedly, a severe interruption of growth was observed when *E. coli* was treated with $CuCl_2$, n-Cu, $CuSO_4$, and n-CuO (the IC_{50} was determined to be 38, 120, 140 and 160 mg/L for these species, respectively, **Table 3.2**). The observed difference in toxicity between $CuCl_2$ and $CuSO_4$ agrees with the previously published data showing the distinct behaviors in bioreduction and biosorption between the two Cu compounds[24] and the influence of chloride and sulfate anions on the bioavailability of Cu and subsequently the uptake of Cu into starch granules in potato and wheat starch.[25] A relatively mild response ($IC_{50} \geq 250$ mg/L) was observed when *E. coli* was treated with n-$Cu(OH)_2$-a and n-$Cu(OH)_2$-b as well as micron-sized particles (m-Cu and m-CuO). Notably, *L. brevis* was more sensitive (as indicated by a smaller IC_{50} value) to each of the Cu species tested than was *E. coli*. n-CuO, n-$Cu(OH)_2$-a, n-Cu, n-$Cu(OH)_2$-b and $CuCl_2$ exhibited IC_{50} values of 4, 4, 6, 6 and 8 respectively in *L. brevis*, which meets the criteria for "toxic to aquatic life" according to the globally harmonized system of classification and labelling of chemicals (GHS) part 4: Environmental hazard).[26] A relatively modest response ($IC_{50} \geq 120$ mg/L) was observed in *L. brevis* for m-Cu and m-CuO (**Figure A2.1, A2.2** in **Appendix 2** and **Table 3.2**). To accurately distinguish between toxic and non-toxic Cu species, the area under the growth inhibition curves (as shown in **Figure A2.1** in **Appendix 2)** was calculated for all of the Cu species (**Figure A2.3** in **Appendix 2**). The calculation provided a continuous measurement for non-toxic particles whose exact IC_{50} could not be determined. (Note that the IC_{50} of these non-toxic particles was listed as ≥ 250 mg/mL in **Table 3.2**). In agreement with the IC_{50} values, nano-sized particles and ionic Cu exhibit a significantly smaller area under their respective growth inhibition curves when compared to their micron-sized particles in both species of bacteria confirming that the nano-sized Cu particles are more toxic than their micron-sized counterparts. In both species of bacteria, the toxicity of the

n-Cu was equivalent to that of toxic ionic Cu species ($CuCl_2$, $CuSO_4$, **Table 3.2**, **Figure A2.3** in **Appendix 2**). Interestingly, the gram-positive *L. brevis* exhibited an elevated toxicity to all of the particles relative to gram-negative *E. coli*, suggesting a possible role for the double membrane structure found specifically in gram negative bacteria in protecting against toxicity of Cu particles. This result is consistent with the previous finding that gram positive bacteria are more sensitive to nanoparticles compared to gram negative counterpart in the case of Cu nanoparticles and nano-sized metal oxide halogen adducts[19, 27] and that gram positive bacteria tend to be more sensitive than gram negative bacteria to ionic copper and other metals ions.[28, 29]

Magnitude of toxicity of Cu species correlates with amount of cell-associated copper

One possible explanation for why bacteria are more sensitive to nano-sized copper species than to micron-sized copper species was proposed previously by Rossetto *et al.* , *i.e.* that the percent dissolution of the nano copper species is greater for nano-sized Cu species than for micron-sized Cu species due to the larger surface to volume ratio for nano-sized particles.[18] To test this possibility, we looked at whether the area under the growth inhibition curve for the different Cu species correlates with the amount of dissolved Cu in the bacterial media. The area under the dose-response curve was determined to provide a continuous measure of toxicity especially for non-toxic Cu species whose IC_{50} could not be determined exactly (*i.e.*, those Cu species where $IC_{50} \geq 250$ mg/L). The correlation between area under the growth inhibition curve and the amount of Cu dissolved in the bacterial media was found to be moderate for *E. coli* (r = -0.64) and weak for *L. brevis* (r = -0.35). (See **Table A2.2** in **Appendix 2**)[30]

Because we had recently observed that the toxicity of silver nanoparticles is dependent upon their ability to bind to the outside of cells and perturb the outer membrane,[14] we also tested whether the nano Cu species were more toxic because they were better able to bind to and deliver Cu to the bacterial cells. To assess this, we used sucrose gradient centrifugation coupled with ICP-MS to determine the concentration of Cu associated with bacteria. In this method, nanoparticles as well as micron-size particles in solution are separated from cells using sucrose gradient centrifugation, and the Cu content of the different fractions was measured using ICP-MS (see **Materials and Methods**); anything firmly adhered to the cells remains in the cellular fraction. As a result, this method provides a measure of the *total Cu associated with the bacteria,* (*i.e.,* both Cu that is bound strongly to the outside of the cells and Cu that has been internalized). A detailed schematic of the sucrose centrifugation experiment is shown in **Figure A2.4** in **Appendix 2**. *E. coli* and *L. brevis* were each treated with 1 mg/mL of each of the Cu species for 24 hours before being centrifuged in a sucrose gradient to separate the bacterial cells from any remaining particles. After centrifugation, any particulate Cu that was not associated with the bacterial cells was pelletized and fractionated to the bottom of the Falcon tube, while the bacterial cells (including any Cu associated with the cells) are visible as a brown band in the middle of the tube. The total number of bacterial cells collected from the sucrose gradient was determined using a linear equation derived from a standard curve relating OD_{600} and total number of cells (colony forming units) as shown in **Figure A2.5** in **Appendix 2**. Generally, there was more Cu associated with cells exposed to the more toxic Cu species than for the cells exposed to the less toxic Cu species (**Table 3.2**). In particular, n-Cu, with the smallest IC_{50} value, exhibited the greatest amount of cell-associated Cu, both in *L. brevis* and *E. coli*. The correlation between the area under the growth inhibition curves and the Cu associated with the

cells were found to be -0.73 and -0.74 for *E. coli* and *L. brevis*, respectively (**Table A2.2**). This correlation is much stronger than that observed between the area under the growth inhibition curves and the amount of Cu dissolved in the bacterial media (-0.64 and -0.35 for *E. coli* and *L. brevis*, respectively). One caveat to the sucrose gradient separation method is that ionic Cu cannot be effectively separated from the cellular components and hence this method cannot be used to ascertain cell-associated Cu for bacteria treated with ionic Cu. However, these results suggest that the ability of the Cu species to associate with cells plays a crucial role in determining their toxicity and suggests the need for more detailed studies on the different mechanisms of toxicity for the Cu species.

To test whether the most important factor in determining toxicity was the amount of Cu *delivered to the inside* of the cells, we used a genetically-engineered bacterial biosensor, *E. coli* MC1061 (pSLcueR/pDNPcopAlux), in which bioluminescence is specifically induced by *intracellular, bioavailable* Cu.[16] The copper species that were found to be most toxic to cells (*i.e.,* $CuCl_2$ and nano-sized Cu particles) resulted in more bioluminescence than did the less toxic Cu species (*i.e.,* micron-sized particles). (See **Figure A2.6** in **Appendix 2**). The level of bioavailable Cu for cells treated with n-Cu was about the same or higher than that of cells treated with $CuCl_2$, suggesting that the nanoparticle form of Cu has a unique advantage over Cu ions in entering the cells. The correlation coefficient between area under the growth inhibition curve and the intracellular amount, bioavailable Cu, was very strong (r = -0.90, **Table A2.2** in **Appendix 2**) suggesting that the best predictor of bacterial toxicity is the amount of intracellular, bioavailable Cu.

Sub-lethal assays reveal that different Cu species exhibit different mechanisms of toxicity

To elucidate the mechanisms of toxicity for the Cu species, a suite of assays measuring membrane potential, membrane damage, cellular ROS generation and electron transport activity were employed in both *E. coli* and *L. brevis*. The outcomes of these four assays are shown in the heat map in **Figure 3.1**. In the heat map, red indicates that the results are similar to the positive control (*i.e.*, NaN_3 for the membrane potential assay, ethanol for membrane damage, H_2O_2 for cellular ROS generation, and CCCP for electron transport activity), and green indicates that the results are identical to the negative controls (*i.e.*, PBS with no added Cu species). While both nano-sized Cu and Cu ions resulted in significant membrane damage and a decrease in electron transport activity in *E. coli*, the micro-sized Cu particles did not. This observation strongly agrees with the growth inhibition results, in which nano-sized Cu and Cu ions exhibit lower IC_{50} values and smaller areas under the growth inhibition curve than the micro-sized Cu species in *E. coli* (**Table 3.2, Figure A2.3** in **Appendix 2**). Strikingly, oxidative stress (measured by biotic ROS generation) was only observed in *E. coli* treated with Cu NPs, but not with *E. coli* treated with ionic copper ($CuCl_2$ or $CuSO_4$) or micron-sized Cu at the concentrations studied herein. Conversely, severe disruption of membrane potential was observed only in *E. coli* treated with Cu ions and not those treated with nano- or micron-sized Cu particles. In both species, the toxicity of the Cu species (as measured by area under the growth curve) was strongly correlated with the decrease in electron transport activity (correlation coefficient = -0.76 in *E. coli*, **Table A2.3A** in **Appendix 2** and -0.64 in *L. brevis*, **Table A2.3B** in **Appendix 2**). Similar trends were observed in *L. brevis* (**Figure 3.1**), with the following exceptions: (1) overall, a stronger response was observed in the sub-lethal assays in *L. brevis* for the more toxic particles; (2) significant membrane damage was observed for both $Cu(OH)_2$ species (CuPro and Kocide) and

$CuCl_2$/$CuSO_4$ in *L. brevis*; and (3) biotic ROS generation was observed in *L. brevis* treated with n-Cu and n-CuO, as well as both of the $Cu(OH)_2$ species (CuPro and Kocide). Inter-species correlation (**Table A2.3C** in **Appendix 2**) revealed that a strong agreement between the two species were observed in biotic ROS generation (r = -0.90) and membrane potential (r = -0.86). Consistent with the results from the growth inhibition assay, however, we typically observed stronger responses in *L. brevis* than in *E. coli* for a given Cu species for each of the assays. The observation that overall toxicity does not correlate strongly with biotic ROS generation for the series of copper species (r = -0.02 in *E. coli* and r = -0.60 in *L.* brevis) is important because it suggests that different toxicity mechanisms are relevant to different Cu species. Although ionic Cu is known to cause oxidative stress,[31] this mechanism does not predominate for ionic Cu at the concentrations studied herein. By contrast, cells treated with particulate forms of Cu (both nano-sized and micron-sized) exhibited significant ROS production even at the low Cu concentrations studied herein. Our observation suggests that n-Cu provokes a particularly strong biotic ROS response — even at these low concentrations — is consistent with prior reports that Cu NPs lead to greater cellular oxidative stress in bacterial cells,[32] yeast cells,[33] and mammalian cells[34] than does ionic Cu. Our finding that, out of the species studied, only ionic Cu severely disrupts membrane potential is consistent with a previous study showing that ionic Cu promotes proton leakage across the plasma membrane and hinders the respiratory chain downstream of coenzyme Q.[35] These results highlight important differences in the mechanistic pathways of toxicity for Cu NPs and Cu ions.

Different Cu species also result in different types of DNA damage *in vitro*

A previous study had demonstrated that ionic Cu, CuO nanoparticles, and micron-sized CuO particles all result in single-stranded DNA damage,[16] but we wished to explore here if *other* types of DNA damage were caused by the different Cu species studied herein. To study the intrinsic potential of the different Cu species to damage double-stranded DNA, we used a plasmid-based *in vitro* DNA damage assay.[36] In this experiment, the plasmid pUC19 (where 90% of the plasmid is supercoiled and 10% is in single-strand nicked form as purchased)[37] was incubated with each of the Cu species for 24 hours; the resulting state of the plasmid was assayed by gel electrophoresis. The gel electrophoresis results for each Cu species are shown in **Figure A3.7** in **Appendix 2**. The positive controls used in this study were a UV-treated plasmid (lane 2 in **Figure A2.7** in **Appendix 2**, which completed degrades the DNA and appears as smeared band) and plasmid treated with the restriction enzyme *Pst*I, (lane 3 in **Figure A2.7** in **Appendix 2**), which results in double strand breaks and hence appears as a linearized plasmid. The DNA damage was classified into linearized DNA (plasmid DNA with a double strand break), single-stranded, nicked DNA (plasmid DNA with single strand breaks) and fragmented DNA (plasmid DNA with multiple strand breaks). Quantification of each type of DNA damage generated by Cu species studied herein is shown in **Figure 3.2A.** All of the Cu species tested resulted in some form of DNA damage, but the nature and the severity of the damage varied significantly from one Cu species to the next. The most severe DNA damage observed for n-Cu and m-Cu, both of which induced complete degradation of plasmid DNA, resulting in smeared bands at lower molecular weights (**Figure 3.2A** and **Figure A2.7** in **Appendix 2**). By contrast, both forms of n-$Cu(OH)_2$ (CuPro and Kocide) resulted in complete conversion of the native form of the supercoiled plasmid to open circular (single-strand breaks) and linearized plasmid (double-strand

breaks). The remaining Cu species tested (n-CuO, m-CuO and ionic Cu) resulted in partial conversion of the supercoiled DNA to open circular and linearized plasmid.

To test whether the ability of the Cu species to cause DNA damage *in vitro* is linked to the ability of the various Cu species to generate ROS abiotically (*i.e.* in the absence of cells), we studied each of the particles using an abiotic ROS generation assay using dichloro-dihydro-fluorescein diacetate (DCFH). In this assay, DCFH is generated *in situ* by cleaving the acetate functional group from H_2DCFDA using NaOH.[38] The solution containing DCFH was mixed with each of the Cu species and the fluorescent signal at 530 nm, which indicates the amounts of oxidized dye, was measured after 2 hours.[38] Only n-Cu and m-Cu — the same two of the particles that resulted in complete DNA degradation — resulted in significant oxidation of DCFH *in vitro* (**Figure 3.2B**). This result strongly suggests that the Cu species studied herein that cause significant DNA damage do so by means of DNA oxidation. This result is consistent with previous findings in mammalian cells that nanoparticles induce single/double stranded DNA breaks as well as chromosomal damage using micronucleus, comet and γ-H_2AX assays.[39]

Cellular imaging studies reveal that Cu nanoparticles enter the bacterial cells intact

The observation that both n-Cu and m-Cu generate significant ROS under abiotic condition and exhibit significant DNA-damage potential *in vitro* but n-Cu exhibits significantly higher toxicity towards bacterial cells begs the question of whether there is a difference in the ability of the two particles to enter the bacterial cells, and hence have direct access to intracellular DNA. To address this question, we examined TEM images of *E. coli* exposed to each of the different Cu species. To ensure that particles loosely associated with the bacteria

were removed, the samples were washed with PBS 3 times prior to obtaining the images. As shown in **Figure 3.3**, *E. coli* treated with nano-sized particles (n-Cu, n-CuO, n-$Cu(OH)_2$-a and n-$Cu(OH)_2$-b) were observed to have particles-associated with them. By contrast, no Cu particles were observed in cells treated with micron-sized particles (m-Cu and m-CuO). Interestingly, n-$Cu(OH)_2$-a, n-$Cu(OH)_2$-b and $CuCl_2$-treated bacteria also showed a marked distorted conformation of the cells, as well as membrane damage.

To ascertain whether the particles were actually inside the cells, we constructed 3D images of *E. coli* treated with n-Cu from a tomogram series. The resulting image (**Figure 3.4**) revealed n-Cu particles inside of the *E. coli*, suggesting that the nanoparticles were able to cross the cell membrane intact. Consistent with the results presented herein, Kumar *et. al* have previously reported the direct uptake of nanoparticles (ZnO and TiO_2) in the bacteria *E. coli*, which was determined using flow cytometry.[40] Together these results support the hypothesis that n-Cu can penetrate into the cells, and mediate toxicity through effects of the nanoparticle surface (e.g., DNA damage) in addition to toxicity due to release of Cu ions. In addition, we conducted confocal imaging of both *E. coli* and *L. brevis* that were stained with Hoechst fluorescent dye (which stains nucleic acids inside the cells blue) and treated with n-CuO labeled with FITC (green fluorescent)[41]. In both cases, we observed co-localization of the n-FITC-CuO and Hoechst signals. (**Figure A2.8** in **Appendix 2**) The results indicate that n-CuO is able to be internalized in both of the species of bacteria studied herein. Taken together, these findings help to explain why we observed both a greater magnitude of toxicity and different mechanisms of toxicity for nano Cu species compared with their micron and ionic analogs. In addition, they offer tantalizing evidence that nano Cu species may persist longer in living organisms than

micron-sized Cu species, and could therefore be transferred to higher trophic levels and bioaccumulated.

CONCLUSIONS

The studies reported herein provide strong evidence that nano-sized Cu particles cannot only be more toxic than their micron-sized analogs, but can also exhibit significantly different mechanisms of toxicity than both ionic Cu and micron-sized Cu. Critically, we found that only nano Cu species were either strongly bound to or internalized within *E. coli* and demonstrated that both n-Cu and n-CuO can be internalized into the bacteria intact. Because n-Cu was also found to generate significant ROS and cause extremely deleterious damage DNA *in vitro*, the potential that n-Cu may exhibit unique genotoxicity inside cells is particularly of concern. Taken together, these studies suggest that nano Cu species should be regulated as distinct (new) materials, differently from their micron and ionic analogs, and that additional safety testing should be conducted on nano Cu species in other organisms.

MATERIALS AND METHODS

Bacterial strains

Two bacterial strains were used in this study: *Escherichia coli* strain ATCC 25922, a standard strain widely used for antimicrobial disk susceptibility tests, and *Lactobacillus brevis* strain (Orla-Jensen) ATCC 14869.

Chemicals and media components

Bacterial growth media for *E. coli* (LB Lennox) was obtained from EMD Chemicals (Merck, Darmstadt, Germany); the pH of the final media was adjusted to 7 using NaOH. Purified water used in all of the experiments consisted of deionized (DI) water that was passed through an Aqua Solutions water purification machine, model RODI-C-12BL (TX, USA). All assays of *E. coli* were conducted in environmentally-relevant media: Modified Minimal Davis, MMD media (1 L H_2O: 0.7 g K_2HPO_4; 0.2 g KH_2PO_4; 0.66 g $(NH_4)_2SO_4$; 0.5 g sodium citrate; 0.1 g $MgSO_4 \bullet 7H_2O$; 3.31g D-glucose, pH 6.9). To prepare agar plates, 15 g of Agar power (Fisher Scientific) was added to 1000 mL of media broth. Kanamycin sulfate was obtained from Sigma-Aldrich. PBS (pH 7.4) was obtained from GIBCO (Invitrogen, CA, USA). Humic acid was obtained from Sigma-Aldrich. Growth media for *L. brevis* (Lactobacilli MRS broth) was obtained from BD (Franklin Lakes, NJ, USA). Plasmid DNA (pUC19) was obtained from Thermo Scientific (Barrington, IL).

Physiochemical characterization of copper species

The copper species tested herein were obtained from a variety of sources as described in **Table A2.1**. Filtered deionized water was used to make stock solution at 20 mg/mL. Dynamic light scattering (DLS, ZetaPALS, Brookhaven Instruments Ltd., UK*)* was utilized to analyze the average size and size distribution of copper species (50 μg/mL) in water, E. coli media (MMD) and L. brevis media (*Lactobacilli* MRS broth). The ζ-potential values of each Cu species in aqueous solution were determined using a ZetaPALS Zeta Potential Analyzer (Brookhaven Instruments Ltd, UK). Transmission Electron Microscopy (TEM) was used to determine the primary size and morphology of the particles. To prepare samples for TEM, a drop of each Cu

species in purified water was applied to carbon-coated TEM grids and evaporated at room temperature. Images were taken with a JEOL 1200 EX TEM microscope.

The percent dissolution of each of the Cu species in water and bacterial media was measured by quantifying dissolved Cu by ICP-OES (ICPE-9000 plasma atomic emission spectrometer, Shimadzu). For the analysis, 1 mg/mL of Cu species was suspended in water or bacterial growth media to yield a final volume of 1 mL for 24 hours and then was centrifuged at 15,000 rpm for 30 minutes to precipitate any remaining particles. The supernatant was collected and transferred to a clean tube for acid digestion. 10 mL of nitric acid (HNO_3, 65-70%, Trace Metal Grade) was added to the supernatant before incubating in a HotBlock (SC100, Environmental Express) at 80ºC for 6 hours. The temperature was then raised to 95ºC overnight to evaporate all liquid present in sample. The dried sample was allowed to cool down at room temperature before being dissolved in 2% (v/v) nitric acid at 80ºC for 3 hours. The extract was transferred to a 15 mL ICP-OES analysis tube to measure Cu ion concentration.

Growth inhibition effects and IC_{50} calculation

To assess the half-maximal inhibitory concentrations (IC_{50}), a growth inhibition curve was constructed for each Cu species. A 20 mg/mL stock of Cu species was diluted to 10 mg/mL with 2X media (MMD for *E. coli* and Lactobacilli MRS broth for *L. brevis*). Humic Acid (HA) was added to a final concentration of 0.01 mg/mL and then the resulting mixture were sonicated in water bath (Branson 2510, CT, USA) for 15 minutes at room temperature. 10 mg/mL of each Cu species was then diluted with 1X media supplemented with 0.01 mg/mL HA to a step-wise concentration gradient at 2, 3.9, 7.8, 15.6, 31.3, 62.5, 125 and 250 mg/mL. 50 μL of NP at each concentration were pipetted into 384-well polystyrene microplates. Nine replicates were

performed for each concentration. In a separate plate, 50 μL of a log-phase bacterial culture (OD_{600} between 0.5 – 0.7) was pipetted into the 384-well plate and then a plastic 384 pin replicator (Genetix Molecular Devices) was used to inoculate bacteria from this plate to the plate containing the serial dilution of Cu species. Sterility and blank controls (bacterial media with no inoculation) were also included for each concentration. A Biotek Synergy plate reader (BioTek, VT) was used to monitor OD_{600} every 30 minute at 37ºC for 24 hours. A growth curve was constructed using equation:

$$\text{Growth (\%)} = \frac{A_{Np,B} - A_{Np,A}}{A_{Bl,B} - A_{Bl,A}} \times 100$$

In the above equation, $A_{Np,B}$ is the absorbance of the bacterial culture in the presence of each concentration of Cu NPs (average of 9 replicates); $A_{Np,A}$ is the absorbance of the Cu NPs at the respective concentrations which contain no bacteria (average of 3 replicates); $A_{Bl,B}$ is the absorbance of the bacterial culture in blank (no Cu species) media (average of 9 replicates), and $A_{Bl,B}$ is the absorbance of media with no bacteria (average of 3 replicates). The growth inhibition curve was plotted using the program Origin version 9 (OriginLab Corporation) using the category Growth/Sigmoidal, function Logistic. The IC_{50} and standard error were calculated for each data set using the same program. The area under the curve was calculated using the software program R with the package "grofit" to provide a continuous variable that could be used as a global measurement of toxicity in the analysis of the correlation between the toxicity outcome and the concentration of Cu.

Suite of sublethal assays

Cellular ROS generation. To study cellular ROS generation, a stock solution of 2′,7′-dichlorodihydrofluorescein diacetate (H_2DCFDA, Molecular Probes, D399) was dissolved in

ethanol to yield a concentration of 1.5 mg/mL.[42] For biotic ROS detection, H_2DCFDA crosses cell membrane and is hydrolyzed by intracellular esterases to nonfluorescent dichlorofluorescin (DCFH). DCFH is then converted to the highly fluorescent 2′,7′-dichlorofluorescein (DCF) in the presence of intracellular reactive oxygen species. In this experiment, a log-phase culture (OD_{600} = 0.5) of *E. coli* or *L. brevis* was treated with a gradient of concentrations of Cu species (0-250 mg/L) for 24 hours before being mixed with H_2DCFDA (final concentration of 15 ng/mL). Three replicates were performed at each concentration. 100 μL of each mixture were then aliquoted into 96 well-plates (Costar, catalog #3915) and the fluorescent signal was measured using a microplate reader (excitation/emission at 485/530 nm; SpectraMax MS, Molecular Devices, CA).

Membrane damage assay. To study the magnitude of bacterial membrane damage, a live/dead BacLight Bacteria Viability kit (L7012, Molecular Probe) was utilized. PI and SYTO 9 were mixed according to the manufacturer's instructions;[43] 0.15 μL of 3.34 mM SYTO 9 dye and 0.15 μL of 20 mM Propidium iodide were added to 100 μL of a log-phase cell culture (*E. coli* and *L. brevis*) that had been treated with Cu species for 24 hours in a 96 well plate (Costar, catalog #3915). In this experiment, PI (red fluorescence signal) specifically penetrates cells with compromised membrane whereas SYTO 9 (green fluorescence signal) non-selectively stains the DNA of every cell. The fluorescence signal was measured using a microplate reader (SpectraMax MS, Molecular Devices, CA) with excitation at 485 nm and the emission at 530 nm (SYTO 9) and 630 nm (PI). The ratio of the green/red fluorescence signals was used to determine the level of membrane damage, where a larger green/red value indicates less cell membrane damage.

Membrane potential assay. To study the proton gradient across the membrane of cells treated with each Cu species, a dye that is sensitive to membrane potential, Bis-(1,3-dibutylbarbituric acid) Trimethine Oxonol or "DiBAC" (Invitrogen & Molecular Probes, catalog #B-438) was used.[44] DiBAC penetrates depolarized cells and binds to intracellular protein and lipid, resulting in an increase in fluorescence. By contrast, hyperpolarized cells excrete the dye from the cells and exhibit lower levels of fluorescence. A fresh stock solution was prepared immediately prior to use by dissolving DiBAC in 70% Ethanol to a concentration of 1 mg/mL. A working concentration of 10 μg/mL DiBAC solution in bacterial media was added to 100 μL of a log-phase bacterial culture that had been treated with Cu species for 24 hours in black plastic 96 wells plates (Costar, catalog #3915). The fluorescent intensity was read after 1 hour of incubation (excitation = 485 nm, emission = 530 nm) using a microtiter plate reader (SpectraMax MS, Molecular Devices, CA).

Electron transport activity. The metabolic activity of bacterial cells exposed to different Cu species was measured using the XTT-base colorimetric assay.[45] In metabolically active cells, the yellow tetrazolium salt XTT (Sigma-Aldrich, catalog #X4626) is reduced by cellular dehydrogenase enzymes to an orange colored formazan product. The reduced product can be quantified by measuring the absorbance at 460 nm. Menadione (Sigma Aldrich) was used as an electron coupling reagent to improve the efficacy of the assays.[46] A fresh stock of XTT was made immediately prior to each use by dissolving XTT to a concentration of 10 mg/mL in PBS. A stock concentration of 10 mM menadione was prepared in acetone and stored at -70ºC. Log-phase *E. coli* and *L. brevis* (OD_{600} = 0.5) were treated with Cu species for 24 hours before being

mixed with XTT and menadione. The working concentrations of XTT and menadione in the solution were 0.5 mg/mL and 50 μM, respectively. 100 μL of the mixture were aliquoted into a 96 well plates. The plates were incubated at 37 ºC for 1 hour wherein the optical density was measured at 460 nm using a microplate reader (SpectraMax MS, Molecular Devices, CA).

In vitro assays

In vitro DNA damage assay. Purified plasmid pUC19 (Thermo Scientific, catalog #SD0061) was incubated in the presence of 100 mg/L Cu species for 24 hours in purified water. Centrifugation at 15000 rpm for 30 minutes was used to separate plasmid DNA from residual Cu NPs. The supernatant containing the plasmid DNA was collected and loaded into a 1.2% Tris-Acetate-EDTA (TAE) agarose gel. Electrophoresis was performed at 5 V/cm for 1 hour and the resulting gel was stained with ethidium bromide for 30 minutes. A Bio-Rad FX^{TM} imaging system was used to image the gel; the band intensities were quantified using QuantityOne^{TM} software. To linearize the pUC19 (first positive control), the restriction enzyme PstI (New England BioLab, catalog #RO140S) was incubated with the plasmid at 37º C for 1 hour. To induce random nicking and DNA fragmentation (second positive control), the plasmid was treated with a xenon arc UV-B lamp (Asahi Spectra, LAX-Cute) for 10 minutes at 1000 mJ/cm^2. For the negative control, pUC19 was loaded into the electrophoresis gel whereas the majority of the plasmid as purchased was in the supercoiled-formed of DNA.

Abiotic ROS Assay. DCFH was used to study the oxidizing properties of each Cu species *in vitro*. DCFH was produced in situ from H_2DCFDA (2',7'-dichlorodihydrofluorescein diacetate,

Molecular Probes, catalog #D399):[38] H_2DCFDA was dissolved in 100% ethanol to yield a stock concentration of 1.5 mg/mL immediately before use and treated with 0.1 M NaOH at room temperature for 30 min to hydrolyze the acetate moiety from the molecule, yielding DCFH. A gradient of concentrations of each Cu species (0-1000 mg/L) was mixed with the dye (final concentration of 30 ng/mL) to determine the oxidizing potential of the different Cu species. After 24 hours, 100 μL of each mixture were aliquoted into a 96 well-plate (Costar, catalog #3915). The fluorescent signal emitted by the oxidized dye molecules was measured using a microplate reader (SpectraMax MS, Molecular Devices, CA) with excitation/emission wavelengths of 485/530 nm. Three replicates were performed at each concentration.

Determining cell-associated Cu using sucrose gradient centrifugation and ICP MS

E. coli and *L. brevis* were treated with 0.5 and 1 mg/L of a series of the Cu species. After 24 hours, the cells were washed 2 times with PBS and then sucrose gradient centrifugation was used to separate the cells from residual particulate Cu. To make the sucrose gradient, 0.3, 0.4 and 0.6 g/mL of sucrose (Sigma-Aldrich) were completely dissolved in water and filtered with a 0.22 μm Millipore filter.[47] 1.2 mL of each sucrose concentration was carefully layered into a 15 mL Falcon tube and then 1 mL of cell suspension was placed on top of the gradient. The mixture was centrifuged (Eppendorf 5810 R) at 2916×g for 5 minutes at room temperature. After centrifugation, a brown band of cells was clearly visible at the upper part of the gradient and Cu species were visibly precipitated at the bottom of the tube. (See **Figure A2.4**, in **Appendix 2**) 1.2 mL of cells suspension were collected. To determine the total number of bacterial cells, a standard curve between OD_{600} and the number of cells was constructed (**Figure A2.5**, in

Appendix 2, A for *E. coli* and B for *L. brevis*). The total amount of cell-associated Cu was normalized as the Cu content per 10^9 cells for each bacterial species. The number of cells was determined by measuring the OD_{600} of 200 μL of this suspension. To determine the amount of cell-associated copper, 1 mL of the suspension was digested with 5 mL of pure HNO_3 for overnight and then was evaporated at 95ºC until no liquid remained. 5% HNO_3 was used to resuspend the sample. Cu content was analyzed using ICP-OES (ICPE-9000, Shimadzu).

Determining bioavailable, intracellular Cu with biosensor strain of *E. coli*

The amount of bioavailable, intracellular Cu was determined using a genetically engineered *E. coli* biosensor strain in which bioluminescence specifically responds to Cu cellular bioavailability (MC1061 pSLcueR/pDNPcopAlux, "Cu-inducible strain"). The luminescent strain was constructed as previously described in Bondarenko *et al*.[16] A colony of the bacteria was inoculated into 3 mL of fresh LB media supplemented with 100 mg/L ampicillin and allowed to grow overnight before being diluted 1:50 using fresh LB media with antibiotic. The culture was allowed to grow to reach log phase (OD_{600} of 0.6) before the cells were harvested for the experiment. Growth was conducted at 30 ºC, shaking at 200 rpm. 25 μL of the Cu species in MMD supplemented with 0.01 mg/mL humic acid were mixed with twenty-five μL of the biosensor bacteria in a 384-well plate to yield a final bacterial OD_{600} of 0.1. The plate was kept at 30 ºC for 2 hours to allow for luminescence induction, at which point the luminescence was quantified using a micro-plate reader (SpectraMax MS, Molecular Devices, CA).

Microscopy of bacterial cells exposed to Cu species

TEM sample preparation and microscopy. *E. coli* cells that had been treated with 0.1 mg/mL Cu species for 24 hours were washed 3 times with phosphate-buffered saline (PBS) before being fixed with 2% glutaraldehyde in 0.1 M PBS. Cells were washed with PBS 3 times before treating with osmium tetroxide (OsO_4) in PBS for 1 hr. After rinsing 3 times with PBS, the cell pellet was dehydrated in a graded series of ethanol (30%, 50%, 70%, 80%, 90%, 95%, and 100% ethanol for two hours each). Propylene oxide was used to remove any residual ethanol before the pellet was embedded in Epon resin (Sigma Aldrich). A Reichert-Jung Ultracut E ultramicrotome was used to cut 100 nm thick sections which were placed onto 1GG200 gold grids (Ted Pell Inc.). Sections were stained with uranyl acetate and Reynolds lead citrate, and examined on an FEI T12 transmission electron microscope operated at 80 kV in the Electron Imaging Center for Nanomachines (EICN) at UCLA.

Electron tomography and 3D reconstruction. *E. coli* cells that had been treated with Cu NPs for 24 hours were washed, dehydrated and embedded in Epon resin as described above. A Reichert-Jung Ultracut E ultramicrotome was used to make 250 nm thick sections from the block, which were placed onto Maxtaform 75/300 Rectangular Mesh copper grids (Ted Pell Inc.). An FEI Tecnai F20 transmission electron microscope was used to capture the tomography tilt series. A Gatan 626 cryo specimen holder was used to collect images in tilt angles ranging from -70º to + 70º, with a 1º increment. The tilt series of 141 images were used to reconstruct 3D volumes using the Etomo tomography processing software in the Imod package (Boulder Laboratory for 3-D Electron Microscopy of Cells).[48]

Confocal microscopy. *E. coli* and *L. brevis* were treated with 50 mg/L of n-FITC-CuO[41] for 24 hours before being washed 3 times with PBS. The bacteria were fixed using 4% paraformaldehyde for 20 minutes at room temperature. After another 3 washes with PBS, the cells were stained with Hoechst 33342, which specifically stains bacterial DNA, yielding blue fluorescence. After 1 hour of incubation with Hoechst dye, the cells were washed 3 times and placed into an 8-well chamber slide (Lab Tek) before being visualized under a confocal microscope (Leica Confocal SP2 1P/FCS). For Hoechst dye, the excitation wavelength used was 358 nm, and E_{max} was monitored at 420-500 nm. For FITC, the excitation wavelength used was 488 nm, and E_{max} was monitored at 520-580 nm.

Safe Handling of Nanomaterials

Nanoparticles as dry powders were handled in a chemical fume hood or powder enclosure, and manipulated while the researcher was wearing a N95 filer mask. After suspension in aqueous solutions, standard good chemical hygiene practices were employed. Sonication can result in aerolization and thus was only performed on solutions that were in closed containers. More detailed recommendations are available in the *Nanotoolkit* developed by the *California Nanosafety Consortium of Higher Education which is available online at:* http://www.cein.ucla.edu/new/p155.php

Supporting information of **Chapter 3** is found in **Appendix 2** which contains the growth inhibition effects of Cu species in *E. coli* and *L. brevis* (**Figure A2.1**), Individual growth inhibition curve including error bars for each of the Cu species (**Figure A2.2**), Area under growth-inhibition curve for Cu species in *E. coli* and *L. brevis* (**Figure A2.3**), Sucrose gradient centrifugation procedure (**Figure A2.4**), Standard curve of OD_{600} and total number of cells

(**Figure A2.5**), Cu bioavailability determined using bacterial biosensor strain (**Figure A2.6**), DNA damage assay (**Figure A2.7**), and Confocal images of cells treated with n-FITC-CuO (**Figure A2.8**). Tables of data include: Sources of Cu particles (**Table A2.1**), Correlation coefficients for area under the growth inhibition curve and amounts of dissolved copper in media, cell-associated Cu, and Cu bioavailable in each of the bacterial species (**Table A2.2**), and Correlation between results from growth inhibition assays and results from the suite of sub-lethal assays (**Table A2.3**).

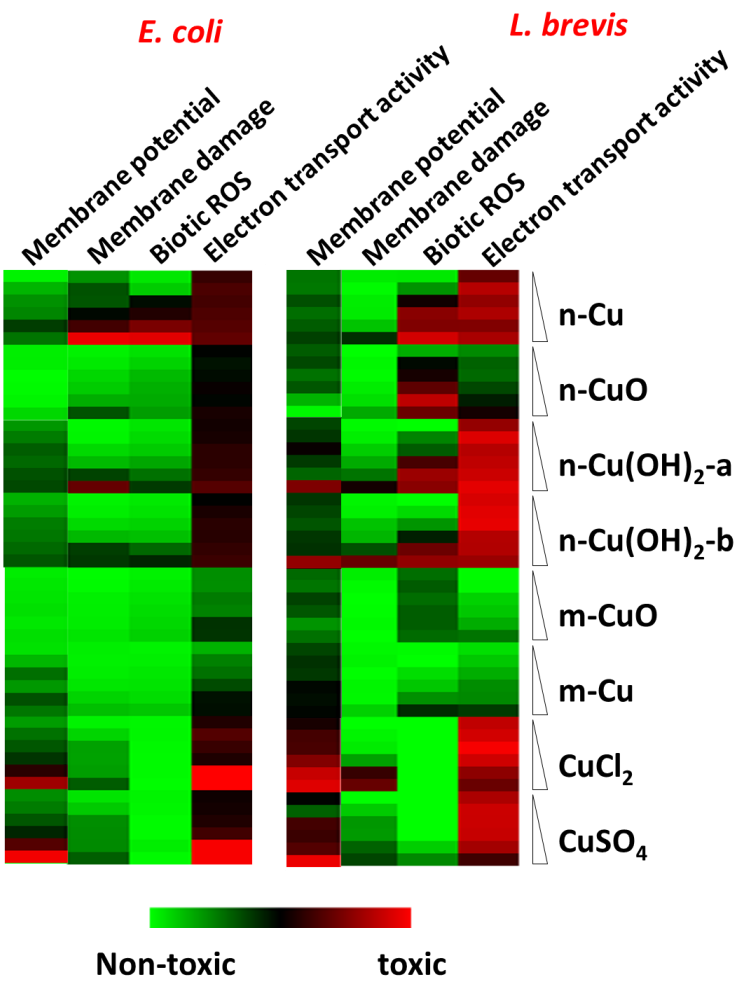

Figure 3.1. A suite of sub-lethal assays was used to elucidate the mechanisms of toxicity of the Cu species. Cells were treated with Cu particles ranging from 2-250 mg/L for 24 hours before being treated with DiBAC, PI/SYTO, H_2DCFDA or XTT to assess membrane potential, membrane damage, biotic ROS generation or electron transport chain activity, respectively. Red indicates similarity for each treatment to the positive controls (NaN_3, Ethanol, H_2O_2 and CCCP for membrane potential, membrane damage, cellular ROS generation and electron transport activity assays, respectively), whereas green indicates the degree of similarity for each treatment

to the negative controls (PBS alone). At least three biological replicates were performed at each concentration for each assay.

A

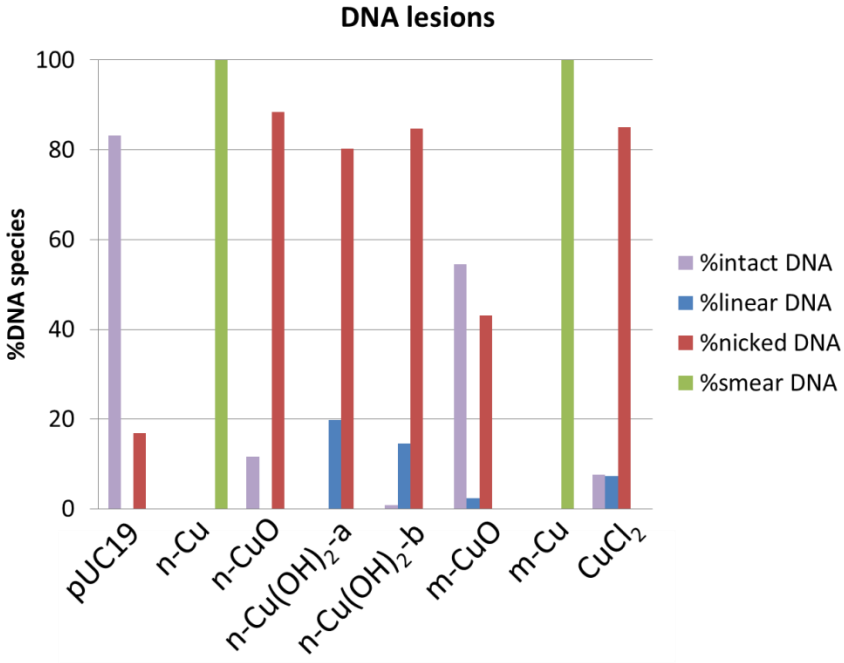
DNA lesions
%DNA species
100
80
60
40
20
0
pUC19
n-Cu
n-CuO
n-Cu(OH)2-a
n-Cu(OH)2-b
m-CuO
m-Cu
CuCl2
%intact DNA
%linear DNA
%nicked DNA
%smear DNA

B

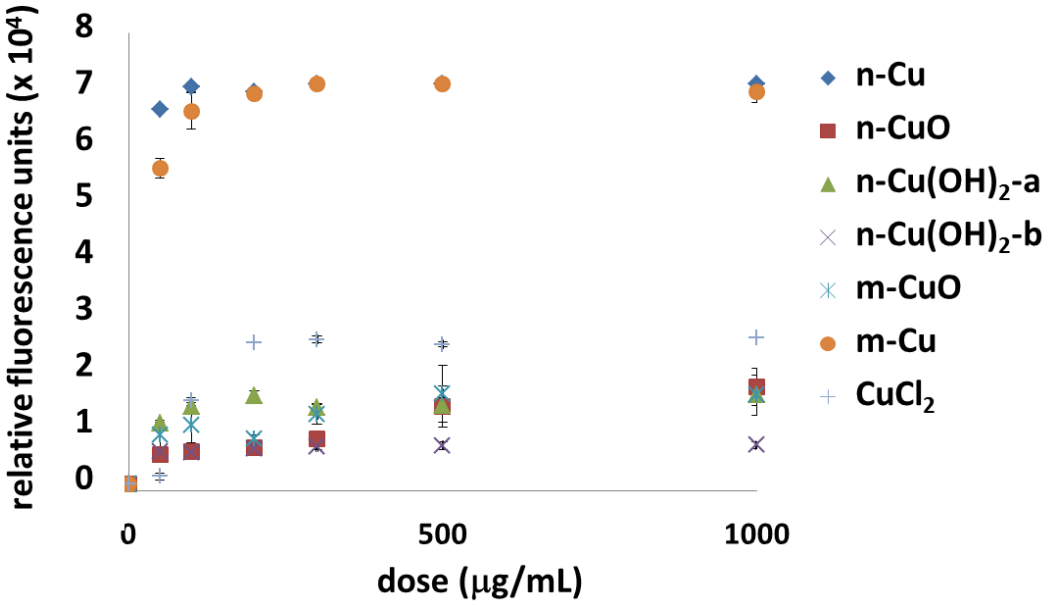
relative fluorescence units (x 10⁴)
8
7
6
5
4
3
2
1
0
0
500
1000
dose (μg/mL)
n-Cu
n-CuO
n-Cu(OH)2-a
n-Cu(OH)2-b
m-CuO
m-Cu
CuCl2

Figure 3.2. Quantification of DNA damage assay and abiotic ROS generation. (A) Plasmid DNA (pUC19) was incubated with Cu species for 24 hours and the resulting plasmid DNA was separated using gel electrophoresis. DNA lesions were classified into 3 categories; 1) linear DNA (plasmid DNA with a double-strand break) 2) nicked DNA (plasmid DNA with single-strand breaks) 3) smeared/fragmented DNA (plasmid DNA with multiple single/double-strands breaks). In the case of the negative control (plasmid used as purchased), the majority of the plasmid is supercoiled DNA and 10-20% of the DNA is in a single-stranded nicked form. Only n-Cu and m-Cu led to a complete degradation of plasmid DNA, appearing as smeared band in the gel (**Figure A2.6** in **Appendix 2**) (B) The capability of each particle to generate reactive oxygen species (ROS) was tested *in vitro* using (2',7' –dichlorofluorescein) DCFH. The particles were treated with DCFH for 2 hours and the fluorescence intensity, which reflects the extent of oxidation, was measured using excitation/emission wavelengths of 530/630 nm. Three replicates were performed at each concentration of each Cu species.

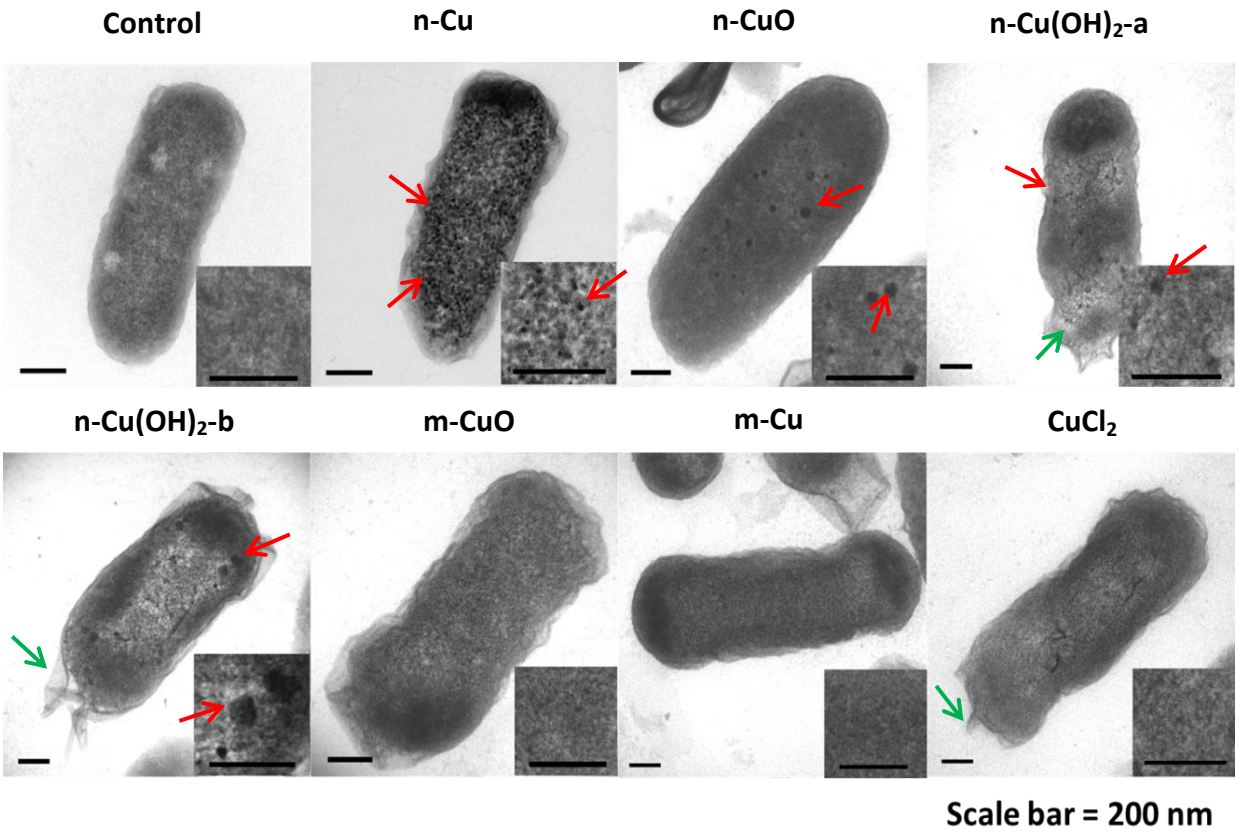

Figure 3.3. TEM images of *E. coli* cells treated with Cu species. Cells were treated with 0.1 mg/mL of the Cu particles for 24 hours before being washed, embedded in resin and negatively stained before being imaged by TEM. Red arrows indicate Cu particles; green arrows indicate membrane damage. Particles-associated with cells were observed in cells treated with nano-sized particles (n-Cu, n-CuO, n-$Cu(OH)_2$-a and n-$Cu(OH)_2$-b).

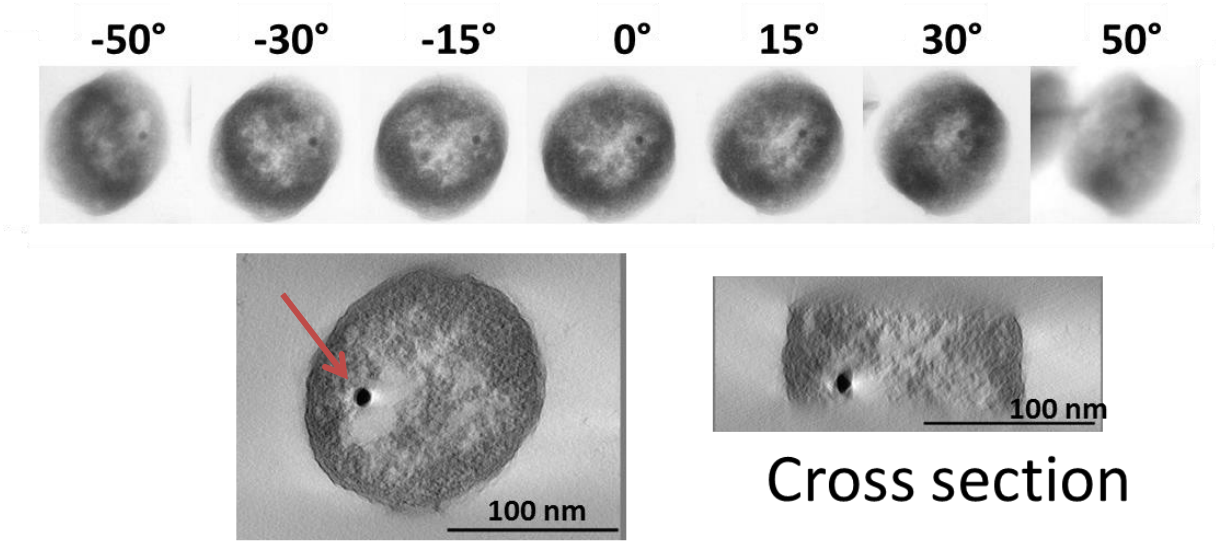

Figure 3.4. Electron tomography 3D construction reveals the presence of intact Cu nanoparticles inside *E. coli* cells. Cells were treated with 0.1 mg/mL of n-Cu for 24 hours before being embedded in the resin, sectioned and stained (see Methods). A tilt series of 141 images was recorded by tilting the sample one degree at a time from -70^0 to $+70^0$ and used to construct a 3D tomogram of the sectioned cell. Example images in the tilt series (top panel) and two orthogonal slabs in the 3D tomogram are shown in the bottom panel, showing a single nano particle inside the cell (black dot).

Table 3.1. Zeta potential, particle size and hydrodynamic diameter of Cu particles in purified water and bacterial media

particles	Zeta potential (mV)	Primary size (nm)[a]	Average Hydrodynamic Diameter (nm)[c]				
			Purified Water	MMD + HA[d]		Lactobacilli media	
				0 hr	24 hr	0 hr	24 hr
n-Cu	-46.3 ± 1.6	200-1000	1200 ± 200	1100 ± 200	1400 ± 300	1600 ± 500	1400 ± 500
n-CuO	-16.5 ± 0.8	20-100	420 ± 20	300 ± 2	460 ± 10	470 ± 4	1600 ± 300
n-$Cu(OH)_2$-a	-45.1 ± 0.8	10	900 ± 200	270 ± 1	300 ± 10	390 ± 10	400 ± 30
n-$Cu(OH)_2$-b	-53.8 ± 0.7	N/A[b]	1400 ± 100	240 ± 2	250 ± 10	280 ± 1	290 ± 2
m-CuO	-28.5 ± 0.9	200-2000	1300 ± 200	1300 ± 500	1500 ± 600	N/A[e]	N/A[e]
m-Cu	-32.5 ± 2.9	>10,000	N/A[e]	N/A[e]	N/A[e]	N/A[e]	N/A[e]

[a] primary sizes were measured by TEM, n = 100

[b] primary size cannot be obtained because particles are of undefined morphology

[c] Standard error was measured from 3 experiments

[d] HA = humic acid, which was added as a stabilizing agent

[e] N/A indicates that particles size exceeds instrumentation range (0.3 nm – 3 μM) according to the manufacturer of the Dynamic Light Scattering machine.

Table 3.2. IC_{50} values, % Cu ion dissolution, amount of cell-associated Cu and % Cu bioavailable for different Cu species

NPs	*E. coli* IC_{50} (μg/mL)	*L. brevis* IC_{50} (μg/mL)	%Cu ion dissolution *in vitro*			Cu associated with cells by sucrose gradient centrifugation (ppm/10^9 cells)		% Cu bioavailable (*E. coli* biosensor)
			water	*E. coli* media	*L. brevis* media	*E. coli*	*L. brevis*	
$CuCl_2$	38 ± 8	7.8 ± 0.5	100	100	100	N/A[a]	N/A[a]	100
$CuSO_4$	140 ± 23	24 ± 3	100	100	100	N/A[a]	N/A[a]	--
n-Cu	120 ± 14	5.7 ± 0.2	0.1 ± 0.0	9.9 ± 0.4	20.7 ± 0.4	10.4 ± 0.1	10.5 ± 0.3	100
n-CuO	160 ± 17	3.6 ± 0.1	0.0 ± 0.0	7.5 ± 0.1	10.9 ± 0.1	4.3 ± 0.1	3.9 ± 0.1	70
n-$Cu(OH)_2$-a	>250	4.0 ± 0.1	2.7 ± 0.1	9.9 ± 0.6	21.8 ± 0.6	8.3 ± 0.3	5.4 ± 0.1	17.5
n-$Cu(OH)_2$-b	>250	6.2 ± 0.9	5.4 ± 0.2	10.8 ± 0.6	17.9 ± 0.6	8.0 ± 0.4	5.6 ± 0.1	--
m-CuO	>250	>250	0.0 ± 0.0	2.9 ± 0.3	3.3 ± 0.3	1.2 ± 0.0	0.9 ± 0.0	4.4
m-Cu	>250	120 ± 24	0.1 ± 0.0	2.1 ± 0.8	5.6 ± 0.8	0.4 ± 0.0	1.5 ± 0.1	10.9

[a] NA = not applicable, because it was not possible to separate ionic Cu from bacterial cells using sucrose gradient centrifugation.

REFERENCES

1. Pham, L. Q.; Sohn, J. H.; Kim, C. W.; Park, J. H.; Kang, H. S.; Lee, B. C.; Kang, Y. S., Copper nanoparticles incorporated with conducting polymer: Effects of copper concentration and surfactants on the stability and conductivity. *J. Colloid Interf. Sci.* **2012,** *365*, 103-109.

2. Saterlie, M.; Sahin, H.; Kavlicoglu, B.; Liu, Y. M.; Graeve, O., Particle size effects in the thermal conductivity enhancement of copper-based nanofluids. *Nanoscale Res. Lett.* **2011,** *6*, 217-223.

3. Almeida, E.; Diamantino, T. C.; de Sousa, O., Marine paints: The particular case of antifouling paints. *Prog. Org. Coat.* **2007,** *59*, 2-20.

4. Ren, G. G.; Hu, D. W.; Cheng, E. W. C.; Vargas-Reus, M. A.; Reip, P.; Allaker, R. P., Characterisation of copper oxide nanoparticles for antimicrobial applications. *Int. J. Antimicrob. Ag.* **2009,** *33*, 587-590.

5. Melegari, S. P.; Perreault, F.; Costa, R. H. R.; Popovic, R.; Matias, W. G., Evaluation of toxicity and oxidative stress induced by copper oxide nanoparticles in the green alga Chlamydomonas reinhardtii. *Aquat. Toxicol.* **2013,** *142*, 431-440.

6. Mwaanga, P.; Carraway, E. R.; van den Hurk, P., The induction of biochemical changes in Daphnia magna by CuO and ZnO nanoparticles. *Aquat. Toxicol.* **2014,** *150*, 201-9.

7. Gomes, T.; Pinheiro, J. P.; Cancio, I.; Pereira, C. G.; Cardoso, C.; Bebianno, M. J., Effects of copper nanoparticles exposure in the mussel Mytilus galloprovincialis. *Environ. Sci. Technol.* **2011,** *45*, 9356-62.

8. Griffitt, R. J.; Weil, R.; Hyndman, K. A.; Denslow, N. D.; Powers, K.; Taylor, D.; Barber, D. S., Exposure to copper nanoparticles causes gill injury and acute lethality in zebrafish (Danio rerio). *Environ. Sci. Technol.* **2007,** *41*, 8178-86.

9. Dasari, T. P.; Pathakoti, K.; Hwang, H. M., Determination of the mechanism of photoinduced toxicity of selected metal oxide nanoparticles (ZnO, CuO, Co3O4 and TiO2) to E. coli bacteria. *J. Environ. Sci.-China* **2013,** *5*, 882-8.

10. Mancuso, L.; Cao, G., Acute toxicity test of CuO nanoparticles using human mesenchymal stem cells. *Toxicol. Mech. Method.* **2014,** *24*, 449-54.

11. Zhang, H. Y.; Ji, Z. X.; Xia, T.; Meng, H.; Low-Kam, C.; Liu, R.; Pokhrel, S.; Lin, S. J.; Wang, X.; Liao, Y. P., et al., Use of Metal Oxide Nanoparticle Band Gap to Develop a Predictive Paradigm for Oxidative Stress and Acute Pulmonary Inflammation. *ACS Nano* **2012,** *6*, 4349-4368.

12. Xiu, Z. M.; Zhang, Q. B.; Puppala, H. L.; Colvin, V. L.; Alvarez, P. J., Negligible particle-specific antibacterial activity of silver nanoparticles. *Nano Lett.* **2012,** *12*, 4271-5.

13. McQuillan, J. S.; Shaw, A. M., Differential gene regulation in the Ag nanoparticle and Ag(+)-induced silver stress response in Escherichia coli: a full transcriptomic profile. *Nanotoxicology* **2014,** *8* 177-84.

14. Ivask, A.; Elbadawy, A.; Kaweeteerawat, C.; Boren, D.; Fischer, H.; Ji, Z.; Chang, C. H.; Liu, R.; Tolaymat, T.; Telesca, D., et al., Toxicity Mechanisms in Escherichia coli Vary for Silver Nanoparticles and Differ from Ionic Silver. *ACS Nano* **2014,** *8*, 374-86.

15. Wang, Z.; Liu, S.; Ma, J.; Qu, G.; Wang, X.; Yu, S.; He, J.; Liu, J.; Xia, T.; Jiang, G. B., Silver nanoparticles induced RNA polymerase-silver binding and RNA transcription inhibition in erythroid progenitor cells. *ACS Nano* **2013,** *7*, 4171-86.

16. Bondarenko, O.; Ivask, A.; Kakinen, A.; Kahru, A., Sub-toxic effects of CuO nanoparticles on bacteria: kinetics, role of Cu ions and possible mechanisms of action. *Environ. Pollut.* **2012,** *169*, 81-9.

17. Dimkpa, C. O.; McLean, J. E.; Britt, D. W.; Johnson, W. P.; Arey, B.; Lea, A. S.; Anderson, A. J., Nanospecific inhibition of pyoverdine siderophore production in Pseudomonas chlororaphis O6 by CuO nanoparticles. *Chem. Res. Toxicol.* **2012,** *25*, 1066-74.

18. Rossetto, A. L.; Melegari, S. P.; Ouriques, L. C.; Matias, W. G., Comparative evaluation of acute and chronic toxicities of CuO nanoparticles and bulk using Daphnia magna and Vibrio fischeri. *Sci. Total Environ.* **2014,** *490*, 807-14.

19. Azam, A.; Ahmed, A. S.; Oves, M.; Khan, M. S.; Habib, S. S.; Memic, A., Antimicrobial activity of metal oxide nanoparticles against Gram-positive and Gram-negative bacteria: a comparative study. *Int. J. Nanomed.* **2012,** *7*, 6003-9.

20. Kaeseberg, T.; Blumensaat, F.; Zhang, J.; Krebs, P., Assessing antibiotic resistance of microorganisms in sanitary sewage. *Water Sci. Technol.* **2015,** *71*, 168-73.

21. Marcus, I. M.; Wilder, H. A.; Quazi, S. J.; Walker, S. L., Linking Microbial Community Structure to Function in Representative Simulated Systems. *Appl. Environ. Microb.* **2013,** *79*, 2552-9.

22. Kato, H.; Fujita, K.; Horie, M.; Suzuki, M.; Nakamura, A.; Endoh, S.; Yoshida, Y.; Iwahashi, H.; Takahashi, K.; Kinugasa, S., Dispersion characteristics of various metal oxide secondary nanoparticles in culture medium for in vitro toxicology assessment. *Toxicol. In Vitro* **2010,** *24*, 1009-1018.

23. Adeleye, A. S.; Conway, J. R.; Perez, T.; Rutten, P.; Keller, A. A., Influence of Extracellular Polymeric Substances on the Long-Term Fate, Dissolution, and Speciation of Copper-Based Nanoparticles. *Environ. Sci. Technol.* **2014,** *48*, 12561-8.

24. Andreazza, R.; Okeke, B. C.; Pieniz, S.; Bento, F. M.; Camargo, F. A. O., Biosorption and Bioreduction of Copper from Different Copper Compounds in Aqueous Solution. *Biol. Trace Elem. Res.* **2013,** *152*, (3), 411-416.

25. Szymonska, J.; Wieczorek, J.; Molenda, M.; Bielanska, E., Uptake of Cu2+ by starch granules as affected by counterions. *J. Agr. Food. Chem.* **2008,** *56*, (11), 4054-4059.

26. GHS, Globally Harmonized System for the classification and labelling of chemicals. **2013**.

27. Haggstrom, J. A.; Klabunde, K. J.; Marchin, G. L., Biocidal properties of metal oxide nanoparticles and their halogen adducts. *Nanoscale* **2010,** *2*, 399-405.

28. Gaber, M.; El-Ghamry, H. A.; Fathalla, S. K., Ni(II), Pd(II) and Pt(II) complexes of (1H-1,2,4-triazole-3-ylimino)methyl]naphthalene-2-ol. Structural, spectroscopic, biological, cytotoxicity, antioxidant and DNA binding. *Spectrochim. Acta. A.* **2014,** *139C*, 396-404.

29. Lo Giudice, A.; Casella, P.; Bruni, V.; Michaud, L., Response of bacterial isolates from Antarctic shallow sediments towards heavy metals, antibiotics and polychlorinated biphenyls. *Ecotoxicology* **2013,** *22*, 240-50.

30. Taylor, R., Interpretation of the Correlation-Coefficient - a Basic Review. *J. Diagn. Med. Sonog.* **1990,** *6*, 35-39.

31. Gaetke, L. M.; Chow, C. K., Copper toxicity, oxidative stress, and antioxidant nutrients. *Toxicology* **2003,** *189*, 147-63.

32. Li, F.; Lei, C.; Shen, Q.; Li, L.; Wang, M.; Guo, M.; Huang, Y.; Nie, Z.; Yao, S., Analysis of copper nanoparticles toxicity based on a stress-responsive bacterial biosensor array. *Nanoscale* **2013,** *5*, 653-62.

33. Kasemets, K.; Suppi, S.; Kunnis-Beres, K.; Kahru, A., Toxicity of CuO nanoparticles to yeast Saccharomyces cerevisiae BY4741 wild-type and its nine isogenic single-gene deletion mutants. *Chem. Res. Toxicol.* **2013,** *26*, 356-67.

34. Liu, Y.; Gao, Y.; Liu, Y.; Li, B.; Chen, C.; Wu, G., Oxidative stress and acute changes in murine brain tissues after nasal instillation of copper particles with different sizes. *J. Nanosci. Nanotechno.* **2014,** *14*, 4534-40.

35. Ciapaite, J.; Nauciene, Z.; Baniene, R.; Wagner, M. J.; Krab, K.; Mildaziene, V., Modular kinetic analysis reveals differences in Cd2+ and Cu2+ ion-induced impairment of oxidative phosphorylation in liver. *FEBS. J.* **2009,** *276*, 3656-68.

36. Leba, L. J.; Brunschwig, C.; Saout, M.; Martial, K.; Vulcain, E.; Bereau, D.; Robinson, J. C., Optimization of a DNA nicking assay to evaluate Oenocarpus bataua and Camellia sinensis antioxidant capacity. *Int. J. Mol. Sci.* **2014,** *15*, 18023-39.

37. https://www.lifetechnologies.com/order/catalog/product/SD0061?ICID=search-product (accessed March 9, 2015)

38. Chin, R. M.; Fu, X.; Pai, M. Y.; Vergnes, L.; Hwang, H.; Deng, G.; Diep, S.; Lomenick, B.; Meli, V. S.; Monsalve, G. C., et al., The metabolite alpha-ketoglutarate extends lifespan by inhibiting ATP synthase and TOR. *Nature* **2014,** *510*, 397-401.

39. Kumbicak, U.; Cavas, T.; Cinkilic, N.; Kumbicak, Z.; Vatan, O.; Yilmaz, D., Evaluation of in vitro cytotoxicity and genotoxicity of copper-zinc alloy nanoparticles in human lung epithelial cells. *Food Chem. Toxicol.* **2014,** *73C*, 105-112.

40. Kumar, A.; Pandey, A. K.; Singh, S. S.; Shanker, R.; Dhawan, A., A flow cytometric method to assess nanoparticle uptake in bacteria. *Cytom. Part A* **2011,** *79*, 707-12.

41. Li, R.; Ji, Z.; Chang, C. H.; Dunphy, D. R.; Cai, X.; Meng, H.; Zhang, H.; Sun, B.; Wang, X.; Dong, J., et al., Surface interactions with compartmentalized cellular phosphates explain rare earth oxide nanoparticle hazard and provide opportunities for safer design. *ACS Nano* **2014,** *8*, 1771-83.

42. Kaweeteerawat, C.; Ivask, A.; Liu, R.; Zhang, H.; Chang, C. H.; Low-Kam, C.; Fischer, H.; Ji, Z.; Pokhrel, S.; Cohen, Y., et al., Toxicity of metal oxide nanoparticles in Escherichia coli correlates with conduction band and hydration energies. *Environ. Sci. Technol.* **2015,** *49*, (2), 1105-12.

43. https://tools.lifetechnologies.com/content/sfs/manuals/mp07007.pdf (accessed March 9, 2015).

44. Wickens, H. J.; Pinney, R. J.; Mason, D. J.; Gant, V. A., Flow cytometric investigation of filamentation, membrane patency, and membrane potential in Escherichia coli following ciprofloxacin exposure. *Antimicrob. Agents Ch.* **2000,** *44*, (3), 682-7.

45. Hatzinger, P. B.; Palmer, P.; Smith, R. L.; Penarrieta, C. T.; Yoshinari, T., Applicability of tetrazolium salts for the measurement of respiratory activity and viability of groundwater bacteria. *J. Microbiol. Meth.* **2003,** *52*, 47-58.

46. Singh, U.; Akhtar, S.; Mishra, A.; Sarkar, D., *J. Microbiol. Meth.* **2011,** *84*, 202-7.

47. Berk, S. G.; Guerry, P.; Colwell, R. R., Separation of small ciliate protozoa from bacteria by sucrose gradient centrifugation. *Appl. Environ. Microbiol.* **1976,** *31*, (3), 450-2.

48. Alexander, J. W., History of the Medical Use of Silver. *Surg. Infect.* **2009,** *10*, (3), 289-292.

CHAPTER 4

Genome-Wide Gene Expression Analysis Reveals That Cationic Silver Nanoparticles and Ionic Silver Up and Down Regulate Different Pathways

ABSTRACT

There has been considerable debate in the scientific literature about whether some metal nanoparticles are toxic simply because they are an efficient source of toxic metals ions or whether nanoparticles exhibit different mechanisms of toxicity that are related to their size. To inform this debate, we used microarray studies (Affymetrix *E.coli* genome 2.0 arrays) to compare the impacts of a cationic silver nanoparticle (Ag-BPEI) with those of silver ions (Ag^+) on gene expression across the entire genome of the bacterium *E. coli*. The microarray analyses revealed that exposure to Ag-BPEI leads primarily to up-regulation of oxidative homeostatic and cellular stress response pathways, including gene involved in heat shock response. By contrast, exposure to Ag^+ leads to up-regulation of cell wall and cell membrane biosynthesis and genes encoding cation-binding proteins. Taken together, these studies demonstrate that Ag-BPEI results in up and down regulation of different pathways than Ag^+ after exposure to 2 mg/L of silver species for two hours.

INTRODUCTION

Silver nanoparticles (Ag NPs) are an important class of nanomaterials, largely due to their outstanding antibacterial properties.[1] Silver has been used as an antimicrobial agent for over a thousand years: the first clear record of silver being used as an antimicrobial agent was in 702-705 A.D. and 980 A.D., where it was used as a blood purifier and to prevent palpitations.[2] In modern times, silver products have been registered as pesticides under the Federal Insecticide, Fungicide, and Rodenticide Act (FIFRA) since the 1950's.[3] Recent studies on silver nanoparticles have revealed that these materials can have superior properties to ionic silver for antimicrobial applications.[4] Ag NP-containing products include odor resistant textiles, food storage containers, antiseptic sprays, wound-dressings and bandages.[5] A key question that has arisen in the literature is whether Ag NPs constitute "new" toxic substances (which would then be subject to stricter regulatory oversight) or whether they are simply a new mechanism for delivering an old toxic substance, namely Ag^+.[6] In March 2015, based on a comprehensive review of the literature, the EPA released a statement indicating that it would, at least for the time being, review applications for registration of pesticide products containing nanosilver as "new" materials (*i.e.*, distinct from ionic silver).[6] Given this decision, additional information about the mechanisms of toxicity of Ag NPs, particularly in bacteria, can prove useful for future regulatory review of these materials.

We recently reported that a series of Ag NPs (Ag-BPEI, Ag-PVP, Ag-cit_{10}, Ag-cit_{20}, and Ag-cit_{40}) and ionic silver (Ag^+) each have different effects when they are examined in the context of their impacts on a genome-wide library of single-gene deletion mutants (GDS) of *E. coli*.[7] Specifically, we reported that the ensemble of effects of each Ag species could be represented using a self-organizing maps (SOMs) that display which gene deletion strains have increased

sensitivity to each Ag species. Through this analysis, we demonstrated that the most toxic Ag NP in the series that we studied, the cationic particle Ag-BPEI, exhibited a "fingerprint" of toxicity (represented by the SOM of sensitive gene clusters) that was more similar to the SOM for a cationic polystyrene nanoparticle (PS-NH_2) than it was to that of the SOM for either Ag^+ or any of the other Ag NPs (Ag-PVP, Ag-cit_{10}, Ag-cit_{20}, and Ag-cit_{40}).[7]

However, there are limitations of this approach used in our prior study on gene deletion strains, including that (1) the library of gene deletion strains does not include deletions of essential genes and hence only represents a portion of the *E. coli* genome (3,985 of 4,288 genes)[8] and (2) due to limitations in the amount of Ag NPs available (and the high cost of these materials), we were only able to focus on genes that, when deleted, resulted in *increased* sensitivity and not those that resulted in *decreased* sensitivity. In addition, a number of studies have demonstrated that phenotypic studies on gene deletion strains only provide a partial picture of global toxicity and that the results from studies on gene deletion strains are well complemented by results from microarray studies.[9] To address these gaps, we report herein a comparison of the impacts of a cationic Ag nanoparticle, Ag-BPEI, and Ag^+ using microarray analysis. These results indicate that while the cationic Ag NP and Ag^+ share some effects on *E. coli* physiology, they result in different patterns of gene expression and confirm our a priori observation that Ag-BPEI and Ag^+ exhibit distinct mechanisms of toxicity.

MATERIALS AND METHODS

Chemicals and nanoparticles

Media components

Bacterial growth media (Luria-Bertani, LB, Lennox) was purchased from EMD Chemicals (Merck, Darmstadt, Germany); the pH of the final media was adjusted to 7.0 using NaOH. All assays of *E. coli* were conducted in environmentally-relevant media: Modified Minimal Davis, MMD media (1 L H_2O: 0.7 g K_2HPO_4; 0.2 g KH_2PO_4; 0.66 g $(NH_4)_2SO_4$; 0.5 g sodium citrate; 0.1 g $MgSO_4 \bullet 7H_2O$; 3.31g D-glucose, pH 6.9). PBS (pH 7.4) was from GIBCO (Invitrogen, CA, USA). Purified water used in all of the experiments consisted of deionized (DI) water that was passed through an Aqua Solutions water purification machine, model RODI-C-12BL (TX, USA).

Nanoparticles

Branched polyethyleneimine (BPEI) stabilized AgNPs (Ag-BPEI) was synthesized in our laboratory as described previously.[7] All the Ag NPs were prepared and stored in liquid state. For dispersion of Ag-BPEI in bacterial (MMD) media, humic acid (HA) at the final concentration of 0.01 mg/mL was used as a dispersing agent. The mixture was then sonicated for 15 minutes in a water bath (Branson 2510, CT, USA). Hydrodynamic diameter (D_h) and Zeta potential of the series of Ag-BPEI as measured by a high-throughput DLS instrument (Wyatt Technology Corporation, CA, US) and ZetaPALS Zeta Potential Analyzer (Brookhaven Instruments Ltd, UK) respectively was analyzed as reported previously.[7]

Microarray analysis

A stock solution of either Ag-BPEI or $AgNO_3$ in purified water was added to a 100 mL sample of *E. coli* that had been grown to mid-log phase (OD_{600} ~ 0.5) in MMD media to yield a final concentration of the silver species of 2 mg/mL. Viability and cell number were checked using colony forming units (CFUs). After 2 hours, cells were harvested and washed 3 times with PBS. Pellets of cells were kept at -80 ºC before RNA extraction. RNA was isolated using an automated nucleic acid purification machine (MagNA Pure Compact machine, Roche, IN) together with RNA isolation kits (MagNA Pure Compact RNA Isolation Kit, Roche, IN). Concentrations of the isolated RNA were measured by a spectrophotometer (Nanodrop ND-8000, Thermo Scientific, DE). Quality of the RNA was assessed using Agilent's 2100 Bioanalyzer (Agilent technologies. Inc. CA). Amplification, labeling and fragmentation of the RNA were achieved using an RNA Amplification Kit (Ambion messageAmpPremier, Life Technologies, NY, ref 4383452). Hybridization of the gene chips (Affymetrix *E.coli* genome 2.0 arrays) were conducted in the Affymetrix GeneChip Hybridization oven 645 (Affymetrix, CA). After that, the arrays were washed using automated Affymetrix Fluidics Station 450 and scanned using Affymetrix Gene Chip Scanner 3000. Data was extracted using Affymetrix Expression Console v 1.2.0.20.

The level of gene expression was calculated from the Affymetrix GeneChip probe level data using the function "rma" from the R library "affy". The significantly expressed genes ($p<0.05$) relative to controls were identified using linear mode fitting (via "lmFit" function of a R library "limma") along with empirical Bayes statistics (via eBayes function of "limma" library) and p-value adjustment for multiple test using the Benjamini-Hochberg (BH) method to control the false discovery rate under positive dependence assumptions.[10]

Gene functional classification

The significantly up-regulated or down-regulated genes identified by microarray analysis were clustered using the DAVID database (http://david.abcc.ncifcrf.gov) to reveal functional relationships and significant pathways responding to the Ag treatments.[11] High classification stringency (similarity threshold 0.5, multiple linkage threshold 0.5, group membership 5) was used in the analysis.

RESULTS AND DISCUSSION

Analysis of genome-wide gene expression in response to Ag NPs and ionic Ag

To thoroughly understand the bacterial response to silver nanoparticles compared to $AgNO_3$, gene expression responses in *E. coli* were determined using microarray analysis. We chose to perform the gene expression studies on the cationic silver nanoparticle Ag-BPEI, which we had previously found to be both the most toxic and to exhibit the most different toxicity mechanisms from Ag^+ out of a series of Ag NPs studied previously (Ag-BPEI, Ag-PVP, Ag-cit_{10}, Ag-cit_{20}, and Ag-cit_{40}).[7] Here, exponential phase *E. coli* cultures (OD_{600} = 0.5) were grown for 2 hours in the presence of 2 mg/mL of either Ag-BPEI NPs or $AgNO_3$ (or no added silver, for the negative controls) and the RNA from each of the samples was extracted. A concentration of 2 mg/mL of silver was selected because it is comparable to the IC_{50} of both silver species (IC_{50} of Ag-BPEI = 2.2 mg/mL; IC_{50} of $AgNO_3$ = 2.0 mg/mL).[7] The extracted mRNA from each sample was converted to cDNA and analysed for changes in gene expression using Affymetrix *E. coli* genome 2.0 arrays, which include approximately 10,000 probes and cover the entire bacterial genome.[12] Genes that were found to be significantly ($p < 0.05$) up- or down-regulated in

the presence of either Ag-BPEI and/or $AgNO_3$ compared to control cells are depicted in the heat map shown in **Figure 4.1.** A complete list of genes that were found to be significantly ($p < 0.05$) up-regulated or down-regulated in the presence of Ag-BPEI and/or $AgNO_3$ is provided in **Table A3.1** in **Appendix 3**. In the presence of Ag-BPEI, 76 and 219 genes were observed to be significantly up-regulated and down-regulated, respectively, compared to the negative control (no silver added). By contrast, 359 and 121 genes were found to be significantly up-regulated and down-regulated, respectively, upon treatment with $AgNO_3$. Interestingly, 47 genes were found to be up-regulated both in the presence of Ag-BPEI and $AgNO_3$ and 61 genes were found to be down-regulated in the presence of both of the silver species (**Figure 4.2A**). The result suggests that Ag-BPEI regulate gene expressions that are different from $AgNO_3$. Among the genes found to be up-regulated both in the presence of Ag-BPEI and in the presence of $AgNO_3$ were *copA* (which encodes for a copper-exporting P-type ATPase)[13] and *cueO* (which encodes a multi-copper oxidase that confers copper tolerance),[14] both of which been shown previously to be important for conferring resistance to silver ions in *E. coli*.[15] This finding is consistent with a previously published microarray study on the impacts of Ag^+ on *E. coli,* which stated that copper resistance ORFs (including c*opA* and *cueO*) were significantly upregulated when the bacteria were challenged with Ag ions.[16] In addition, these results are consistent with those reported for prior microarray study on the impacts of a different silver nanoparticle on gene expression in *E. coli* exposure to Ag NPs, in which changes in the expression of genes involved in Cu homeostasis (Cu stress response) were also observed.[17]

Cellular pathways significantly affected by Ag NPs and ionic Ag

To understand the cellular pathways affected by Ag-BPEI NPs and $AgNO_3$, gene ontology (GO) analysis was used to group genes which were observed to be significantly up- or

down-regulated in response to either Ag-BPEI or ionic Ag compared to the negative (untreated) control. Using this approach, we were able to identify those functional pathways important for the cellular response to Ag-BPEI and $AgNO_3$, respectively (**Table 4.1).** The cellular processes that were most significantly up-regulated when the cells were treated with Ag-BPEI based on the Database for Annotation, Visualization and Integrated Discovery (DAVID) program were ribosomal protein/ribonucleoprotein complexes, heat shock protein/stress response/molecular chaperone, metal-binding/cation binding and oxidative stress/cell redox homeostasis response. The processes that were down-regulated most significantly in the presence of Ag-BPEI included transcription regulation/DNA binding protein, cold shock protein, fatty acid metabolism and cellular respiration. These results suggest that exposure of bacterial cells to Ag-BPEI leads to activation of cellular stress response including oxidative stress and chaperone/heat shock pathways and Cu homeostasis pathways, whereas energy generating processes and cold shock pathways were down-regulated. This result is consistent with a prior study by McQuillan *et al*. who reported that exposure to a different type of Ag NPs (with no surface ligand) lead to significant regulation of gene expression for heat shock response genes and Cu stress response in *E. coli* (as shown by microarray analysis).[17] Up-regulated pathways we observed for *E. coli* exposed to $AgNO_3$ (Ag^+) treatment included ribonucleoprotein complex biogenesis, peptidoglycan/cell wall, oxidative phosphorylation/ATP synthesis, metal binding/cation binding proteins. Pathways that we observed to be down-regulated in the presence of $AgNO_3$ were lipoprotein, starch and sucrose metabolism, and purine and nucleoside biosynthesis. The results we observed for Ag^+ are consistent with those reported in a previous study in *Arabidopsis thalina* in which it was observed that exposure to Ag^+ leads to changes in the level of expression of genes involved in metabolic process, cellular organization or biogenesis and metal binding

process.[18] The result and the findings reported herein suggest that treatment of cells with $AgNO_3$ results in increases in the synthesis of cell wall subunits and metal-binding proteins, possibly to chelate excess silver ions and results in decreased levels of the metabolism of sugar, lipid and nucleic acid. Interestingly, the finding that exposure to Ag-BPEI lead to regulation of gene expression that overlap only partially which those observed for $AgNO_3$ exposure, is consistent with previous results of microarray analysis in *E. coli*[17] suggesting that the type of silver (nanoparticle versus ionic Ag) plays an important role in determining the mechanisms of toxicity in *E. coli*.

It is important to note that we intentionally performed the microarray analyses reported herein after treating the bacterial cells with 2 mg/mL Ag-BPEI or $AgNO_3$ for 2 hours to study the "early" or "first" response of the bacteria to the silver insults in the interest of determining the primary toxic pathways as well as the principal defense mechanisms of the bacteria. By contrast, earlier study of gene expression analysis in the presence of AgNPs in *E. coli* was performed after 10 minutes of treatment with silver insults, which might not provide enough exposure time to allow the changes in gene expression in the bacteria.[17] Likewise, the GDS studies (growth inhibition effects and calculation of IC_{50}) were performed after 24 hours.[7] Previously, Xu *et al*. found that prolonged exposure of AgNPs (48 hours) to HeLa cells lead to significantly decrease in number of genes with altered expression compared to shorter exposure of 24 hours suggesting that it is important to study early time points.[19]

Comparison of Ag NPs-affected pathways identified from gene expression analysis and those obtained from phenotypic analysis of single gene deletion strains of *E.coli*

In a previous paper, we reported the sensitivities of 4000 single gene deletion strains of *E. coli* towards various Ag NPs and ionic Ag.[7] The results showed that ionic silver and Ag NPs

affected different classes of gene deletion mutants of *E. coli*. For example, $AgNO_3$ were found to affect metal binding pathways, whereas, cell surface antigen activity (lipopolysaccharides) was found to be important for cell survival after being treated with Ag-BPEI NPs. In this study, we sought to compare results from microarray analysis with those derived from using a library of 4000 *E.coli* gene deletion mutant strains and focused on early changes in gene expression. As shown in **Figure 4.2B,** 680 genes were identified to be significantly altered when treated with $AgNO_3$ by microarray analysis whereas 460 genes were found to significantly sensitize the growth of the mutant strains in the previous single gene deletion strain study. Strikingly, 332 genes were commonly identified by both approaches. Likewise, 440 genes were identified to be significantly altered by Ag-BPEI NPs in the microarray gene expression analysis and 398 genes were identified to affect bacterial sensitivity to these NPs in single gene deletion analysis assay. Among these genes, 236 were consistently identified by both methods. Genes that were commonly identified by both approaches when treated with Ag-BPEI NPs included *cspD cspG* (cold shock protein), *cueO cueR* (Cu/Ag exporter), *dnaJ dnaK dnaT* (molecular chaperone/heat shock protein), *sodA sodB* (superoxide dismutase). In addition, *cyoB cyoD cyoE* (cytochrome subunits), *flgB flgD flgF* (flagellar proteins), *recJ recO recR* (DNA recombination/DNA repair protein) were identified to be significantly important when cells were treated with $AgNO_3$ both by gene expression analysis using microarray and from the phenotypic experiment on single gene deletion strains. It is important to note that in this study, we measured the gene expressions of the cells after treatment with the silver species after 2 hours therefore measuring the specific response that took place early on as opposed to measuring the generic phonotypic response (growth inhibition effects) after 24 hours using single gene deletions bacteria.

As discussed above, one of the advantages of using microarray methods (compared to the using a phenotypic screen of gene deletion strains) is that changes in regulation of essential genes can be determined using microarrays. Examples of essential genes identified to be involved in the bacterial responses to Ag-BPEI by microarray analysis are *ipbB* (heat shock protein that is essential for chaperone activity) and *adhP* (xenobiotic transforming enzyme). Likewise, *clpB* (stress-induced chaperone protein) and soxS (an essential gene that act as transcriptional activator of the superoxide response regulation in *E. coli*) were identified by microarray analysis to be important in the bacterial responses to $AgNO_3$. These observations suggest that anti-oxidant mechanisms, chaperone proteins and pathways of transforming xenobiotic are crucial for the bacterial cells in responding to the silver species. It is important to note that the timeframe used for the microarray experiment (2 hours of exposure to silver species) and the GDS experiment (24 hours of exposure to silver species) may also be responsible for some of the differences observed in the two approaches[20]. For instance, we would expect that early response genes (*e.g.*, those in generic stress response pathways such as heat shock genes) would be more likely to show up in the microarray experiment (at 2 hours) than in the gene deletion strain experiment (at 24 hours). Conversely, we would expect to see genes involved in how the organism responds to specific toxicants to show up more prominently in the GDS experiment (at 24 hours). Nonetheless, we still observed substantial differences in which genes were differentially expressed in the presence of AgBPEI and Ag+ even in the microarray experiment (after 2 hours).

Supporting information of **Chapter 4** is found in **Appendix 3** which contains the expression level and fold change of genes that have been identified to be significantly up or

down regulated compared to untreated controls (*p-value* < 0.05 after BH adjustment to restrict the false discovery rate) (**Table A3.1**)

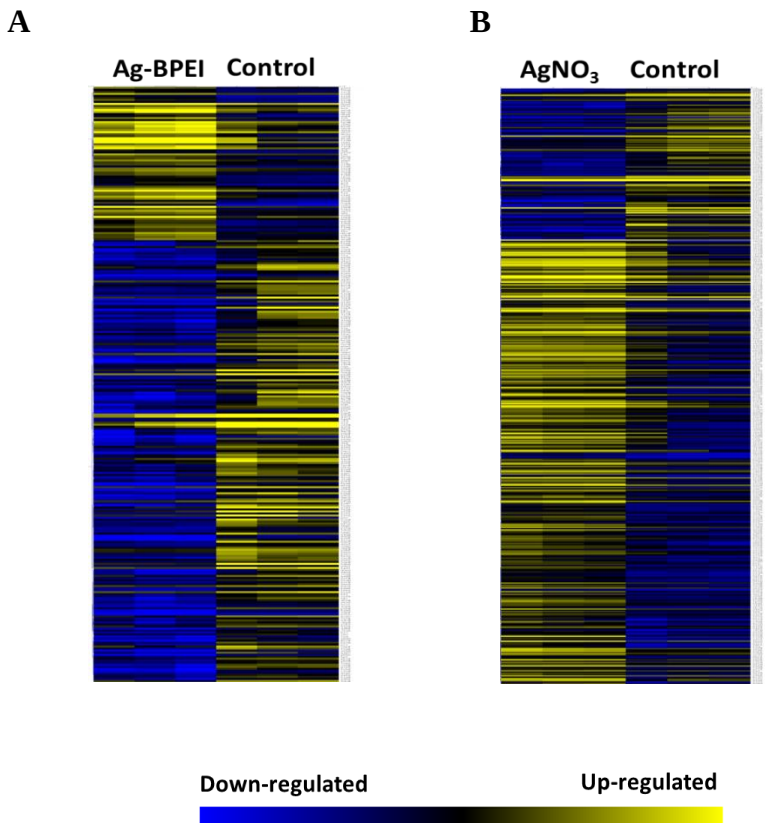

Figure 4.1. Heat map of differential gene expression observed after treatment with Ag-BPEI NPs **(A)** and $AgNO_3$ **(B)** compared to a negative control (no added silver). The RNA used for the microarray analysis was extracted from *E. coli* that had been cultured in the presence of 2 mg/mL Ag-BPEI, 2 mg/mL $AgNO_3$, or no added silver for 2 hours. Yellow in the heat map indicates genes that were significantly up-regulated ($p < 0.5$) whereas blue indicates genes that were significantly down-regulated ($p < 0.5$) compared to the negative (untreated) controls.

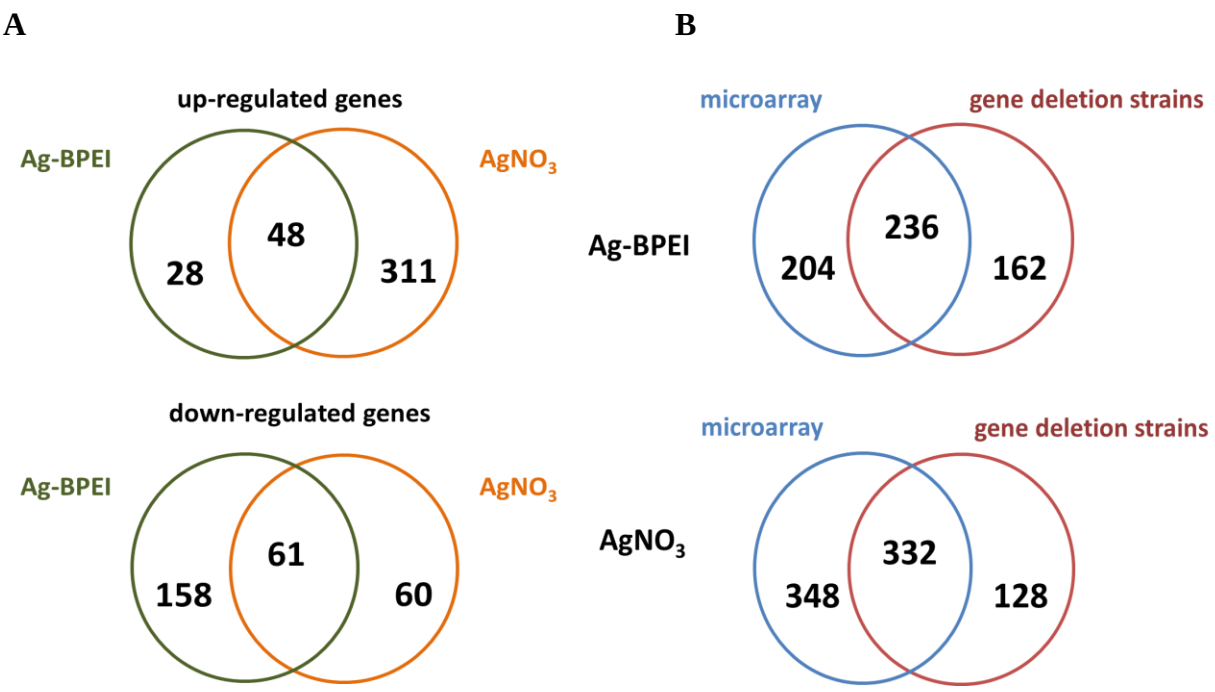

Figure 4.2. (A) Comparison of the genes found to be significantly up- or down- regulated by Ag-BPEI compared to $AgNO_3$ compared to untreated control in the microarray experiments reported herein. **(B)** Comparison of genes found to be differentially expressed after Ag-BPEI and $AgNO_3$ treatment (*i.e.* either up- or down-regulated compared to the negative control as shown by microarray analysis performed in this study) with genes previously shown to confer sensitivity of *E. coli* to the same Ag species in the phenotypic analysis of a library of single gene deletion strains reported previously.[7]

Table 4.1. Physiological pathways in bacterial cells that were significantly affected ($p < 0.05$) by Ag-BPEI and $AgNO_3$. Gene clusters were annotated based on their molecular function.

Silver formulation	number of genes	cluster	main molecular function annotation	*p* value
Ag-BPEI NPs (up regulated)	76	Cluster 1.1	ribosome (7)	3.30E-10
		Cluster 1.2	molecular chaperone/heat shock protein/stress response (5)	2.50E-09
		Cluster 1.3	metal-binding/cation binding (12)	2.50E-05
		Cluster 1.4	disulfide bond/redox-active center (5)	8.60E-05
		Cluster 1.5	pyruvate metalbolism (4)	2.50E-04
		Cluster 1.6	ATP/nucleotide binding (6)	6.80E-06
		Cluster 1.7	inorganic cation transmembrane transporter activity (5)	9.80E-03
		Cluster 1.8	membrane/peptidoglycan-based cell wall (15)	5.50E-04
		Cluster 1.9	repressor/transcription regulation (4)	7.10E-03
Ag-BPEI NPs (down regulated)	219	Cluster 2.1	DNA binding/regulators of transcription (15)	4.10E-13
		Cluster 2.2	cold shock protein (6)	1.10E-05
		Cluster 2.3	fatty acid metabolism (4)	1.30E-04
		Cluster 2.4	cellular respiration (11)	5.40E-04
		Cluster 2.5	tryptophan metabolism (3)	2.20E-03
		Cluster 2.6	palmitate/lipoprotein (8)	8.40E-06
		Cluster 2.7	beta-alanine metabolism (3)	3.30E-03
		Cluster 2.8	butanoate metabolism (4)	1.50E-03
		Cluster 2.9	membrane protein (41)	3.40E-09
		Cluster 2.10	ABC transporters (7)	2.60E-03
		Cluster 2.11	galactitol/hexitol metabolic process (3)	2.70E-03
		Cluster 2.12	nitrogen metabolism (4)	2.90E-04
		Cluster 2.13	alanine, aspartate and glutamate metabolism (7)	1.20E-03
		Cluster 2.14	starch and sucrose metabolism (3)	2.10E-02
		Cluster 2.16	amine biosynthetic process (10)	2.10E-02

Silver formulation	number of genes	cluster	main molecular function annotation	*p* value
		Cluster 2.17	hexose metabolic process (11)	9.00E-04
		Cluster 2.18	metalloprotein (5)	6.50E-04
		Cluster 2.19	peptidoglycan-based cell wall (17)	8.90E-03
		Cluster 2.20	phosphoprotein (7)	4.40E-03
		Cluster 2.21	phosphotransferase system (PTS) (4)	8.60E-03
$AgNO_3$ (up regulated)	359	Cluster 3.1	ribosome/protein biosynthesis (41)	1.90E-49
		Cluster 3.2	cell inner membrane (62)	3.30E-24
		Cluster 3.3	oxidative phosphorylation/membrane-associated complex (14)	9.90E-21
		Cluster 3.4	nucleotide-binding (63)	1.00E-23
		Cluster 3.5	metal binding/cation binding (51)	3.00E-18
		Cluster 3.6	coenzyme metabolic process (27)	2.30E-07
		Cluster 3.7	nitrogen compound biosynthetic process (50)	8.50E-09
		Cluster 3.8	pyrimidine metabolism (11)	8.40E-07
		Cluster 3.9	tricarboxylic acid (citrate)/TCA cycle (8)	4.00E-07
		Cluster 3.10	Alanine, aspartate and glutamate metabolism (8)	4.80E-06
		Cluster 3.11	monosaccharide biosynthetic process (11)	8.10E-07
		Cluster 3.12	aminoacyl-tRNA ligase activity/ligase (22)	1.20E-14
		Cluster 3.13	ncRNA metabolic process (22)	3.40E-06
		Cluster 3.14	cation ion transport (18)	1.30E-10
		Cluster 3.15	glycolysis (8)	2.00E-07
		Cluster 3.16	aldehyde catabolic process/pyruvate metabolism (5)	5.80E-05
		Cluster 3.17	pentose phosphate pathway (6)	7.50E-04
		Cluster 3.18	C5-branched dibasic acid metabolism (4)	9.40E-04
		Cluster 3.19	regulation of cellular protein metabolic process (7)	2.50E-05
		Cluster 3.20	glutamine metabolic process/glutamine amidotransferase (5)	4.60E-05
		Cluster 3.21	GTP binding (6)	8.90E-08
		Cluster 3.22	FAD/Flavoprotein (12)	9.80E-08
		Cluster 3.23	repressor/regulation of transcription (19)	9.30E-13
		Cluster 3.24	Glycine, Serine and threonine metabolism (6)	1.20E-03

Silver formulation	number of genes	cluster	main molecular function annotation	*p* value
		Cluster 3.25	iron/iron-sulfur cluster binding (21)	1.30E-07
		Cluster 3.26	glucoside transport (4)	1.30E-03
		Cluster 3.27	nucleotide biosynthetic process/ATP biosynthesis (19)	8.10E-07
		Cluster 3.28	valine, leucine and isoleucine biosythesis (6)	2.21E-05
		Cluster 3.29	bacterial flagellum/flagellar assembly (5)	9.10E-05
		Cluster 3.30	phosphotransferase/sugar transport (11)	5.10E-09
		Cluster 3.31	purine ribonucleotide biosynthetic process (11)	6.20E-05
		Cluster 3.32	cell wall/peptidoglycan biosynthesis (6)	2.60E-05
		Cluster 3.33	thiamine pyrophosphate (5)	2.40E-04
		Cluster 3.34	arginine and proline metabolism (5)	1.90E-02
		Cluster 3.35	molybdenum cofactor biosynthesis (4)	8.50E-05
		Cluster 3.36	fatty acid metabolic process (4)	4.60E-03
		Cluster 3.37	ubiquinone biosynthesis (3)	6.10E-03
		Cluster 3.38	protein export/bacterial secretion system (4)	8.00E-03
		Cluster 3.39	polyketide sugar/lipopolysaccharide biosynthesis (3)	9.80E-03
		Cluster 3.40	glutathione metabolism (4)	1.30E-02
		Cluster 3.41	Cystathionine beta-synthase/CBS domain (3)	6.10E-03
		Cluster 3.42	detection of stimulus/phage recognition (3)	6.90E-03
		Cluster 3.43	topoisomerase (3)	1.60E-02
		Cluster 3.44	redox-active center/cell redox homeostasis (5)	3.60E-03
		Cluster 3.45	homologous recombination/DNA repair (5)	6.00E-03
		Cluster 3.46	ABC transporters (11)	1.80E-02
$AgNO_3$ (down regulated)	121	Cluster 4.1	membrane (32)	1.50E-10
		Cluster 4.2	response to osmotic stress (5)	2.70E-06
		Cluster 4.3	palmitate lipoprotein (6)	6.70E-05
		Cluster 4.4	metalloprotein (5)	8.50E-05
		Cluster 4.5	purine salvage/purne metabolism (3)	2.40E-03
		Cluster 4.6	sugar transport (5)	1.00E-02
		Cluster 4.7	cell inner membrane (16)	3.00E-05
		Cluster 4.8	DNA-binding (9)	1.80E-01

REFERENCES

1. Klaine, S. J.; Alvarez, P. J.; Batley, G. E.; Fernandes, T. F.; Handy, R. D.; Lyon, D. Y.; Mahendra, S.; McLaughlin, M. J.; Lead, J. R., *Environ. Toxicol. Chem.* **2008,** *27,* 1825-51.

2. Alexander, J. W., History of the Medical Use of Silver. *Surg. Infect.* **2009,** *10,* (3), 289-292.

3. *See Comments of the Silver Nanotechnology Working Group for Review by the FIFRA Scientific Advisory Panel (Oc-tober 30, 2009), at p. 3. Available online at http://www.silver-institute.org/images/stories/silver/PDF/epa_hq_opp2009.pdf.*

4. Mijnendonckx, K.; Leys, N.; Mahillon, J.; Silver, S.; Van Houdt, R., Antimicrobial silver: uses, toxicity and potential for resistance. *Biometals* **2013,** *26,* (4), 609-21.

5. Wei, L.; Lu, J.; Xu, H.; Patel, A.; Chen, Z. S.; Chen, G., *Drug Discov. Today* **2014**, in press.

6. Housenger, J. E., EPA response to Petition from International Center for Technology Assessment Relating to Regulation of Nanoscale Silver as a Pesticide. *Supporting & Related Material from EPA* **2015**, 1-23.

7. Ivask, A.; Elbadawy, A.; Kaweeteerawat, C.; Boren, D.; Fischer, H.; Ji, Z.; Chang, C. H.; Liu, R.; Tolaymat, T.; Telesca, D., et al., Toxicity Mechanisms in Escherichia coli Vary for Silver Nanoparticles and Differ from Ionic Silver. *ACS Nano* **2014,** *8,* 374-86.

8. Baba, T.; Ara, T.; Hasegawa, M.; Takai, Y.; Okumura, Y.; Baba, M.; Datsenko, K. A.; Tomita, M.; Wanner, B. L.; Mori, H., Construction of Escherichia coli K-12 in-frame, single-gene knockout mutants: the Keio collection. *Mol. Syst. Biol.* **2006,** *2.*

9. Fry, R. C.; Begley, T. J.; Samson, L. D., Genome-Wide Responses to DNA-Damaging Agents. *Annu. Rev. Microbiol.* **2005,** *59,* 357-77.

10. Benjamini, Y.; Hochberg, Y., Controlling the False Discovery Rate - a Practical and Powerful Approach to Multiple Testing. *J. Roy. Stat. Soc. B. Met.* **1995,** *57,* (1), 289-300.

11. Dennis, G., Jr.; Sherman, B. T.; Hosack, D. A.; Yang, J.; Gao, W.; Lane, H. C.; Lempicki, R. A., *Genome Biol.* **2003,** *4*, 3.

12. http://www.osa.sunysb.edu/udmf/ArraySheets/ecoli2_datasheet.pdf (accessed on May 4th, 2015).

13. Rensing, C.; Fan, B.; Sharma, R.; Mitra, B.; Rosen, B. P., CopA: An Escherichia coli Cu(I)-translocating P-type ATPase. *Proc. Natl. Acad. Sci. U.S.A.* **2000,** *97*, (2), 652-656.

14. Grass, G.; Rensing, C., CueO is a multi-copper oxidase that confers copper tolerance in Escherichia coli. *Biochem Bioph. Res. Co.* **2001,** *286*, (5), 902-908.

15. Franke, S.; Grass, G.; Nies, D. H., The product of the ybdE gene of the Escherichia coli chromosome is involved in detoxification of silver ions. *Microbiol-UK* **2001,** *147*, 965-972.

16. Wu, M. Y.; Suryanarayanan, K.; van Ooij, W. J.; Oerther, D. B., Using microbial genomics to evaluate the effectiveness of silver to prevent biofilm formation. *Water Sci.Techno.* **2007,** *55*, (8-9), 413-419.

17. McQuillan, J. S.; Shaw, A. M., Differential gene regulation in the Ag nanoparticle and Ag(+)-induced silver stress response in Escherichia coli: a full transcriptomic profile. *Nanotoxicology* **2014,** *8* 177-84.

18. Kaveh, R.; Li, Y. S.; Ranjbar, S.; Tehrani, R.; Brueck, C. L.; Van Aken, B., Changes in Arabidopsis thaliana Gene Expression in Response to Silver Nanoparticles and Silver Ions. *Environ. Sci. Technol.* **2013,** *47*, (18), 10637-10644.

19. Xu, L. M.; Takemura, T.; Xu, M. S.; Hanagata, N., Toxicity of Silver Nanoparticles as Assessed by Global Gene Expression Analysis. *Mater. Express* **2011,** *1*, (1), 74-79.

20. Sahu, S. C.; Zheng, J.; Yourick, J. J.; Sprando, R. L.; Gao, X., Toxicogenomic responses of human liver HepG2 cells to silver nanoparticles. *J. Appl. Toxicol.* **2015**.

CHAPTER 5

Overarching Conclusions and Recommendations for Future Studies

High-throughput screening assays as an integral component in the iterative design of safe materials. The suite of growth inhibition and sub-lethal assays in bacteria that were developed and implemented in this work (**Chapters 2** and **3**) constitute a powerful tool for rapidly screening toxicity potential of uncharacterized materials. We recommend that this methodology be applied to assess the safety of new nanoparticles (NPs) at an early stage of research and development. Our proposed approach for the development of safe (*i.e.* low toxicity potential) nanomaterials involves screening for toxicity early on, at the same time as candidate new materials are being screened for desired physicochemical properties. This is a much more efficient way to approach design or optimization of new materials, as an optimal balance between maximizing desired properties and minimizing toxicity properties is built in to the development process.[1, 2] This approach can also be applied to materials that are already in the consumer market by allowing regulators to prioritize materials that are likely to be toxic for further studies in animal models, which require extensive time and budget commitment.[3] This method will help speed up the process of initial screening for toxicity of NPs to keep pace with new particle synthesis, as well as provide mechanistic insights into how these NPs might affect bacterial communities in the environment.

Safer design principles for metal oxide nanoparticles (MOx NPs). By thoroughly studying toxicological outcomes of a comprehensive set of 24 MOx NPs, we have been able to identify those physicochemical parameters that correlate significantly with toxicity levels

(Chapter 2).[4] Interestingly, we found that conduction band energy and hydration enthalpy were predictive of the toxicity of MOx NPs in bacteria, similar to what had been reported earlier in mammalian cells.[5] Specifically, the probability for a MOx NP in our set of 24 NPs to be highly toxic increased as the hydration enthalpy of the materials became less negative and as the conduction band energy of the MOx NP approached the redox potential of biological molecules.[4] These principles should help guide the development of future generations of MOx NPs that exhibit desirable properties but are relatively safer by design.

Toxicities of NPs are distinct from their ionic- or micron-sized counterparts. In the side-by-side comparison between Cu NPs and their ionic and micron-sized analogs[6] (**Chapter 3**), we found that toxicity of nano-sized particles (nano-Cu, nano-CuO, nano-$Cu(OH)_2$) was higher than the micron-sized counterparts (micro-Cu and micro-CuO) and approached that of ionic Cu ($CuCl_2$ and $CuSO_4$) in both the gram-negative bacterium *E. coli* and gram-positive bacterium *L. brevis*. The suite of sub-lethal assays also revealed that the mechanisms of toxicity were distinct between these substances. Whereas ionic Cu led to a decrease of cellular membrane potential, Cu nanoparticles led to severe oxidative stress in the bacterial cells at an order of magnitude higher than their ionic counterparts. Confocal microscopy, TEM imaging as well as a 3D tomography reconstruction also suggested that particles at nano-sized Cu, *but not* at micro-sized Cu, are internalized into the cells as intact particles. This is a concern because these internalized particles could accumulate up through the food chain. Based on the data so far for Cu NPs, we suggest that NPs to be subject to regulatory scrutiny as new materials.

Genotoxic and mutagenic effects of NPs need to be studied in more detail. We observed that both zero-valence Cu species (nano-Cu and micro-Cu) resulted in extensive DNA damage in an *in vitro* assay (**Chapter 3**). However, TEM imaging and electron tomography revealed that

nano-Cu particles were found to be internalized into bacterial cells, whereas micro-Cu particles were not. This suggested that it is possible for nano-Cu to enter cells, where they could catalyzes the production of intracellular reactive oxygen species that would lead to DNA damage and genomic stability *in vivo*. Clearly, additional studies are needed to determine whether nano-Cu results in DNA damage and/or results in increased rates of mutations in bacteria (and other species) *in vivo*. If so, this would have important ramifications for how nano-Cu is regulated compared to other Cu species.

Gram-positive bacteria are more sensitive to Cu NPs than gram-negative bacteria. Toxicity of Cu NPs (as well as ionic Cu and micron-sized copper) was found to be greater in the gram positive bacterium we investigated (*L. brevis*) than gram-negative bacterium we studied (*E. coli*). The observation that Cu nanoparticles exhibit differential toxicity for different phyla of bacteria has important implications for potential impact of these agents on population dynamics in natural systems (*e.g.,* for soil bacteria when applying Cu antimicrobials and/or for marine bacteria when using anti-fouling paints as well as in waste water treatment system). Studies should be performed to examine which of the differences (*e.g.* structure of cell membrane/cell wall or the presence of lipopolysaccharide) between these two species of bacteria are responsible for the differential toxicity of nano Cu species. In addition, micro/mesocosm and modeling studies should be performed to determine whether these affects are recapitulated in systems with multiple species of bacteria present.

New sucrose-gradient centrifugation method developed herein can be used to determine the amount of Cu associated with cells. In **Chapter 3**, I report the development of a method to separate the bacterial cells from the excess Cu species by mean of sucrose-gradient centrifugation.[6] A strong correlation between overall toxicity in *E. coli* and *L.* brevis and the

amount of Cu associate with the bacterial cells was observed. Using sucrose-gradient centrifugation is simple, fast and cost-effective method to separate NPs from cells and provides an essential tool for further study of toxicity of nanoparticles. When used in concert with other method such as biosensor strain, which exhibit luminescent signal in response with cellular bioavailable Cu,[7] the sucrose gradient method provides complementary information about the role of Cu that bind tightly to the outer layers of the bacterial cells in mediating toxicity.

A cationic silver nanoparticle (Ag-BPEI) results in up and down regulation of different genes than Ag^+. From genome-wide gene expression analysis of the bacterial response to a cationic Ag NP (Ag-BPEI) and to ionic silver (**Chapter 4**), we found that these different forms of silver led to up- or down- regulation of different cellular pathways.[8] We observed that exposure to Ag-BPEI led to up-regulation of oxidative homeostatic and cellular stress response pathways, including the heat shock response.[8] By contrast, we found that Ag^+ led to up-regulation of cell wall and cell membrane biosynthesis and genes encoding cation-binding proteins, similar to what had been reported previously for ionic silver.[9] In addition, we found that exposure to Ag-BPEI results in down-regulation of energy generating processes and cold shock pathways, whereas the pathways that were down-regulated when the cells were treated with ionic silver were lipoprotein biosynthesis, starch and sucrose metabolism, and purine and nucleoside biosynthesis. These results are consistent with prior reports that Ag-BPEI exhibits mechanisms of toxicity that are distinct from those observed for Ag^+ or other Ag NPs.[10, 11] These studies support the assertion that Ag NPs are fundamentally new antimicrobial substances[10, 12] and that, as a class, Ag NPs should be subject to additional regulatory scrutiny and not just assumed to be a new delivery system for Ag^+.

Microarray studies on NPs provide information that is complementary to that obtained from phenotypic assays (using gene deletion strains & sub-lethal assays) Microarray studies are a useful tool because they provide a comprehensive understanding of cellular responses to external insults at the level of gene transcription.[13] Prior studies comparing the results obtained from microarray studies and those obtained from phenotypic assays (including genome-wide phenotypic assays such as those performed on libraries of gene deletion strains) on conventional (organic) toxicants provide complementary information.[14] The results of the studies reported in Chapter 4, taken together with prior reports looking at the impacts of Ag-BPEI and other Ag NPs on a library of gene deletion strains,[10] suggest that microarray and phenotypic studies can provide complementary toxicity information about NPs as well. For instance, microarray analysis revealed that heat shock pathway was crucial for the bacterial response to Ag-BPEI,[6] whereas cell surface antigen activity (lipopolysaccharides) were found to be important for *E. coli* when being treated with the same nanoparticles.[10]

The ensemble of mechanisms of toxicity can be used as a "fingerprint" of cellular response to a specific nanoparticle. Both the results from the microarray studies (**Chapter 4**) and from the sub-lethal assays (**Chapters 2-4**) reported herein support the general observation that nanoparticles – similar to other toxicants – tend not to exhibit a single "mechanism" of toxicity but rather are characterized by a "fingerprint" or set of biological responses[15] and that the "fingerprint" observed for toxic NPs is often distinct from those of ionic or micron-sized analogs.[6, 10] These studies suggest that, as the field of nanotoxicology moves forward, characterization of the *suite* of toxicological impacts (as opposed to simply characterizing the magnitude of toxicity or the effects on a single toxicological outcome (e.g., ROS generation) will be critical to achieving an accurate understanding of the toxicity of these important materials.

References

1. Nel, A.; Xia, T.; Meng, H.; Wang, X.; Lin, S. J.; Ji, Z. X.; Zhang, H. Y., Nanomaterial Toxicity Testing in the 21st Century: Use of a Predictive Toxicological Approach and High-Throughput Screening. *Acc. Chem. Res.* **2013,** *46*, (3), 607-621.

2. Zhu, M. T.; Nie, G. J.; Meng, H.; Xia, T.; Nel, A.; Zhao, Y. L., Physicochemical Properties Determine Nanomaterial Cellular Uptake, Transport, and Fate. *Acc. Chem. Res* **2013,** *46*, (3), 622-631.

3. Godwin, H.; Nameth, C.; Avery, D.; Bergeson, L. L.; Bernard, D.; Beryt, E.; Boyes, W.; Brown, S.; Clippinger, A. J.; Cohen, Y., et al., Nanomaterial Categorization for Assessing Risk Potential To Facilitate Regulatory Decision-Making. *ACS Nano* **2015**.

4. Kaweeteerawat, C.; Ivask, A.; Liu, R.; Zhang, H.; Chang, C. H.; Low-Kam, C.; Fischer, H.; Ji, Z.; Pokhrel, S.; Cohen, Y., et al., Toxicity of Metal Oxide Nanoparticles in Escherichia coli Correlates with Conduction Band and Hydration Energies. *Environ. Sci. Technol.* **2015**.

5. Zhang, H. Y.; Ji, Z. X.; Xia, T.; Meng, H.; Low-Kam, C.; Liu, R.; Pokhrel, S.; Lin, S. J.; Wang, X.; Liao, Y. P., et al., Use of Metal Oxide Nanoparticle Band Gap to Develop a Predictive Paradigm for Oxidative Stress and Acute Pulmonary Inflammation. *ACS Nano* **2012,** *6*, 4349-4368.

6. Kaweeteerawat, C.; Chang, C.; Roy, K.; Rong, L.; Li, R.; Toso, D.; Fischer, H.; Ivask, A.; Ji, Z.; Zink, J., et al., Cu Nanoparticles Have Different Impacts in *E. coli* And *L. brevis* Than Their Micron-Sized and Ionic Analogs. **2015**, manuscript submitted to *ACS Nano*

7. Bondarenko, O.; Ivask, A.; Kakinen, A.; Kahru, A., Sub-toxic effects of CuO nanoparticles on bacteria: kinetics, role of Cu ions and possible mechanisms of action. *Environ. Pollut.* **2012,** *169*, 81-9.

8. Kaweeteerawat, C.; Ivask, A.; Liu, R.; ElBadawy, A.; Chang, C.; Fischer, H.; Ji, Z.; Cohen, Y.; Zink, J.; Tolaymat, T., et al., Genome-Wide Gene Expression Analysis Reveals That Silver Nanoparticles and Ionic Silver Up and Down Regulate Different Pathways. **2015**, Manuscript under preparation.

9. Kaveh, R.; Li, Y. S.; Ranjbar, S.; Tehrani, R.; Brueck, C. L.; Van Aken, B., Changes in Arabidopsis thaliana Gene Expression in Response to Silver Nanoparticles and Silver Ions. *Environ. Sci. Technol.* **2013,** *47*, (18), 10637-10644.

10. Ivask, A.; Elbadawy, A.; Kaweeteerawat, C.; Boren, D.; Fischer, H.; Ji, Z.; Chang, C. H.; Liu, R.; Tolaymat, T.; Telesca, D., et al., Toxicity Mechanisms in Escherichia coli Vary for Silver Nanoparticles and Differ from Ionic Silver. *ACS Nano* **2014,** *8*, 374-86.

11. Silva, T.; Pokhrel, L. R.; Dubey, B.; Tolaymat, T. M.; Maier, K. J.; Liu, X., Particle size, surface charge and concentration dependent ecotoxicity of three organo-coated silver nanoparticles: comparison between general linear model-predicted and observed toxicity. *Sci. Total. Environ.* **2014,** *468*, 968-76.

12. Rai, M.; Yadav, A.; Gade, A., Silver nanoparticles as a new generation of antimicrobials. *Biotechnol. Adv.* **2009,** *27*, (1), 76-83.

13. Bammler, T.; Beyer, R. P.; Bhattacharya, S.; Boorman, G. A.; Boyles, A.; Bradford, B. U.; Bumgarner, R. E.; Bushel, P. R.; Chaturvedi, K.; Choi, D., et al., Standardizing global gene expression analysis between laboratories and across platforms. *Nat. Methods* **2005,** *2*, (5), 351-356.

14. Fry, R. C.; Begley, T. J.; Samson, L. D., Genome-Wide Responses to DNA-Damaging Agents. *Annu. Rev. Microbiol.* **2005,** *59*, 357-77.

15. Judson, R.; Houck, K.; Martin, M.; Knudsen, T.; Thomas, R. S.; Sipes, N.; Shah, I.; Wambaugh, J.; Crofton, K., In vitro and modelling approaches to risk assessment from the U.S. Environmental Protection Agency ToxCast programme. *Basic Clin. Pharmacol. Toxicol.* **2014,** *115*, (1), 69-76.

APPENDIX 1

Supporting Information for **Chapter 2**

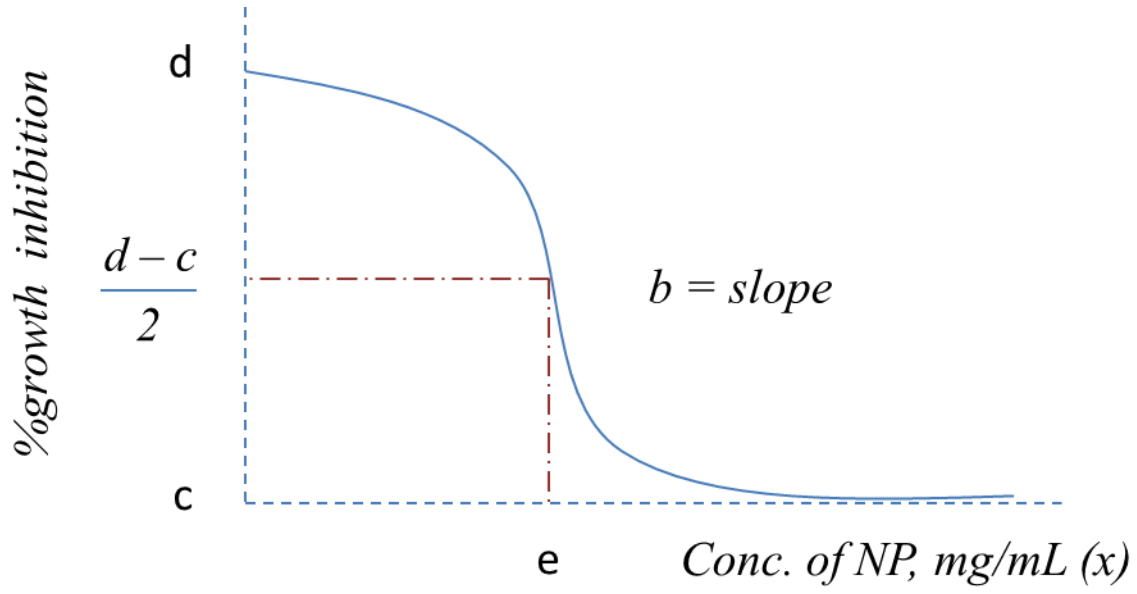

$$\%growth\ inhibition = c + \frac{d-c}{1+\exp\left(b\left(\log(x)-\log(e)\right)\right)}$$

Figure A1.1. Calculation of IC_{50} from growth-inhibition curves. The growth inhibition curve of each NP was fitted using a log-logistic model in the software program R. The curves are characterized by 4 parameters: maximum response (d), minimum response (c), IC_{50} (mg/L) (e) and the slope (b). The IC_{50} of each MOx NP was calculated using the equation shown above.

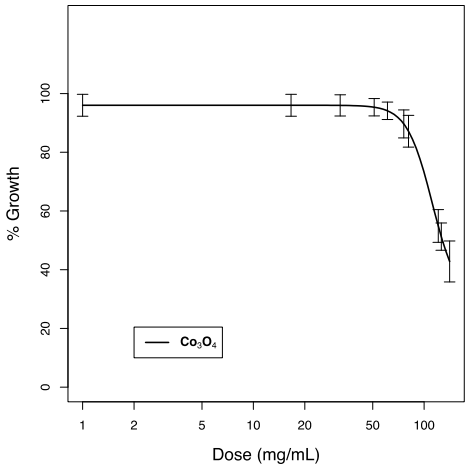
% Growth
0
20
40
60
80
100
1
2
5
10
20
50
100
Dose (mg/mL)
Co3O4

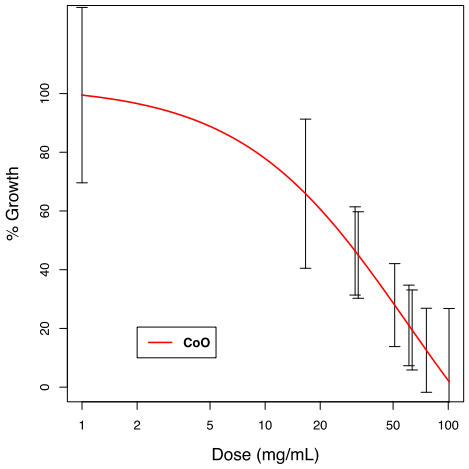
% Growth
0
20
40
60
80
100
1
2
5
10
20
50
100
Dose (mg/mL)
CoO

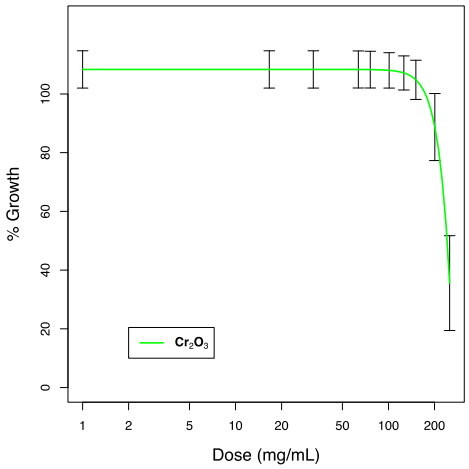
% Growth
0
20
40
60
80
100
1
2
5
10
20
50
100
200
Dose (mg/mL)
Cr2O3

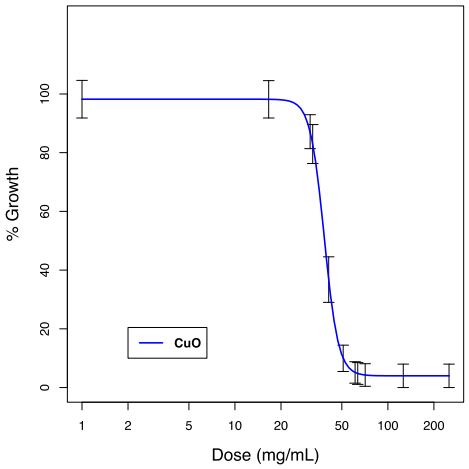
% Growth
0
20
40
60
80
100
1
2
5
10
20
50
100
200
Dose (mg/mL)
CuO

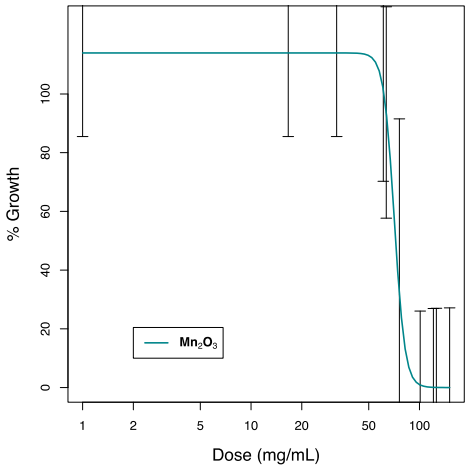
% Growth
0
20
40
60
80
100
1
2
5
10
20
50
100
Dose (mg/mL)
Mn_2O_3

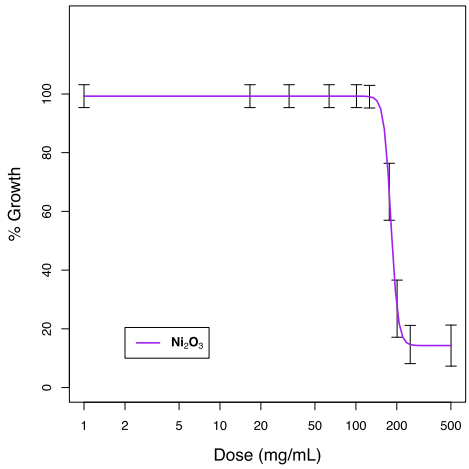
% Growth
0
20
40
60
80
100
1
2
5
10
20
50
100
200
500
Dose (mg/mL)
Ni_2O_3

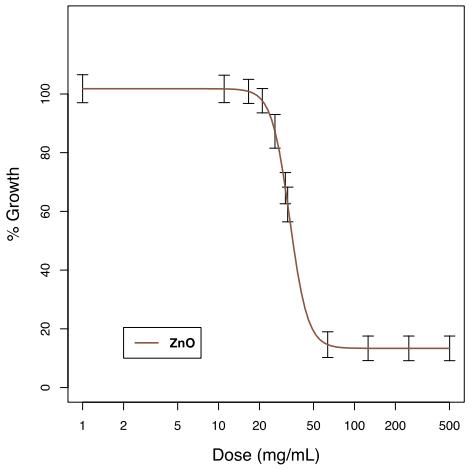
% Growth
0
20
40
60
80
100
1
2
5
10
20
50
100
200
500
Dose (mg/mL)
ZnO

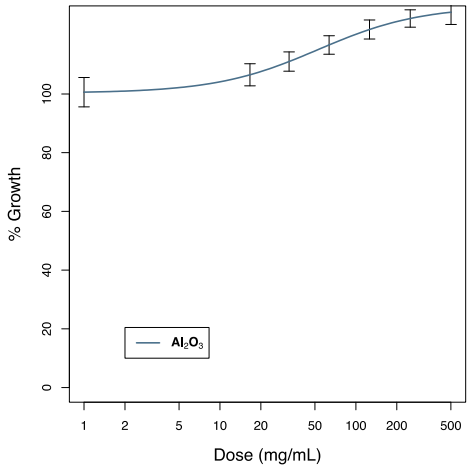
% Growth
0
20
40
60
80
100
1
2
5
10
20
50
100
200
500
Dose (mg/mL)
Al_2O_3

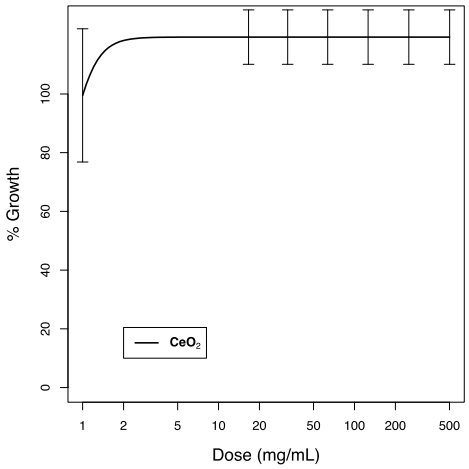
% Growth
0
20
40
60
80
100
1
2
5
10
20
50
100
200
500
Dose (mg/mL)
CeO2

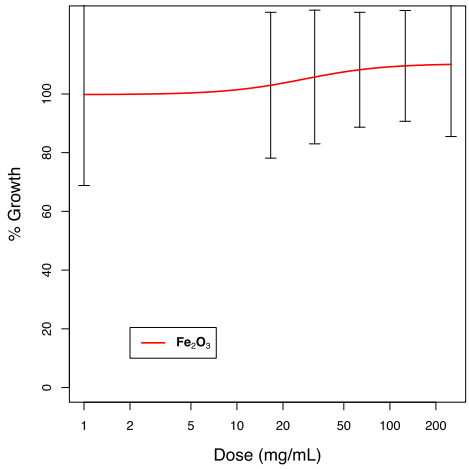
% Growth
0
20
40
60
80
100
1
2
5
10
20
50
100
200
Dose (mg/mL)
Fe2O3

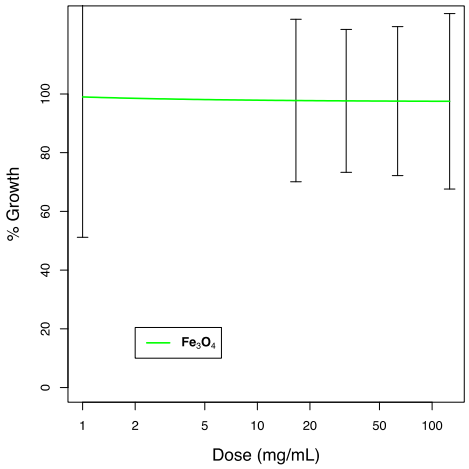
% Growth
0
20
40
60
80
100
1
2
5
10
20
50
100
Dose (mg/mL)
Fe3O4

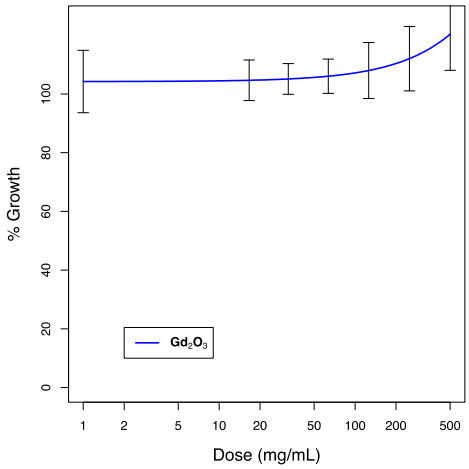
% Growth
0
20
40
60
80
100
1
2
5
10
20
50
100
200
500
Dose (mg/mL)
Gd2O3

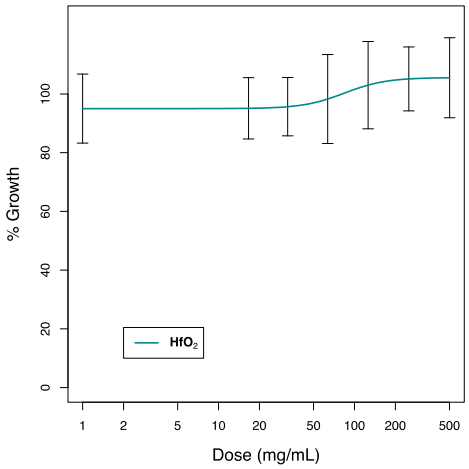
% Growth
0
20
40
60
80
100
HfO2
1
2
5
10
20
50
100
200
500
Dose (mg/mL)

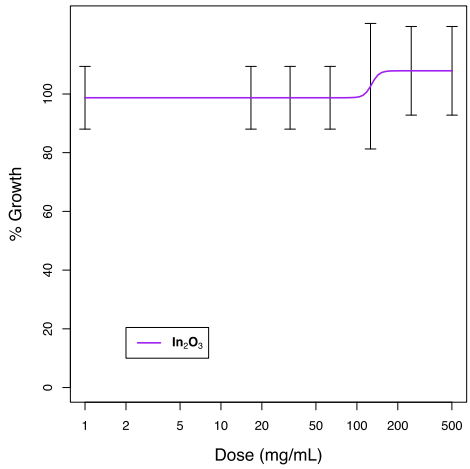
% Growth
0
20
40
60
80
100
In2O3
1
2
5
10
20
50
100
200
500
Dose (mg/mL)

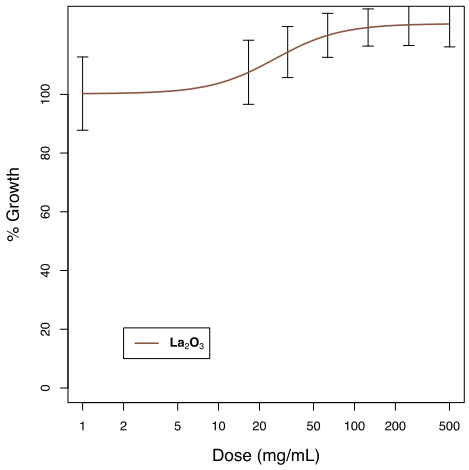
% Growth
0
20
40
60
80
100
La2O3
1
2
5
10
20
50
100
200
500
Dose (mg/mL)

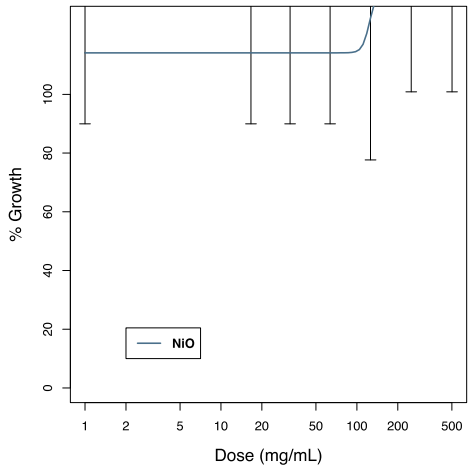
% Growth
0
20
40
60
80
100
NiO
1
2
5
10
20
50
100
200
500
Dose (mg/mL)

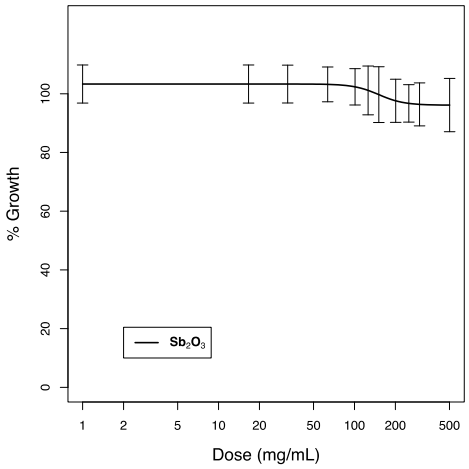
% Growth
0
20
40
60
80
100
Sb2O3
1
2
5
10
20
50
100
200
500
Dose (mg/mL)

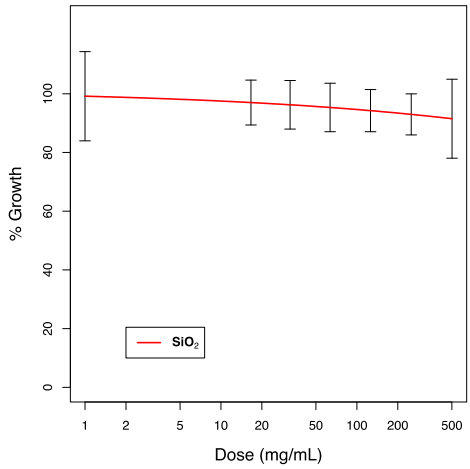
% Growth
0
20
40
60
80
100
SiO2
1
2
5
10
20
50
100
200
500
Dose (mg/mL)

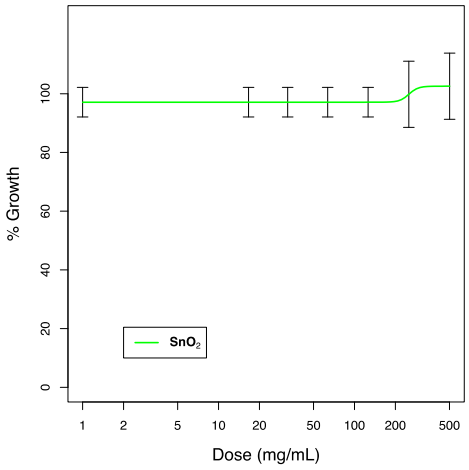
% Growth
0
20
40
60
80
100
1
2
5
10
20
50
100
200
500
Dose (mg/mL)
SnO2

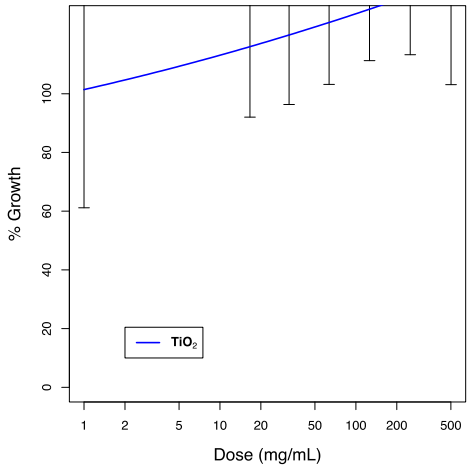
% Growth
0
20
40
60
80
100
1
2
5
10
20
50
100
200
500
Dose (mg/mL)
TiO2

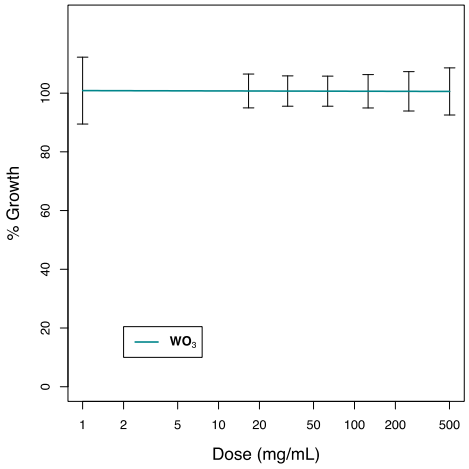
% Growth
0
20
40
60
80
100
1
2
5
10
20
50
100
200
500
Dose (mg/mL)
WO3

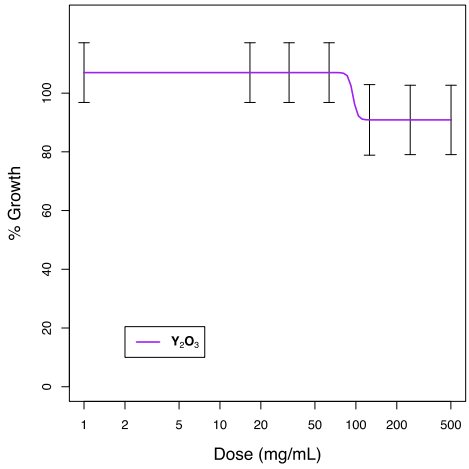
% Growth
0
20
40
60
80
100
1
2
5
10
20
50
100
200
500
Dose (mg/mL)
Y2O3

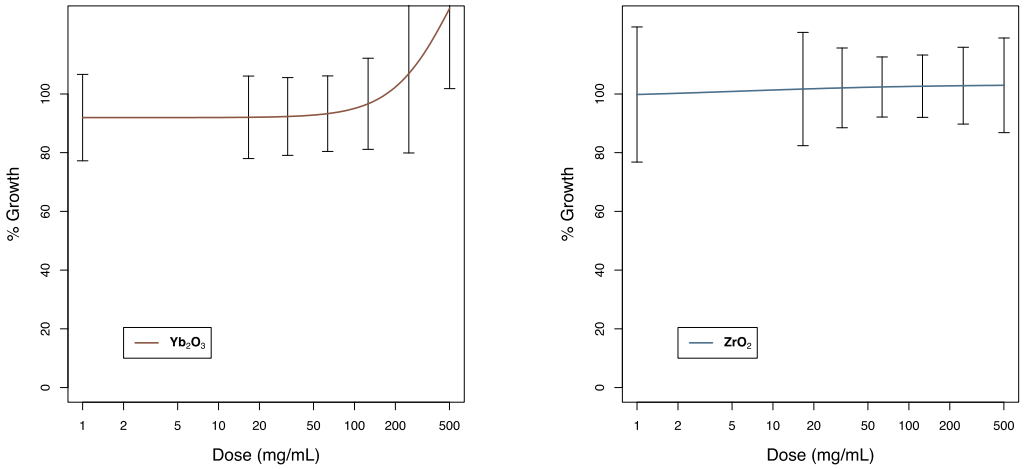

Figure A1.2. Individual growth inhibition curve including error bars for each of the 24 MOx NPs. Log-phased *E. coli* was cultured in the presence of each of the 24 MOx NPs. OD_{600} at 24 hours (in MMD with 0.01 % HA) was used to calculated the percent growth inhibition compared to *E. coli* (untreated) control. Curves shown are fit to the average of at least nine independent measurements; the model-based standard error for each point is indicated by error bars.

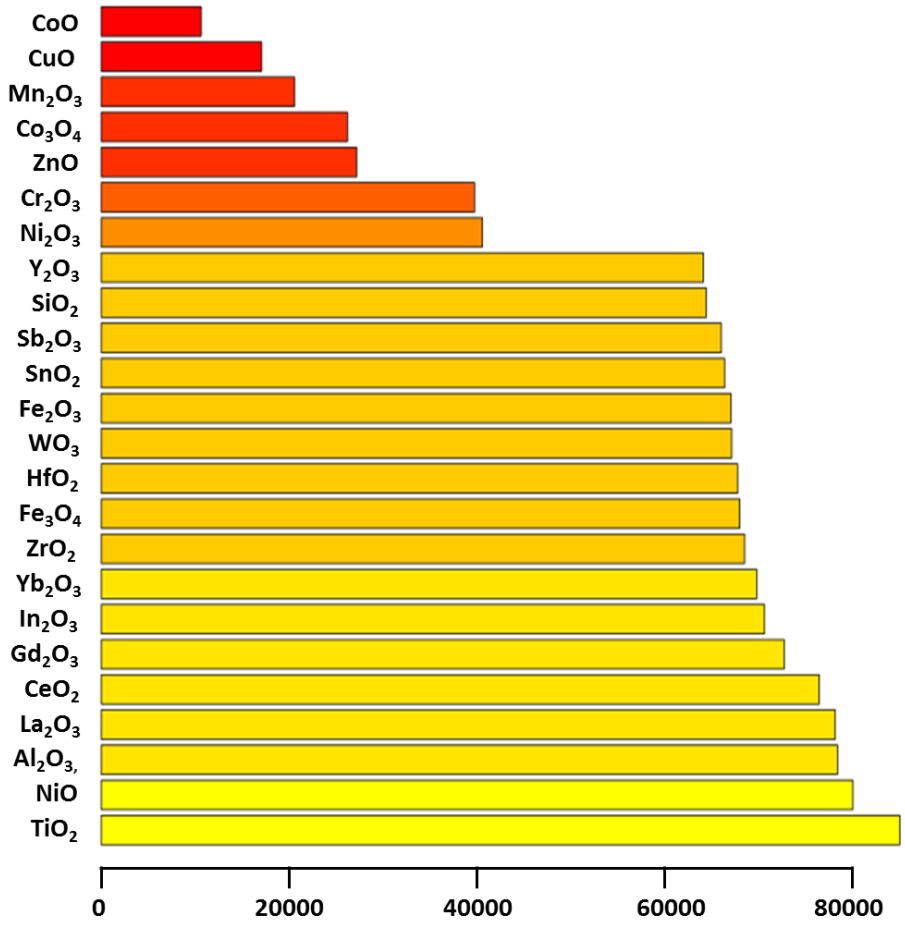

Figure A1.3. Area under growth-inhibition curve for 24 metal oxide nanoparticles in *E. coli*. To accurately distinguish between toxic and non-toxic particles, the area under the growth inhibition curves (shown in **Figure 1 and Figure A1.2**) was calculated by using the grofit package of R software. All seven toxic particles (Co_3O_4, CoO, Cr_2O_3, CuO, Mn_2O_3, Ni_2O_3 and ZnO) exhibit a significantly smaller area under their respective growth inhibition curves when compared to the non-toxic particles. The calculation provided a continuous measurement for non-toxic particles whose exact IC_{50} could not be determined. (The IC_{50} of these non-toxic NPs was listed as ≥ 500 mg/mL in **Table 1**). Continuous variables are needed to perform the

Structure Activity Relationship (SAR) analysis, which elucidates which properties of NPs are linked to their toxicity.

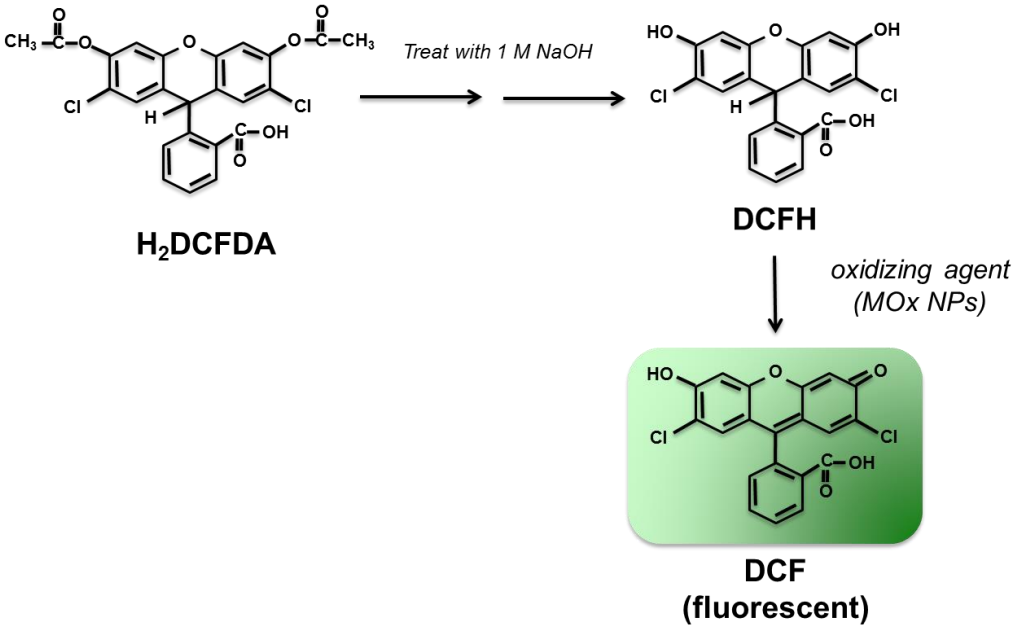

Figure A1.4. DCFH can be used to measured abitic ROS generation. H_2DCFDA was treated with 1 M NaOH for 30 min at room temperature to cleave acetate group and yield DCFH. Upon oxidation, DCFH converts into the fluorecent molecule DCF. By measuring the fluorescence signal, this method can be used to determine the oxidizing potential of each of the 24 MOx NPs *in vitro*.

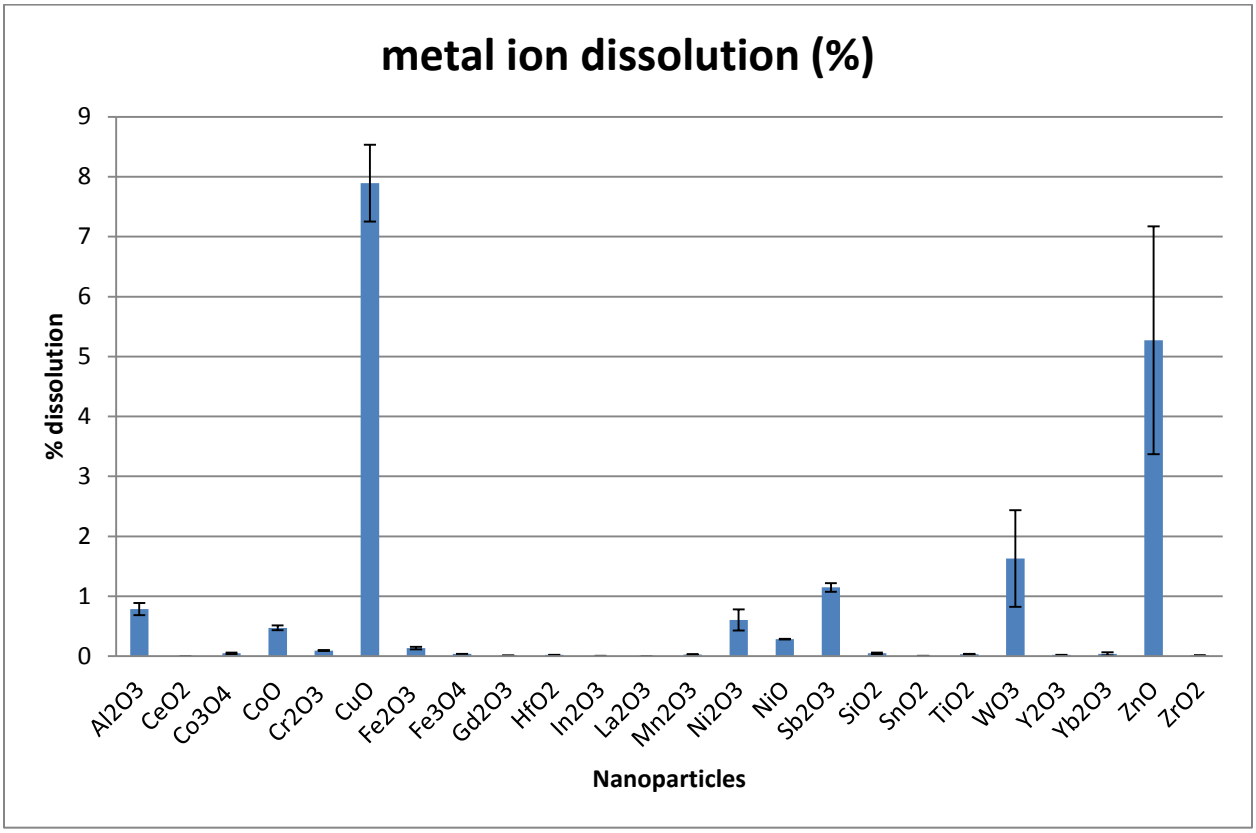

Figure A1.5. Metal ion dissolution. Metal ion dissolution from each MOx NP in MMD media was analyzed either by Inductively Coupled Plasma Mass Spectrometry (ICP-MS) or Atomic Absorption Spectrophotometry (AAS) as described in the text. In this experiment, 100 mg/L of well-dispersed MOx NPs in MMD were incubated at 37ºC for 24 hours. The sample was centrifuged (21,130 RCF, 30 min) and supernatant was collected in order to determine the dissolved metal ion concentration. Out of 24 particles, ZnO and CuO were shown to exhibit the highest amount of metal ion dissolution. The values shown represent the mean of the results obtained from three indpendent experiments and the error bars represent the standard deviation of the results.

Table A1.1: Quantitative effects of humic acid on aggregation of nanoparticles. Humic acid (HA) was added to the nanoparticles in bacterial media (MMD) to prevent aggregation. To determine the minimum concentration of HA that could be used to prevent significant aggregation, the effect of various concentrations of HA on hydrodynamic diameter was explored. The hydrodynamic diameter in deionized water was used as a target for optimal diameter. CuO, Mn_2O_3, and WO_3 were selected as representative nanoparticles. The average hydrodynamic size of CuO, Mn_2O_3, and WO_3 in the presence of varying concentrations of humic acid (HA) in minimal media (MMD), or in deionized water, was measured in triplicate using dynamic light scattering (DLS). Because lower concentrations of HA did not robustly prevent aggregation (particularly of Mn_2O_3, and WO_3), a concentration of 0.01% HA was used for the toxicity studies reported herein.

	Hydrodynamic diameter (nm)		
Solution Components	**CuO**	**Mn_2O_3**	**WO_3**
deionized water	263.3 ± 4.5	286.8 ± 2.8	176.6 ± 1.8
MMD + 0.01 mg/mL HA	311.3 ± 2.3	479.9 ± 9.1	260.7 ± 8
MMD + 0.001 mg/mL HA	341.2 ± 9.2	535.4 ± 9.6	360.8 ± 16.2
MMD + 0.0001 mg/mL HA	364.2 ± 2.5	643.9 ± 13.2	371.9 ± 6.7
MMD	1108.2 ± 13	691.9 ± 32.6	548.5 ± 22.2

Table A1.2: Correlations between results obtained from diffferent assays performed on MOx NPs. To demonstrate the agreement between the four different assays used herein, a correlation analysis was performed. Three of the sublethal assays (Biotic ROS, Abiotic ROS and Membrane damage) exhibit strong correlations with the growth inhibitory effects (IC_{50}) (Correlation coefficient = -0.84, -0.79 and 0.82, respectively), suggesting that all of these mechanistic pathways lead to toxicity and eventually cell death in *E. coli*. A moderate correlation (between -0.66 to -0.76) was also observed among each three of sublethal assays.

Assay	Biotic ROS	Abiotic ROS	Membrane damage	IC50
Biotic ROS	1.00	0.74	-0.76	-0.84
Abiotic ROS	0.74	1.00	-0.66	-0.79
Membrane damage	-0.76	-0.66	1.00	0.82
IC50	-0.84	-0.79	0.82	1.00

APPENDIX 2

Supporting Information for **Chapter 3**

(A) ***E. coli***

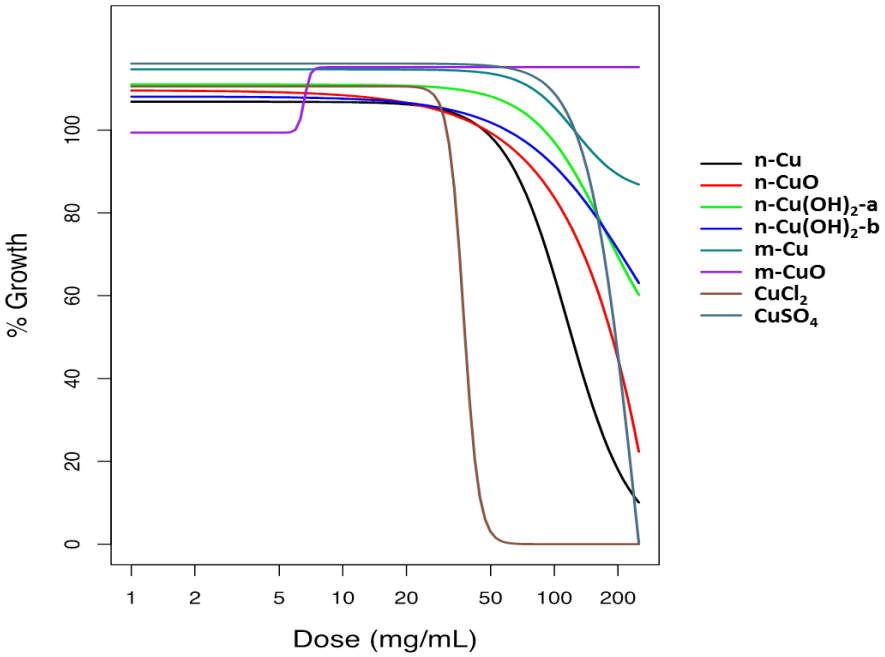

(B) ***L. brevis***

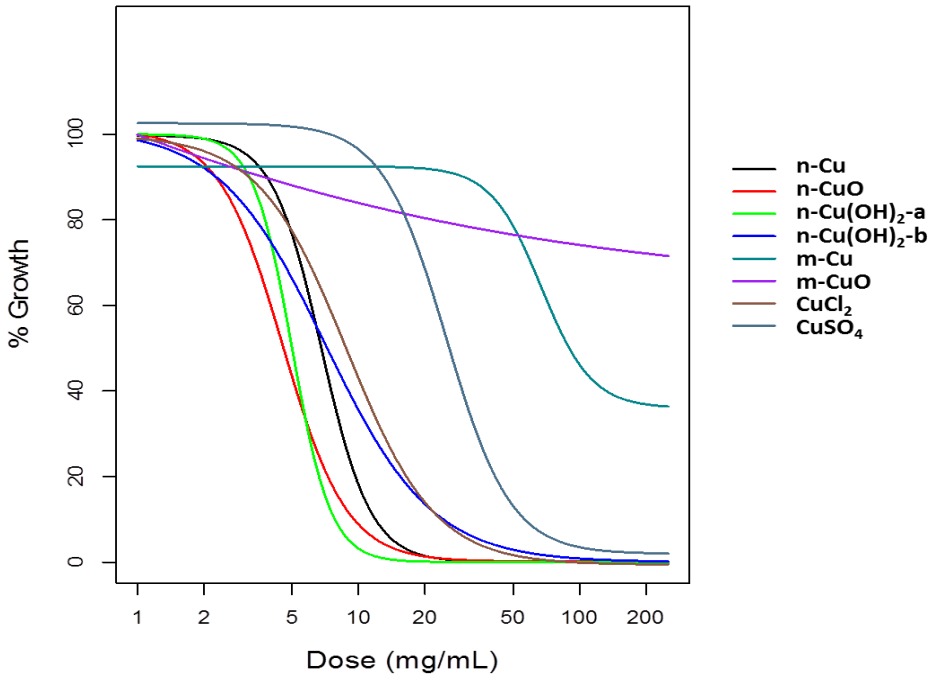

Figure A2.1. Growth inhibition effects of Cu species in *E. coli* and *L. brevis* *E. coli* (A) and *L. brevis* (B) were cultured in the presence of Cu particles ranging from 2 to 250 mg/L. OD_{600} was measured every 30 minute for 24 hours. Growth inhibition was plotted as the function of OD_{600} at different doses. At least 9 replicates were conducted for each concentration in each bacterial species.

(A) *E. coli*

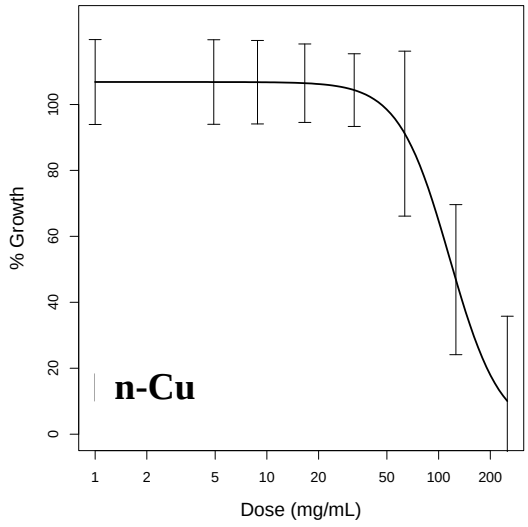
% Growth
0
20
40
60
80
100
n-Cu
1
2
5
10
20
50
100
200
Dose (mg/mL)

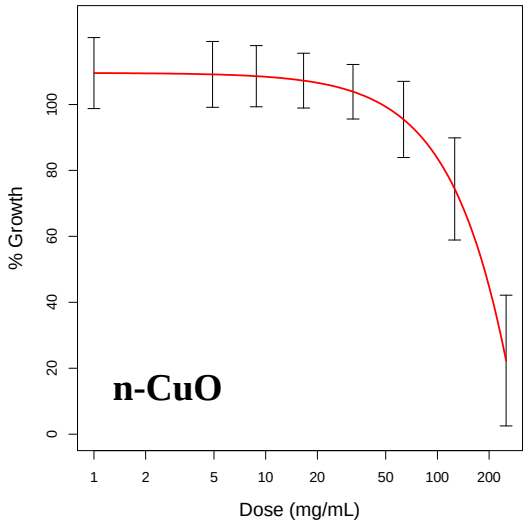
% Growth
0
20
40
60
80
100
n-CuO
1
2
5
10
20
50
100
200
Dose (mg/mL)

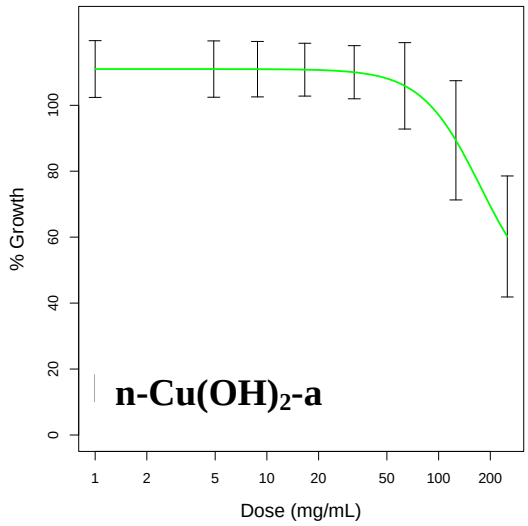
% Growth
0
20
40
60
80
100
n-Cu(OH)2-a
1
2
5
10
20
50
100
200
Dose (mg/mL)

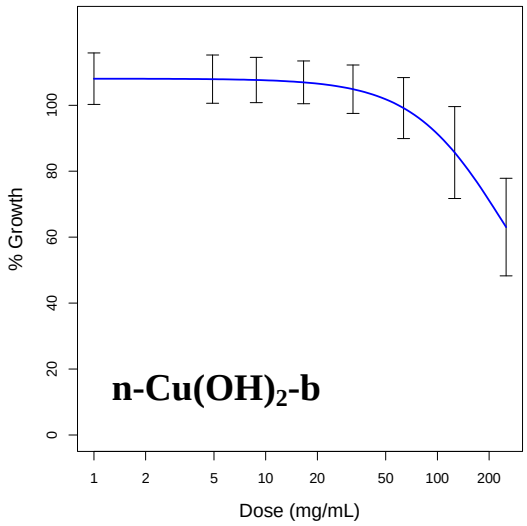
% Growth
0
20
40
60
80
100
n-Cu(OH)2-b
1
2
5
10
20
50
100
200
Dose (mg/mL)

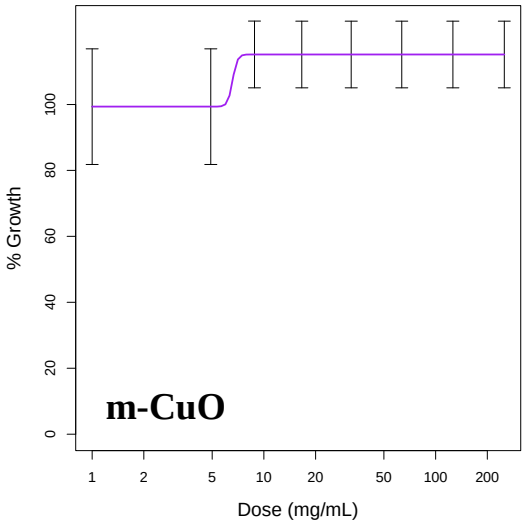
% Growth
0
20
40
60
80
100
1
2
5
10
20
50
100
200
Dose (mg/mL)
m-CuO

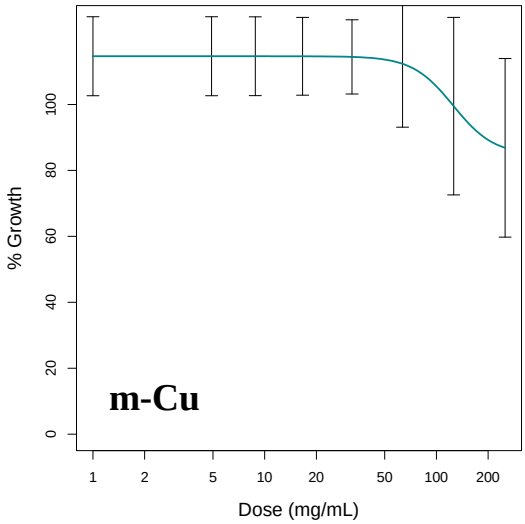
% Growth
0
20
40
60
80
100
1
2
5
10
20
50
100
200
Dose (mg/mL)
m-Cu

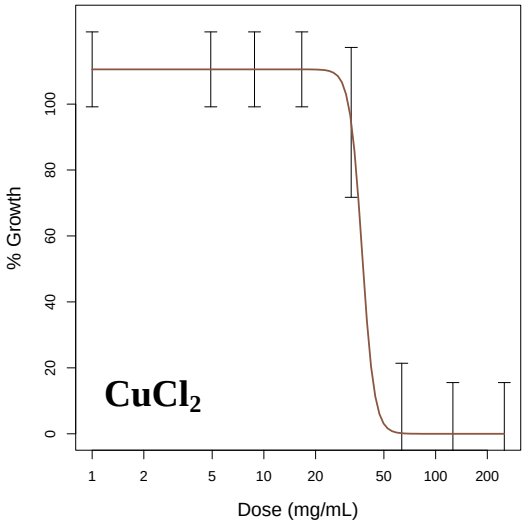
% Growth
0
20
40
60
80
100
1
2
5
10
20
50
100
200
Dose (mg/mL)
CuCl2

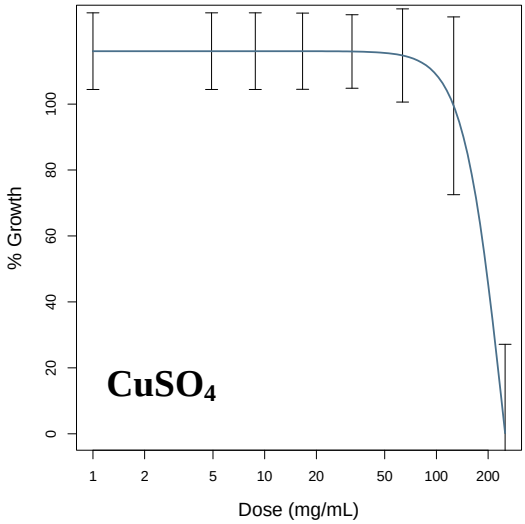
% Growth
0
20
40
60
80
100
1
2
5
10
20
50
100
200
Dose (mg/mL)
CuSO4

(B) *L. brevis*

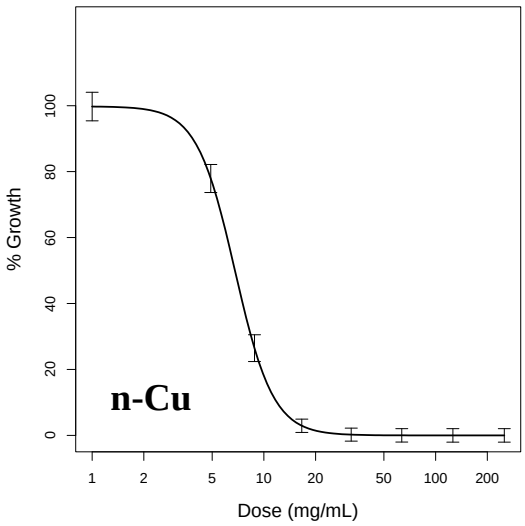
n-Cu
% Growth
0
20
40
60
80
100
1
2
5
10
20
50
100
200
Dose (mg/mL)

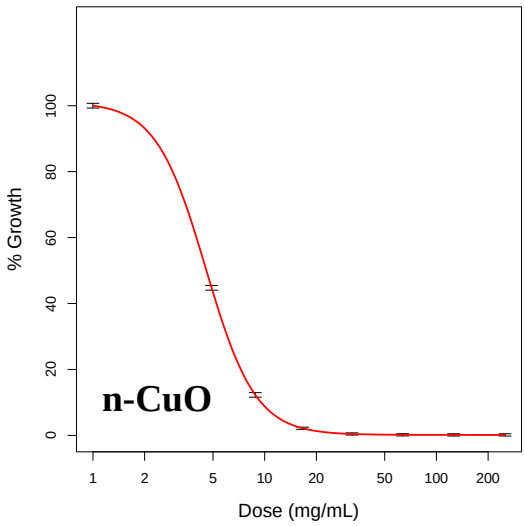
n-CuO
% Growth
0
20
40
60
80
100
1
2
5
10
20
50
100
200
Dose (mg/mL)

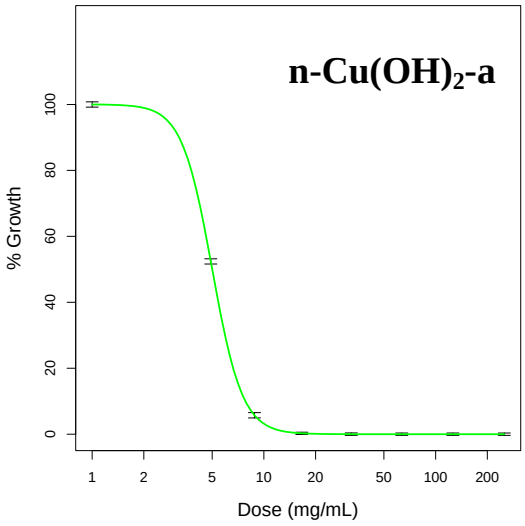
n-Cu(OH)2-a
% Growth
0
20
40
60
80
100
1
2
5
10
20
50
100
200
Dose (mg/mL)

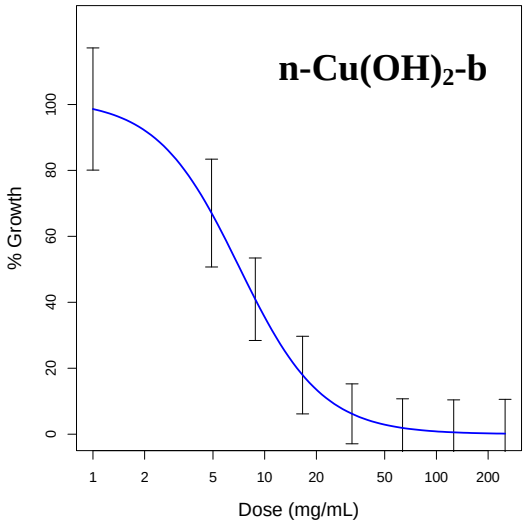
n-Cu(OH)2-b
% Growth
0
20
40
60
80
100
1
2
5
10
20
50
100
200
Dose (mg/mL)

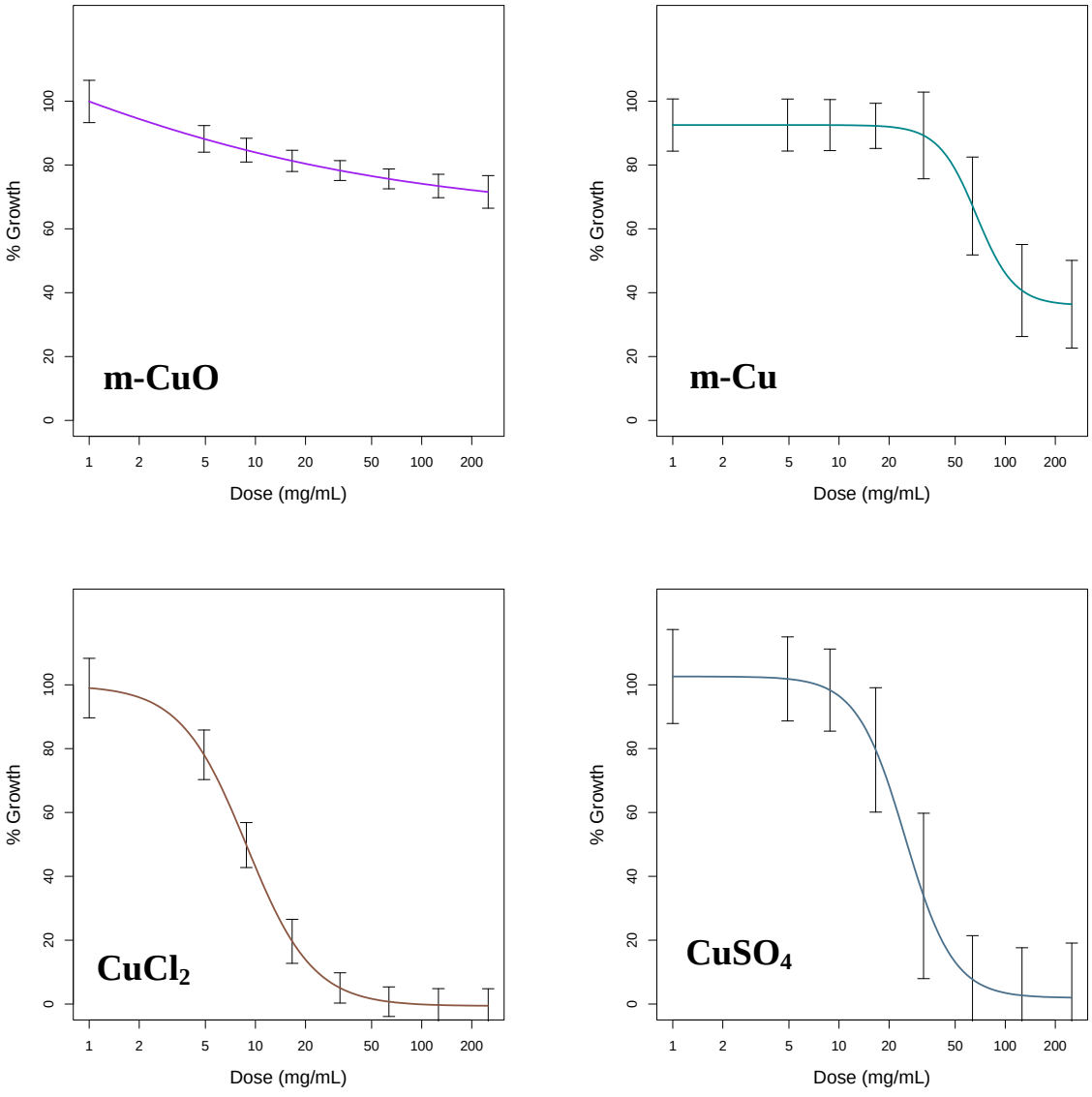

Figure A2.2. Individual growth inhibition curves including error bars for each of the Cu species. Curves shown are fit through eight different concentrations and at least nine replicates at each concentration; the model-based standard error for each point is indicated by the error bars. (A) *E. coli* (B) *L. brevis.*

(A) *E. coli*

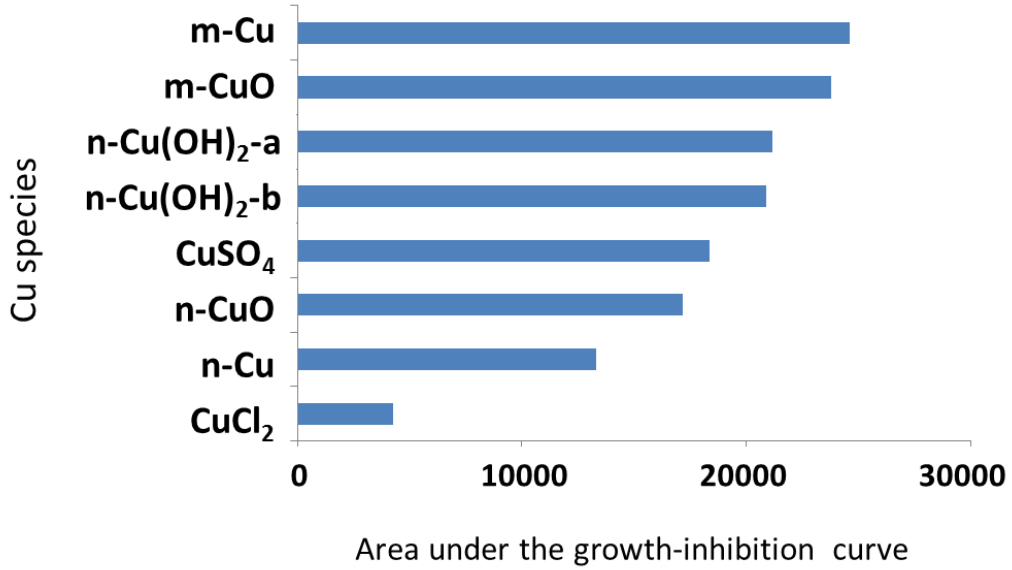

(B) *L. brevis*

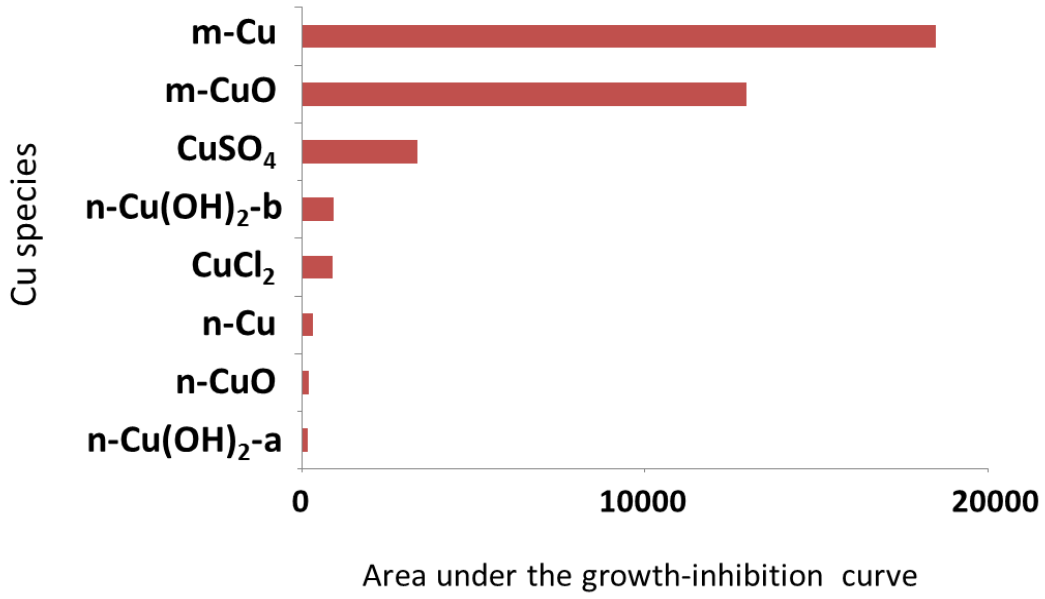

Figure A2.3. Area under the growth-inhibition curve for different Cu species in *E. coli* and *L. Brevis*. The area under the growth inhibition curves was calculated for (A) *E. coli* and (B) *L. brevis* to accurately distinguish between toxic and non-toxic Cu species. The toxic nano-sized

and ionic Cu treatments exhibit significantly smaller areas under their respective growth inhibition curves when compared to the less toxic micron-sized particles.

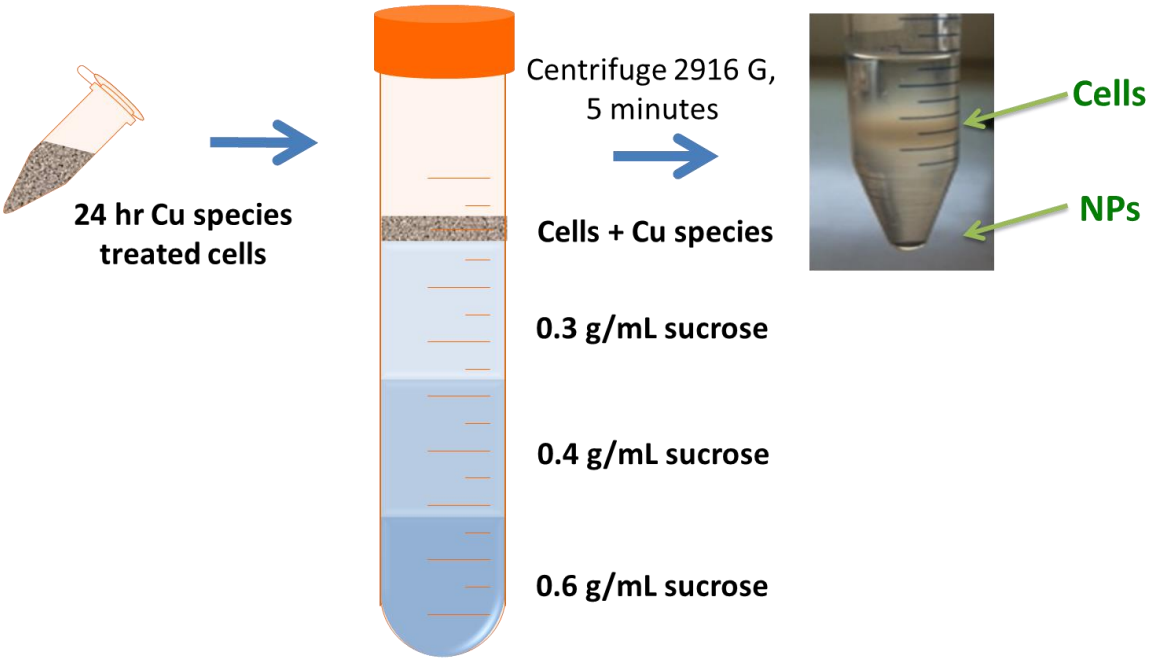

Figure A2.4. Schematic of sucrose gradient centrifugation procedure Bacterial cells were treated with Cu particles for 24 hours before being laid on top of the sucrose gradient to separate excessive particles from the bacterial cells. Sucrose gradients were constructed by carefully layering 0.6 g/mL at the bottom of the Falcon tube followed, by 0.4 and 0.3 g/mL of sucrose solutions. For each concentration, sucrose was dissolved in purified water to a completion before being filtered using a 0.22 μm Millipore filters. After centrifugation (5 minutes)a brown band of cells was visible in the middle of the gradient, with Cu particles are localized at the bottom of the tube

(A) *E. coli*

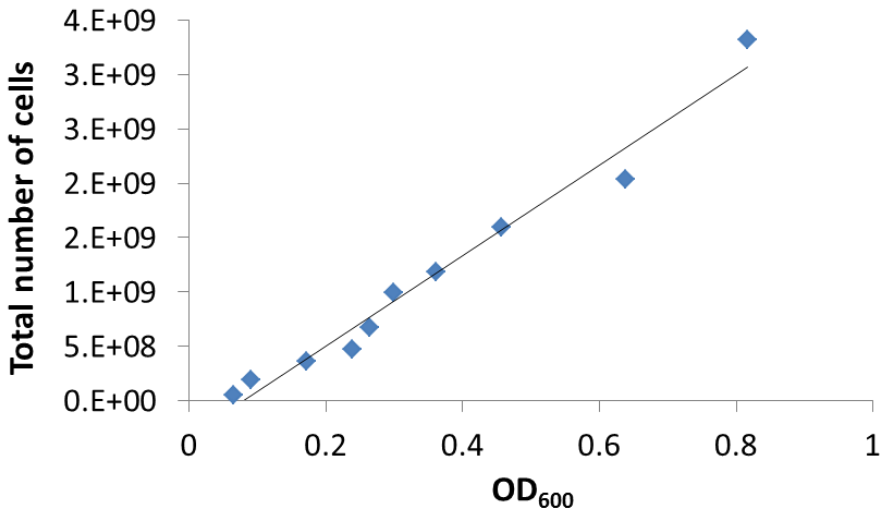

(B) *L. brevis*

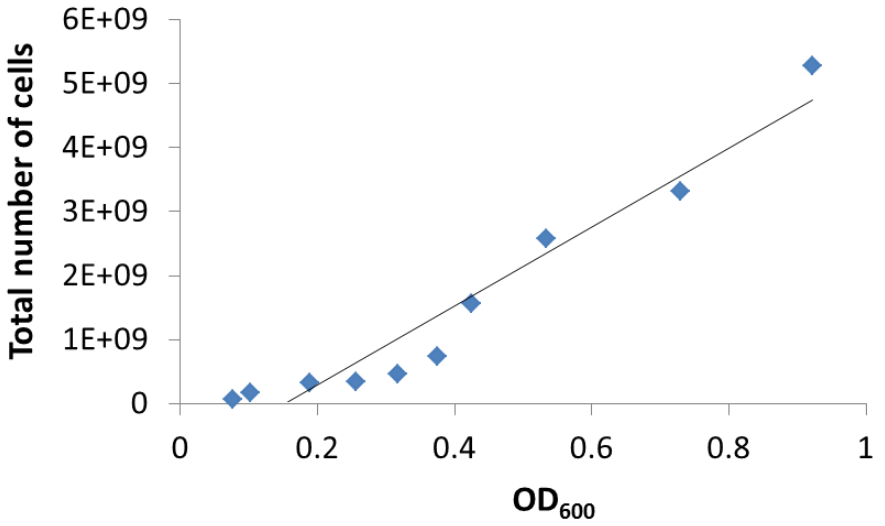

Figure A2.5. Standard curve of total number of cells versus OD_{600}. Total number of cells was calculated from counting colony forming units (CFUs) after plating the bacterial cells onto solid media (agar). Standard curves between OD_{600} and total number of cells were constructed for (A) *E. coli* and (B) *L. brevis*. For *E. coli*, the linear equation was Y = 4E+09x – 3E+08 and R^2 = 0.9748. For *L. brevis*, the linear equation was Y = 6E+09x – 9E+08 and R^2 = 0.9362.

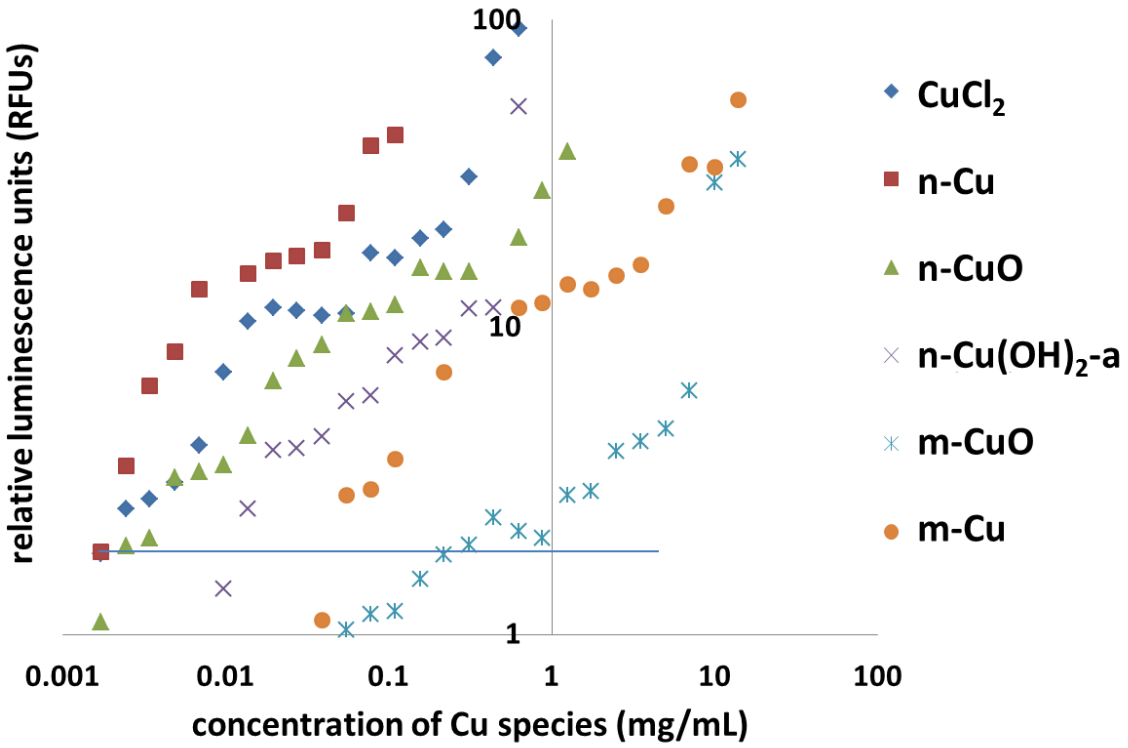

Figure A2.6. Cu bioavailability was determined using bacterial biosensor strain. A bacterial biosensor strain, which bioluminesces in response to intracellular bioavailable Cu, was used to quantify Cu inside of the cells exposed to the different Cu species. The sensor strain was cultured in the presence of Cu species for 2 hours, at which point the luminescence signal was measured. Three biological replicates were performed at each concentration. The concentration of copper required to induce a doubling of the amount of lumniscence signal compared to baseline ("concentration of bioavailable copper", shown on graph above as the intersection of each curve with the horizontal line) was determined for each copper species. Nano-Cu and $CuCl_2$ led to the highest induction of bioluminescence signal, followed by n-CuO and n-$Cu(OH)_2$, while the micron-sized particles (m-Cu and m-CuO) led to the lowest amount of bioluminescent signal.

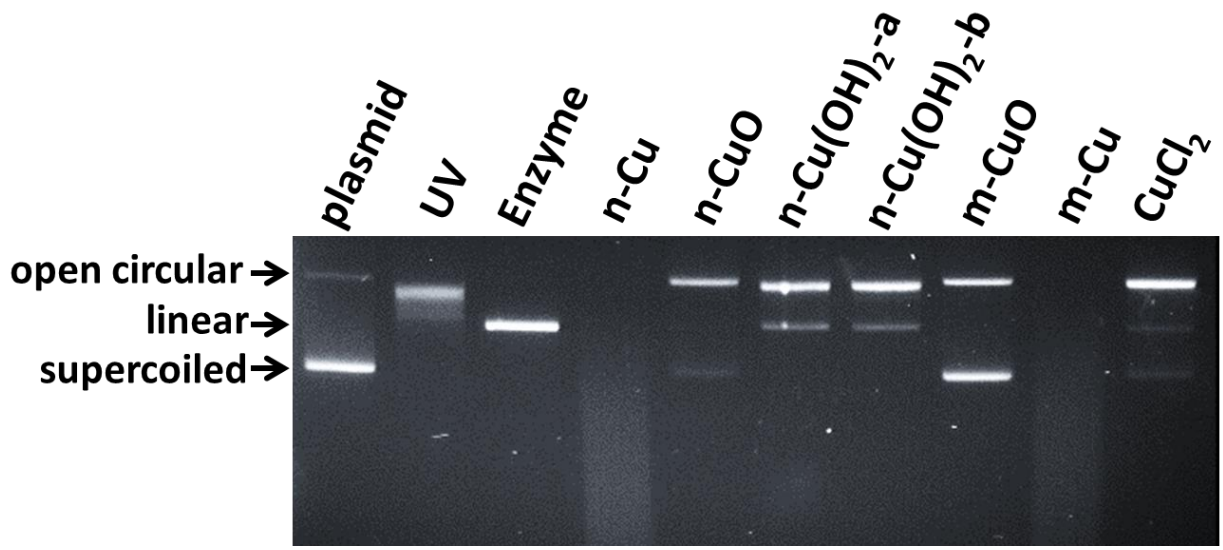

Figure A2.7. Results from DNA damage assay. The plasmid pUC19 was treated with the different Cu species for 24 hours and the resulting DNA species were separated and analyzed using gel electrophoresis. UV and restriction enzyme (*Pst*I) were used as positive controls for fragmented and linearized DNA, respectively. Electrophoresis was run at 5 V/cm for 1 hour. N-Cu and m-Cu generated the most severe DNA damage and resulted in complete degradation of the plasmid DNA. N-$Cu(OH)_2$-a and n-$Cu(OH)_2$-b induced complete conversion of supercoiled DNA to open circular and linear DNA, while exposure to the other Cu species resulted in only partial conversion of the plasmid DNA.

(A) *E. coli* control

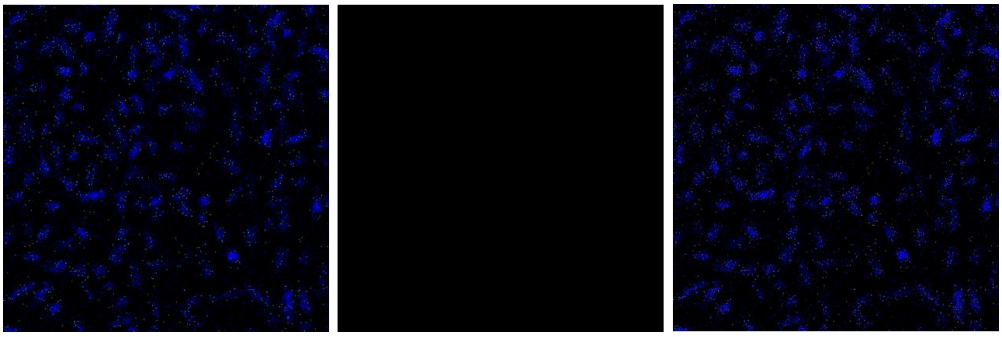

(B) *E. coli* treated with n-FITC-CuO

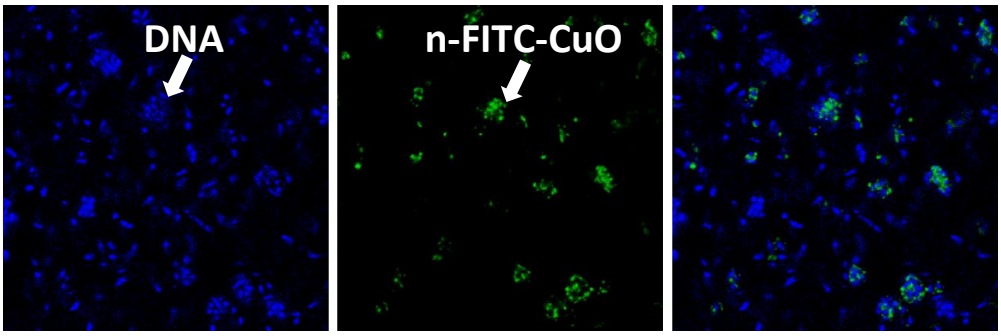

(C) *L. brevis* control

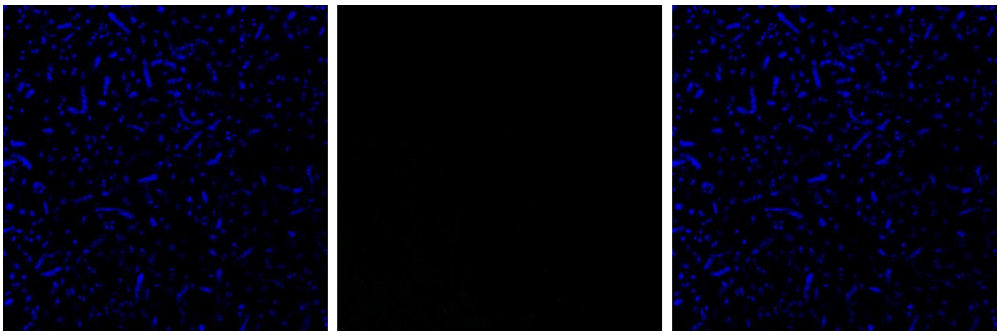

(D) *L. brevis* treated with n-FITC-CuO

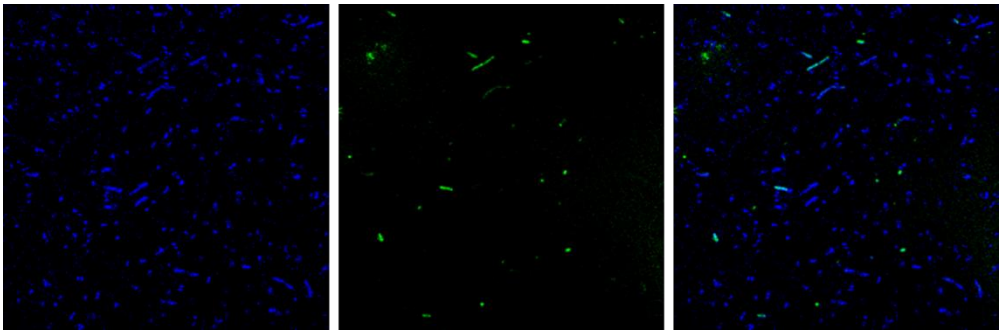

Figure A2.8. Confocal images of cells treated with n-FITC-CuO (green fluorescence). *E. coli* and *L. brevis* were treated with 0.1 mg/mL n-FITC-CuO for 24 hours before being washed and stained with Hoechst dye. (A) *E. coli* control (B) *E. coli* treated with n-FITC-CuO (C) *L. brevis* control (D) *L. brevis* treated with n-FITC-CuO. Co-localization of the DNA (Hoescht dye) and the nanoparticle (n-FITC-CuO) inside of the bacteria was observed for both species.

Table A2.1. Sources of Cu particles used herein

NPs	Source	Cat number
n-Cu	US Research Nanomaterials, InC	US1090
n-CuO	Sigma Aldrich	544868-25G
n-$Cu(OH)_2$-a	TreeGeek	CuPro 2005
n-$Cu(OH)_2$-b	Solution Self-Chem	Kocide 3000
m-CuO	Sigma Aldrich	208841-2KG
m-Cu	Sigma Aldrich	12806-1KG-R

Table A2.2. Correlation coefficients (*r*) for area under growth inhibition curve and amounts of dissolved copper in media, cell-associated Cu, and Cu bioavailable in each of the bacterial species.

r	Cu dissolution in media	Cu associated with cells (sucrose gradient)	biosensor
IC_{50} (*E.coli*)	-0.64	-0.73	-0.90
IC_{50} (*L. brevis*)	-0.35	-0.74	

Table A2.3. To demonstrate the agreement between five different assays studied herein, a correlation analysis was performed. (A) Correlation between results from the growth inhibition assay (area under curve) and the results from the suite of sub-lethal assays (area under the curve for membrane damage, biotic ROS generation, electron transport chain activity and membrane potential) in *E. coli*. (B) Correlation between results from the growth inhibition assay (area under curve) and the results from the suite of sub-lethal assays (area under the curve for membrane damage, biotic ROS generation, electron transport chain activity and membrane potential) in *L. brevis*. These correlations reveal that the best predictor overall of IC_{50} in each of the bacterial species is the assay for respiration rate. (C) Cross-correlation of results for the different assays between the two species of bacteria. Overall, a strong correlation between the results in the two species of bacteria was observed for biotic ROS generation and membrane potential, but only a moderate correlation was observed for IC_{50}, membrane damage, and electron transport chain activity.

(A) *E. coli*

Assays	IC_{50}	Membrane damage	Biotic ROS	Electron transport activity	Membrane potential
IC_{50}	1.00	0.43	0.02	0.76	0.31
Membrane damage	0.43	1.00	0.60	0.62	0.50
Biotic ROS	0.02	0.60	1.00	0.21	0.33
Electron transport activity	0.76	0.62	0.21	1.00	0.83
Membrane potential	0.31	0.50	0.33	0.83	1.00

(B) *L. brevis*

Assays	IC_{50}	Membrane damage	Biotic ROS	Electron transport activity	Membrane potential
IC_{50}	1.00	0.43	0.60	0.64	0.26
Membrane damage	0.43	1.00	0.24	0.88	0.71
Biotic ROS	0.60	0.24	1.00	0.14	0.76
Electron transport activity	0.64	0.88	0.14	1.00	0.43
Membrane potential	0.26	0.71	0.76	0.43	1.00

(C) cross-species comparison

Assays	IC_{50} (*L. brevis*)	Membrane damage (*L. brevis*)	Biotic ROS (*L. brevis*)	Electron transport activity (*L. brevis*)	Membrane potential (*L. brevis*)
IC_{50} (*E. coli*)	0.52	0.55	0.07	0.36	0.21
Membrane damage (*E. coli*)	0.62	0.60	0.45	0.81	0.19
Biotic ROS (*E. coli*)	0.45	0.05	0.90	0.33	0.52
Electron transport activity (*E. coli*)	0.38	0.79	0.26	0.62	0.67
Membrane potential (*E. coli*)	0.07	0.76	0.52	0.62	0.86

APPENDIX 3

Supporting Information for **Chapter 4**

Table A3.1. Expression level and fold change of genes that have been identified to be significantly up or down regulated in (A) Ag-BPEI and (B) $AgNO_3$ compared to untreated controls (*p-value* < 0.05 after BH adjustment to restrict the false discovery rate). Fold changes that are <1 indicate down regulated genes and fold changes that are >1 indicate up regualted genes.

(A) Ag-BPEI

Gene	expression level		fold change
	Ag-BPEI	control	
acpT	4.90	6.76	0.73
adhP	4.39	6.48	0.68
alaC	5.75	8.23	0.70
aldB	5.98	8.41	0.71
alkA	3.32	5.42	0.61
amiD	5.21	7.09	0.73
ansB	5.36	8.30	0.65
arnC	4.63	6.54	0.71
aroL	5.18	7.48	0.69
arpB	8.68	12.08	0.72
artQ	3.32	8.08	0.41
asd	8.40	9.96	0.84
asnS	5.93	7.94	0.75
aspA	7.27	10.01	0.73
atoC	6.16	9.00	0.68
bdm	4.89	9.63	0.51
bfr	6.41	8.27	0.78
blc	5.37	7.48	0.72
bolA	6.36	9.51	0.67
bsmA	6.27	11.01	0.57
bssR	6.57	9.03	0.73
can	7.52	9.05	0.83
cbpA	5.32	7.96	0.67
ccmC	5.50	8.13	0.68
cfa	6.66	8.61	0.77
chbB	6.29	8.73	0.72
chbC	5.74	8.06	0.71
cra	5.51	7.39	0.75
csgF	3.86	7.38	0.52
csiE	5.36	7.88	0.68
cspA	6.87	12.27	0.56
cspB	5.13	10.68	0.48

(B) $AgNO_3$

Gene	expression level		fold change
	$AgNO_3$	control	
aldB	4.97	7.88	0.63
allD	5.31	6.85	0.78
bdm	6.40	9.53	0.67
bfr	7.24	8.50	0.85
bolA	7.91	9.56	0.83
chbB	7.07	9.05	0.78
chbC	4.73	6.39	0.74
cheA	5.97	7.12	0.84
citD	6.59	8.11	0.81
csgD	6.30	8.43	0.75
csgG	5.39	6.46	0.83
cysW	4.50	6.20	0.73
dps	8.13	10.06	0.81
elfG	6.90	9.37	0.74
evgS	8.98	10.04	0.89
fdrA	4.48	6.03	0.74
fhuE	5.66	7.13	0.79
frvB	5.39	6.51	0.83
gadB	2.88	6.39	0.45
gadE	7.67	10.05	0.76
gadW	8.20	10.13	0.81
hdeA	8.81	13.28	0.66
hdeB	8.17	11.13	0.73
hdeD	7.43	10.65	0.70
hdhA	8.96	10.20	0.88
hlyE	2.87	5.10	0.56
hyaA	4.20	6.27	0.67
hyaF	4.69	7.37	0.64
hycF	6.16	9.18	0.67
lsrB	5.54	9.33	0.59
lsrG	5.03	8.57	0.59
mdtE	5.46	6.59	0.83

Gene	expression level		fold change
	Ag-BPEI	control	
cspC	6.06	9.15	0.66
cspD	4.81	7.07	0.68
cspE	5.89	9.88	0.60
cspG	4.77	8.87	0.54
cysB	5.76	7.73	0.75
dld	6.02	8.15	0.74
elaB	6.55	8.88	0.74
emtA	5.26	7.44	0.71
erfK	6.18	8.00	0.77
evgS	9.12	10.97	0.83
fadD	4.30	6.45	0.67
fadJ	5.39	7.76	0.69
frdA	7.43	9.22	0.81
gadB	3.55	6.56	0.54
gadE	8.01	10.13	0.79
gadW	7.87	10.69	0.74
gapC	4.83	9.46	0.51
gapC	6.12	9.06	0.68
gatA	7.22	11.48	0.63
gatY	11.09	14.12	0.79
gatZ	9.23	13.03	0.71
glgC	5.27	7.00	0.75
glgS	5.50	8.86	0.62
glmU	7.43	9.26	0.80
glmY	8.36	13.06	0.64
glmZ	8.24	10.08	0.82
glnQ	4.94	7.76	0.64
glpQ	3.80	5.73	0.66
hdeA	8.57	13.34	0.64
hdeD	6.58	10.70	0.62
hemA	5.49	7.75	0.71
hisL	6.54	9.40	0.70
hlyE	7.11	9.32	0.76
hokB	6.88	9.25	0.74
hokD	4.31	8.33	0.52
hpt	6.29	8.30	0.76
hyaF	4.12	6.85	0.60
hycF	6.46	9.71	0.67
hypE	2.30	5.59	0.41
ilvL	8.68	11.76	0.74
iraP	6.45	9.43	0.68
lsrB	5.27	9.55	0.55
lsrR	8.95	10.97	0.82
manA	5.26	7.79	0.68
melB	7.00	9.46	0.74
mglB	5.75	7.71	0.75

Gene	expression level		fold change
	$AgNO_3$	control	
melA	5.43	7.91	0.69
melB	7.11	9.64	0.74
mlrA	6.15	7.74	0.79
nadR	6.34	7.60	0.84
nlpA	8.65	10.66	0.81
npr	7.00	9.07	0.77
osmE	8.06	9.31	0.87
otsA	6.99	8.58	0.81
otsB	12.46	14.11	0.88
perR	6.51	8.43	0.77
pgaC	5.96	7.84	0.76
pnuC	6.97	8.58	0.81
prpB	6.44	9.24	0.70
prr	5.68	7.83	0.72
rffT	7.67	8.82	0.87
rhaM	6.29	8.07	0.78
rspB	5.37	7.82	0.69
rutE	4.86	6.44	0.75
rzpR	6.23	8.24	0.76
sgcA	4.72	6.87	0.69
sgcE	5.61	7.36	0.76
slp	5.37	7.77	0.69
sra	11.63	13.00	0.89
tam	4.19	5.97	0.70
treA	7.27	8.67	0.84
wcaA	6.45	7.57	0.85
wrbA	4.25	7.14	0.59
xanQ	6.52	8.91	0.73
xdhA	6.74	8.10	0.83
xdhB	6.45	7.89	0.82
xdhC	6.22	7.43	0.84
yahE	7.85	9.60	0.82
yahO	5.81	8.57	0.68
ybaS	5.83	7.50	0.78
ybdK	7.00	8.22	0.85
ybfB	7.33	9.23	0.79
ybfO	6.99	10.14	0.69
ycaC	6.75	8.72	0.77
ycaP	6.60	8.06	0.82
ycbK	7.87	9.21	0.85
yccJ	6.00	7.85	0.76
yceK	8.07	9.18	0.88
ycgB	6.96	9.21	0.76
yciW	7.36	8.90	0.83
ycjN	8.72	9.92	0.88
ycjY	5.86	7.94	0.74

Gene	expression level		fold change
	Ag-BPEI	control	
mgrB	5.38	9.03	0.60
micF	8.03	10.60	0.76
minE	4.90	8.56	0.57
mlrA	3.91	6.86	0.57
msrB	7.73	9.47	0.82
mtfA	4.51	8.26	0.55
nagC	5.67	7.60	0.75
nagK	6.58	8.32	0.79
npr	5.05	9.28	0.54
nuoE	8.49	10.37	0.82
omrA	4.12	6.63	0.62
oppA	8.96	11.05	0.81
oppB	7.19	9.51	0.76
osmC	6.11	8.03	0.76
osmE	4.72	9.29	0.51
otsA	6.61	8.08	0.82
otsB	10.92	14.14	0.77
paaX	5.55	7.51	0.74
pgaA	5.70	8.12	0.70
pgl	3.89	7.46	0.52
phr	4.79	6.60	0.73
pitA	6.40	7.87	0.81
preA	6.85	9.50	0.72
prr	5.92	8.01	0.74
prs	4.56	8.59	0.53
pspE	6.63	9.31	0.71
pth	4.86	6.49	0.75
queG	4.27	8.21	0.52
relA	6.02	7.51	0.80
rfaC	7.73	9.13	0.85
rfbA	7.04	8.81	0.80
rho	6.91	8.34	0.83
rnlA	4.96	8.09	0.61
rpoE	5.86	8.55	0.69
rsd	4.45	6.22	0.71
rssB	4.37	6.69	0.65
ryfA	6.21	8.29	0.75
rzpR	4.94	7.84	0.63
sapF	4.44	6.34	0.70
sbmC	6.48	9.00	0.72
sibA	3.50	6.24	0.56
sibC	5.86	7.56	0.77
slp	5.91	8.30	0.71
slyA	8.19	9.68	0.85
sokB	7.38	10.38	0.71
spr	5.87	9.11	0.64

Gene	expression level		fold change
	$AgNO_3$	control	
ydcS	6.01	8.41	0.71
ydcU	7.07	8.64	0.82
ydhS	5.73	7.83	0.73
ydhX	5.55	7.30	0.76
ydiH	12.24	13.65	0.90
yeaG	7.02	9.35	0.75
yeaH	6.49	8.71	0.75
yeaN	6.03	7.57	0.80
yeaQ	6.86	9.29	0.74
yebV	6.41	9.11	0.70
yfdC	7.96	10.36	0.77
yfhL	5.80	7.78	0.75
yfiL	8.44	9.80	0.86
ygaM	11.84	12.97	0.91
ygbM	4.73	5.95	0.79
ygeX	6.83	9.87	0.69
ygeY	7.39	9.12	0.81
ygfM	5.80	7.94	0.73
yghX	6.75	8.14	0.83
yhbY	8.48	9.49	0.89
yhcO	6.06	7.49	0.81
yhiD	7.90	9.70	0.81
yhiL	5.70	8.76	0.65
yiaG	5.82	8.82	0.66
yjdF	7.58	9.25	0.82
yjdI	8.83	10.75	0.82
yjdJ	9.53	10.91	0.87
yliI	6.03	7.37	0.82
yliL	9.65	10.64	0.91
yncG	6.30	8.04	0.78
yncG	6.18	8.55	0.72
ynfC	6.69	8.58	0.78
ynfE	6.05	8.14	0.74
ynfF	7.39	9.57	0.77
ynfH	6.11	7.60	0.80
yoaC	8.23	9.53	0.86
yodC	7.33	8.83	0.83
yodD	10.37	12.18	0.85
yohC	5.14	7.01	0.73
yohF	4.08	6.05	0.68
yqjD	8.99	10.03	0.90
yqjE	8.53	9.91	0.86
ytfQ	11.57	13.27	0.87
aas	7.49	6.36	1.18
accD	8.89	7.00	1.27
aceE	9.95	8.13	1.22

Gene	expression level		fold change
	Ag-BPEI	control	
sra	9.95	13.19	0.75
tdcB	8.13	10.22	0.79
tdcE	6.79	8.90	0.76
tdcG	5.75	7.49	0.77
tnaA	6.20	9.59	0.65
tnaC	3.69	10.08	0.37
tusC	6.42	8.24	0.78
uidR	6.58	8.45	0.78
uspE	6.30	8.52	0.74
uspF	8.46	10.67	0.79
uvrC	5.18	7.17	0.72
uxaA	6.62	9.26	0.71
wrbA	2.97	7.23	0.41
yagN	6.65	10.30	0.65
yahB	5.73	8.60	0.67
yahO	3.98	8.51	0.47
yaiI	6.33	7.81	0.81
ybdD	5.64	7.94	0.71
ybeD	6.70	8.40	0.80
ybfB	5.94	8.21	0.72
ybgT	6.94	8.88	0.78
ybhQ	6.36	8.48	0.75
ybhT	6.96	9.07	0.77
ycaC	6.97	8.58	0.81
ycbJ	6.79	8.69	0.78
ycbK	6.82	9.31	0.73
yccF	6.45	8.29	0.78
yccJ	6.24	8.76	0.71
yceK	5.69	9.27	0.61
ycfH	4.71	7.66	0.61
ycfL	5.81	7.78	0.75
ycfP	5.65	8.68	0.65
ycgB	6.34	9.57	0.66
ycgE	6.58	9.22	0.71
ycgE	6.28	7.93	0.79
ychH	5.42	9.04	0.60
yciB	5.87	7.56	0.78
yciU	3.49	5.02	0.70
ycjY	5.70	8.03	0.71
ydaS	6.76	9.33	0.72
ydcJ	5.26	8.26	0.64
ydcS	4.97	8.18	0.61
ydcU	6.91	8.63	0.80
ydhI	6.39	7.97	0.80
ydhS	5.19	7.39	0.70
ydhU	6.53	8.22	0.79

Gene	expression level		fold change
	$AgNO_3$	control	
aceF	10.98	7.98	1.38
acnB	8.25	6.01	1.37
acrA	8.31	6.02	1.38
acrB	7.34	5.84	1.26
adk	9.81	8.14	1.21
ahpC	9.89	8.29	1.19
ahpF	6.79	5.21	1.30
alaS	10.31	7.65	1.35
amiD	9.10	7.64	1.19
araC	8.74	7.35	1.19
asnA	10.78	8.26	1.31
aspA	12.06	10.41	1.16
atpA	10.77	8.37	1.29
atpC	11.80	9.64	1.22
atpE	11.18	9.54	1.17
atpG	10.89	8.97	1.21
atpI	9.97	8.59	1.16
bacA	8.26	6.96	1.19
bamB	8.82	7.18	1.23
bamC	8.96	6.49	1.38
bcsE	9.61	8.14	1.18
betB	7.25	5.66	1.28
betI	7.69	6.05	1.27
carA	8.58	6.99	1.23
carB	8.29	6.92	1.20
cdaR	9.54	7.67	1.24
chpS	10.60	9.09	1.17
clpB	9.49	7.00	1.36
cmoB	6.39	4.78	1.34
copA	9.92	5.82	1.71
csdL	7.25	5.85	1.24
cueO	5.24	3.72	1.41
cyoB	10.02	7.11	1.41
cyoD	10.90	8.63	1.26
cyoE	11.78	9.01	1.31
cysS	8.69	7.19	1.21
dadA	9.76	7.10	1.37
dadX	10.46	8.18	1.28
dcp	7.49	6.45	1.16
dcrB	9.43	7.14	1.32
degP	7.92	6.34	1.25
dmlR	8.19	6.63	1.24
dnaJ	10.02	7.23	1.38
eda	7.59	5.57	1.36
emrA	7.54	6.28	1.20
envC	7.25	5.92	1.23

Gene	expression level		fold change
	Ag-BPEI	control	
ydhW	5.14	6.83	0.75
ydiH	10.97	13.66	0.80
ydiK	5.94	7.37	0.81
yeaG	5.30	9.28	0.57
yeaH	7.10	8.82	0.80
yeaZ	6.06	7.56	0.80
yebF	5.39	7.38	0.73
yebO	8.44	10.14	0.83
yebS	5.13	7.45	0.69
yebV	6.36	8.30	0.77
yecR	5.68	7.88	0.72
yeeU	4.65	9.47	0.49
yehT	5.83	7.73	0.75
yfcZ	6.52	9.41	0.69
yfdC	8.10	10.11	0.80
yfgG	8.91	10.96	0.81
yfgJ	6.27	7.91	0.79
yfiL	7.97	9.50	0.84
yfjH	8.95	10.68	0.84
yfjK	5.77	9.76	0.59
ygaM	10.10	13.04	0.77
ygdI	9.08	11.53	0.79
ygeX	7.41	10.17	0.73
yhbJ	9.38	11.02	0.85
yheO	6.20	9.04	0.69
yheU	3.75	6.06	0.62
yhfK	4.97	6.98	0.71
yiaG	6.07	8.95	0.68
yjbJ	6.47	9.84	0.66
yjbQ	5.48	7.52	0.73
yjcE	5.13	7.24	0.71
yjdF	7.26	9.02	0.80
yjfN	5.78	8.79	0.66
ykgA	4.26	9.52	0.45
yneF	5.51	7.50	0.73
ynfE	5.65	7.90	0.72
ynfF	8.02	9.60	0.84
ynhG	7.99	9.53	0.84
yoaC	8.21	10.10	0.81
yobF	8.56	10.63	0.81
yodC	6.08	8.51	0.71
yodD	8.96	12.54	0.71
yohF	4.29	6.30	0.68
yqeF	4.95	7.74	0.64
yqjD	8.94	10.26	0.87
yqjE	5.97	9.88	0.60

Gene	expression level		fold change
	$AgNO_3$	control	
era	7.60	6.17	1.23
exbD	8.08	5.19	1.56
fabA	9.38	8.37	1.12
fabF	9.20	7.54	1.22
fabR	10.85	8.47	1.28
fadE	8.64	6.23	1.39
fecA	9.79	7.08	1.38
fecC	7.96	5.70	1.40
fecD	7.93	6.50	1.22
fecR	7.73	5.97	1.30
feoB	9.29	6.21	1.50
feoC	7.68	5.54	1.39
fepD	7.41	6.23	1.19
fes	7.14	5.50	1.30
flgB	7.30	5.85	1.25
flgD	7.82	5.88	1.33
flgF	6.11	4.63	1.32
fliG	7.20	4.89	1.47
fliN	7.17	4.53	1.58
fliO	7.58	5.57	1.36
frmA	9.98	7.34	1.36
frmR	10.66	7.44	1.43
ftsE	9.21	7.20	1.28
fumA	11.93	10.39	1.15
fusA	12.90	10.17	1.27
gapA	10.44	8.07	1.29
glcB	10.64	8.93	1.19
glcC	8.67	7.05	1.23
glcG	11.05	8.66	1.28
glnA	8.22	7.07	1.16
glnE	8.93	6.27	1.42
glnG	7.38	4.69	1.57
gltB	7.14	5.80	1.23
glyA	8.80	7.28	1.21
glyQ	9.12	7.60	1.20
glyS	9.74	8.27	1.18
gnd	8.83	6.82	1.29
gnd	9.59	7.78	1.23
gpmA	9.10	7.46	1.22
groS	14.25	12.97	1.10
gshA	10.45	8.89	1.18
gshB	9.55	6.85	1.39
guaA	8.51	6.66	1.28
guaB	8.95	6.07	1.48
gutQ	9.30	6.83	1.36
gyrA	10.14	7.71	1.31

Gene	expression level		fold change
	Ag-BPEI	control	
yqjK	5.66	9.78	0.58
ytfK	8.50	11.66	0.73
zitB	6.91	9.33	0.74
aceE	10.18	8.45	1.21
aceF	11.26	8.03	1.40
ahpC	10.29	8.26	1.25
ahpF	8.08	5.61	1.44
arfA	9.68	7.29	1.33
argH	9.65	7.44	1.30
atpC	12.08	9.82	1.23
clpB	9.36	6.91	1.35
copA	9.37	5.71	1.64
cueO	6.79	4.15	1.64
cysN	7.93	6.50	1.22
dcp	8.17	6.48	1.26
degP	8.50	6.62	1.28
deoB	10.34	8.21	1.26
dnaJ	9.66	7.40	1.31
dnaK	13.42	11.01	1.22
dsbA	11.03	8.66	1.27
fecA	8.94	6.84	1.31
fes	7.35	5.40	1.36
fhuA	7.79	6.49	1.20
fpr	8.72	6.75	1.29
frmA	9.62	7.75	1.24
frmR	9.35	7.22	1.29
gcd	8.29	6.83	1.21
gshB	10.23	6.82	1.50
hflC	9.36	7.87	1.19
hns	10.58	9.02	1.17
htpG	9.39	6.53	1.44
ibpA	12.64	9.24	1.37
ibpB	12.03	8.81	1.37
idi	10.52	8.86	1.19
inaA	7.21	5.94	1.21
ldhA	8.50	6.45	1.32
lnt	10.29	8.22	1.25
metQ	9.48	7.73	1.23
mgtA	9.06	6.17	1.47
miaA	12.73	9.52	1.34
mlaF	11.36	8.48	1.34
mprA	11.76	8.69	1.35
mqsR	9.33	7.56	1.23
nrdH	9.19	7.65	1.20
pflD	7.30	5.88	1.24
ratB	11.40	8.52	1.34

Gene	expression level		fold change
	$AgNO_3$	control	
gyrB	9.28	7.73	1.20
hda	8.00	6.25	1.28
hemC	11.15	10.03	1.11
hemL	8.90	7.00	1.27
hns	10.72	9.25	1.16
hokD	9.73	8.30	1.17
holA	6.04	4.71	1.28
hscA	9.29	7.49	1.24
hspQ	10.31	7.98	1.29
htpG	8.20	6.33	1.30
hupA	9.97	8.00	1.25
ibpA	11.82	9.43	1.25
ibpB	11.60	8.82	1.31
ileS	9.31	7.05	1.32
ilvB	9.38	7.05	1.33
ilvE	9.98	8.82	1.13
ilvG	8.86	6.31	1.40
ilvY	6.41	4.25	1.51
inaA	7.42	6.24	1.19
insG	8.12	6.30	1.29
iscX	8.80	7.55	1.16
kdgK	8.16	6.95	1.17
lamB	11.13	9.02	1.23
lepA	9.01	6.99	1.29
leuS	8.80	6.73	1.31
lpcA	7.24	5.82	1.24
lpd	10.81	8.65	1.25
lpoA	8.27	7.03	1.18
lpp	12.42	9.88	1.26
lptB	8.29	7.05	1.18
lptE	11.10	9.35	1.19
lptF	8.04	6.56	1.23
lspA	11.67	10.23	1.14
maeB	8.64	6.93	1.25
malE	9.17	7.67	1.20
malG	8.65	7.31	1.18
malK	11.35	8.74	1.30
malT	8.27	5.86	1.41
manX	9.12	7.35	1.24
manY	10.13	8.24	1.23
mdh	10.53	8.29	1.27
menC	9.16	7.58	1.21
menD	7.82	6.22	1.26
metQ	8.96	7.91	1.13
mgsA	10.22	7.57	1.35
mhpD	7.15	6.04	1.18

Gene	expression level		fold change
	Ag-BPEI	control	
rimI	9.87	7.77	1.27
rplI	8.22	6.09	1.35
rplW	12.27	10.15	1.21
rplY	10.70	8.16	1.31
rpmG	11.12	9.28	1.20
rpmI	12.45	10.08	1.24
rpoD	8.76	6.34	1.38
rpoD	10.81	8.06	1.34
rpsB	9.42	7.05	1.34
rpsR	10.24	8.09	1.27
rrsH	14.41	8.12	1.77
rtcR	8.12	6.52	1.25
secA	12.86	9.74	1.32
sodA	10.43	9.02	1.16
soxS	8.99	7.23	1.24
spy	9.59	7.61	1.26
sseB	9.95	8.60	1.16
tig	9.04	7.67	1.18
tsf	9.90	6.82	1.45
yacH	8.58	6.41	1.34
ybaQ	9.14	7.16	1.28
ybbN	8.01	5.88	1.36
ybdH	8.20	6.51	1.26
ybjC	12.95	10.49	1.23
ydbK	9.65	7.16	1.35
yhcN	11.97	9.67	1.24
yhfT	8.00	5.95	1.35
yicH	8.76	6.34	1.38
yjbD	7.81	6.37	1.23
yjeJ	9.46	7.36	1.28
yjeP	7.16	5.24	1.37
ylbE	7.37	5.58	1.32
ytfF	9.27	7.65	1.21

Gene	expression level		fold change
	$AgNO_3$	control	
mioC	8.72	7.25	1.20
mlaF	10.81	8.53	1.27
mmuM	8.75	6.25	1.40
mnmA	9.44	8.05	1.17
mnmG	9.11	7.55	1.21
moaC	7.68	6.46	1.19
moaD	10.02	8.25	1.22
moaE	8.19	6.51	1.26
mog	8.97	7.59	1.18
mprA	11.37	8.83	1.29
mqo	7.47	5.58	1.34
mrcB	8.87	6.68	1.33
mreB	9.67	7.44	1.30
murA	8.57	5.90	1.45
murF	7.99	5.80	1.38
murG	9.07	7.10	1.28
murP	7.65	6.29	1.22
nagC	9.40	7.52	1.25
nanA	9.14	6.64	1.38
nanE	8.62	6.25	1.38
nanK	8.65	6.75	1.28
nanT	8.44	6.80	1.24
napF	7.94	6.72	1.18
narG	9.97	7.73	1.29
narK	8.94	7.05	1.27
ndk	7.88	6.17	1.28
nirB	8.32	6.12	1.36
norR	7.40	5.31	1.40
nrdD	8.95	7.19	1.25
nrdH	8.90	7.65	1.16
nrdI	7.71	6.22	1.24
nrdR	7.81	5.90	1.32
nuoG	8.55	5.95	1.44
nuoH	11.10	8.05	1.38
nuoI	12.56	9.95	1.26
nuoJ	13.32	11.17	1.19
nuoK	10.64	8.75	1.22
nuoL	10.24	8.11	1.26
nuoM	9.17	7.61	1.21
nuoN	9.66	7.64	1.26
nupC	8.72	6.88	1.27
nusG	8.58	7.18	1.19
obgE	8.49	6.72	1.26
ompA	10.10	7.81	1.29
ompF	11.10	9.33	1.19
ompR	7.99	6.25	1.28

Gene	expression level		fold change
	$AgNO_3$	control	
ompX	10.34	8.57	1.21
oxyR	8.22	6.74	1.22
pal	10.23	9.14	1.12
panB	8.63	7.07	1.22
parC	8.62	7.21	1.20
pcnB	8.62	7.02	1.23
pfkA	10.74	9.69	1.11
pitA	8.78	7.62	1.15
plaP	7.79	6.01	1.30
plsB	7.63	6.45	1.18
ppa	8.67	7.39	1.17
prfC	8.97	7.05	1.27
priB	10.39	7.56	1.37
proB	9.29	7.51	1.24
proS	9.38	7.37	1.27
proW	10.68	8.88	1.20
purL	8.92	6.40	1.39
purR	9.20	6.95	1.32
putA	8.97	6.41	1.40
putP	8.61	5.94	1.45
pyrB	8.63	6.54	1.32
pyrG	8.22	6.99	1.18
pyrH	9.40	7.12	1.32
ratA	10.32	8.86	1.16
rbsK	8.69	7.24	1.20
recJ	8.89	7.46	1.19
recO	7.19	5.91	1.22
recR	9.74	8.43	1.16
rfbD	7.84	6.56	1.19
rffG	9.06	8.00	1.13
rffH	8.91	6.23	1.43
rimM	9.53	6.53	1.46
rlmI	9.94	7.65	1.30
rlmN	8.91	7.20	1.24
rluA	9.00	6.83	1.32
rluB	7.60	6.39	1.19
rnk	7.63	6.28	1.22
rob	9.32	7.51	1.24
rpiA	9.00	7.47	1.21
rplA	10.31	8.70	1.19
rplD	13.02	10.63	1.22
rplI	7.99	5.46	1.46
rplJ	11.49	9.14	1.26
rplK	9.77	7.97	1.23
rplL	11.56	8.98	1.29
rplM	10.81	8.20	1.32

Gene	expression level		fold change
	$AgNO_3$	control	
rplQ	11.66	9.48	1.23
rplS	10.85	7.98	1.36
rplT	11.02	9.25	1.19
rplU	9.68	8.05	1.20
rplV	11.75	8.78	1.34
rplW	11.98	10.13	1.18
rplY	9.76	8.19	1.19
rpmA	8.24	6.01	1.37
rpmB	11.05	9.63	1.15
rpmC	10.29	7.21	1.43
rpmE	9.88	8.65	1.14
rpmF	10.97	8.58	1.28
rpmG	11.38	9.66	1.18
rpoA	12.77	9.70	1.32
rpoC	10.04	8.61	1.17
rpoD	9.95	6.42	1.55
rpoD	10.49	8.08	1.30
rpsA	10.87	7.74	1.41
rpsB	10.04	6.56	1.53
rpsD	11.04	8.35	1.32
rpsF	9.98	7.30	1.37
rpsG	11.27	9.20	1.23
rpsI	10.60	9.17	1.16
rpsK	11.26	9.71	1.16
rpsL	11.10	8.53	1.30
rpsO	11.49	9.67	1.19
rpsQ	11.33	8.86	1.28
rpsR	9.80	7.57	1.29
rrsH	14.66	8.18	1.79
rsmG	13.26	11.26	1.18
sdaB	9.55	6.60	1.45
sdaC	8.44	5.92	1.43
secA	10.65	9.45	1.13
secE	8.86	7.55	1.17
serC	8.34	7.25	1.15
sgrS	9.47	7.32	1.29
sodA	10.42	9.07	1.15
soxS	10.96	7.89	1.39
speA	9.58	6.41	1.49
spy	9.51	7.89	1.21
srlB	8.36	6.31	1.32
srlD	7.73	6.47	1.20
srlE	7.95	6.58	1.21
sseB	9.95	8.59	1.16
sspB	9.92	7.95	1.25
sucA	10.85	9.49	1.14

Gene	expression level		fold change
	$AgNO_3$	control	
sucC	10.90	8.56	1.27
sucD	9.39	7.51	1.25
tadA	8.70	6.83	1.27
tdh	9.04	7.09	1.28
tff	10.47	6.92	1.51
thrC	8.31	6.72	1.24
thyA	6.64	5.37	1.24
tig	9.69	7.84	1.24
tilS	8.39	6.77	1.24
tmcA	7.72	5.65	1.36
tolB	9.16	7.08	1.29
treB	11.85	8.09	1.47
treC	10.42	7.76	1.34
trmJ	10.43	8.92	1.17
truD	9.06	7.59	1.19
trxB	8.49	6.39	1.33
tsf	9.72	7.06	1.38
ubiA	9.14	7.00	1.31
ubiD	10.18	8.70	1.17
ubiF	8.94	6.92	1.29
ucpA	10.90	9.22	1.18
uhpB	8.21	6.21	1.32
ulaR	8.81	7.53	1.17
upp	13.72	11.44	1.20
uraA	7.66	6.57	1.17
uup	7.79	6.65	1.17
yaeP	8.58	6.14	1.40
yafJ	6.71	5.65	1.19
yagE	7.46	5.71	1.31
yagF	8.50	5.86	1.45
yaiZ	9.98	8.30	1.20
yajQ	7.70	5.39	1.43
ybbN	8.76	6.14	1.43
ybdH	8.89	6.54	1.36
ybgF	9.22	8.11	1.14
ybhC	7.14	5.25	1.36
ybiJ	7.63	6.44	1.18
ybjC	12.85	10.38	1.24
ycbC	8.69	5.71	1.52
ycdY	8.34	7.02	1.19
yceM	8.99	7.06	1.27
ycfD	8.89	7.08	1.26
ychF	8.27	6.47	1.28
ycjQ	9.21	7.93	1.16
ydbK	8.28	7.26	1.14
yeaC	8.23	6.57	1.25

Gene	expression level		fold change
	$AgNO_3$	control	
yeaD	9.33	7.72	1.21
yedE	10.57	7.82	1.35
yedF	10.48	8.68	1.21
yeeZ	9.33	7.67	1.22
yeiH	8.81	7.75	1.14
yejG	10.31	7.61	1.35
yfcH	9.43	7.93	1.19
yfiH	7.99	6.76	1.18
yfjD	9.34	7.77	1.20
ygbI	8.68	7.48	1.16
yghB	11.34	10.01	1.13
ygiF	7.96	5.54	1.44
yhaM	8.49	6.68	1.27
yhcN	11.57	9.70	1.19
yhdE	9.30	8.05	1.16
yhiI	7.66	5.98	1.28
yibF	8.28	7.09	1.17
yicH	7.88	6.32	1.25
yidC	8.95	7.27	1.23
yjaH	7.20	5.39	1.34
yjiA	8.17	7.10	1.15
yjjK	9.66	8.19	1.18
ykgE	8.73	6.79	1.29
ymgG	9.40	8.14	1.15
ynjB	7.81	5.60	1.40
yoeB	8.65	6.51	1.33
ypeB	6.47	4.99	1.30
ysaA	8.94	7.19	1.24
ytfN	7.70	6.33	1.22
zapB	10.22	8.63	1.18
zipA	8.20	6.09	1.35
zraP	9.44	5.69	1.66
zraR	8.26	6.00	1.38
zraS	9.11	7.43	1.23